DISSERTATION

A NOVEL METHOD FOR RAPID IN VITRO RADIOBIOASSAY

Submitted by

Evan Bogert Crawford

Department of Environmental and Radiological Health Sciences

In partial fulfillment of the requirements

For the Degree of Doctor of Philosophy

Colorado State University

Fort Collins, Colorado

Spring 2015

Doctoral Committee:

Advisor: John Zimbrick

Alexander Hulpke
Jerome LaRosa
Howard Ramsdell
Georg Steinhauser

ABSTRACT

A NOVEL METHOD FOR RAPID IN VITRO RADIOBIOASSAY

Rapid and accurate analysis of internal human exposure to radionuclides is essential to the effective triage and treatment of citizens who have possibly been exposed to radioactive materials in the environment. The two most likely scenarios in which a large number of citizens would be exposed are the detonation of a radiation dispersal device (RDD, "dirty bomb") or the accidental release of an isotope from an industrial source such as a radioisotopic thermal generator (RTG). In the event of the release and dispersion of radioactive materials into the environment in a large city, the entire population of the city – including all commuting workers and tourists – would have to be rapidly tested, both to satisfy the psychological needs of the citizens who were exposed to the mental trauma of a possible radiation dose, and to satisfy the immediate medical needs of those who received the highest doses and greatest levels of internal contamination – those who would best benefit from rapid, intensive medical care.

In this research a prototype rapid screening method to screen urine samples for the presence of up to five isotopes, both individually and in a mixture, has been developed. The isotopes used to develop this method are Co-60, Sr-90, Cs-137, Pu-238, and Am-241. This method avoids time-intensive chemical separations via the preparation and counting of a single sample on multiple detectors, and analyzing the spectra for isotope-specific markers. A rapid liquid-liquid separation using an organic extractive scintillator can be used to help quantify the activity of the alpha-emitting isotopes. The method provides quantifiable results in less than five minutes for the activity of beta/gamma-emitting isotopes when present in the sample at the

intervention level as defined by the Centers for Disease Control and Prevention (CDC), and quantifiable results for the activity levels of alpha-emitting isotopes present at their respective intervention levels in approximately 30 minutes of sample preparation and counting time.

Radiation detector spectra – e.g. those from high-purity germanium (HPGe) gamma detectors and liquid scintillation detectors – which contain decay signals from multiple isotopes often have overlapping signals: the counts from one isotope's decay can appear in energy channels associated with another isotope's decay, complicating the calculation of each isotope's activity. The uncertainties associated with analyzing these spectra have been traced in order to determine the effects of one isotope's count rate on the sensitivity and uncertainty associated with each other isotope.

The method that was developed takes advantage of activated carbon filtration to eliminate quenching effects and to make the liquid scintillation spectra from different urine samples comparable. The method uses pulse-shape analysis to reduce the interference from beta emitters in the liquid scintillation spectrum and improve the minimum detectable activity (MDA) and minimum quantifiable activity (MQA) for alpha emitters. The method uses an HPGe detector to quantify the activity of gamma emitters, and subtract their isotopes' contributions to the liquid scintillation spectra via a calibration factor, such that the pure beta and pure alpha emitters can be identified and quantified from the resulting liquid scintillation spectra. Finally, the method optionally uses extractive scintillators to rapidly separate the alpha emitters from the beta emitters when the activity from the beta emitters is too great to detect or quantify the activity from the alpha emitters without such a separation. The method is able to detect and quantify all five isotopes, with uncertainties and biases usually in the 10-40% range, depending upon the isotopic mixtures and the activity ratios between each of the isotopes.

ACKNOLWEDGEMENTS

I would be remiss if the first person I acknowledged were to be anyone other than Dr. Jerome LaRosa, my committee member, mentor, adviser, colleague, and friend. Without Jerry's patience, guidance, kindness, and generosity, neither I – nor possibly anyone else in the Radioactivity Group at NIST – ever would have gotten much done. The only thing Jerry may enjoy more than doing radiochemistry in the lab is teaching it to others, and I am sincerely grateful to him for all of his help.

Of course, I am also deeply grateful to my parents and family for their love and for their support of my academic and personal endeavors.

I also extend a sincere thanks to Dr. Zimbrick and the rest of my committee, including Drs. Steinhauser, Ramsdell, and Hulpke, as well as the former members of my committee, Drs. Johnson, Ibrahim, and Borak, for their support and patience over the past nine years. And of course, many thanks to Julie Asmus and Jeanne Brockway for helping me navigate the bureaucratic waters at CSU, often from 1500 miles away.

I would also like to recognize the memory of Dr. D. Allan Bromley, my former professor and advisor when I was an undergraduate at Yale University, who first encouraged me to pursue my interests in this field.

I certainly can't forget to mention and thank the National Institute of Standards and Technology, my former employer – and, in many ways, my home – for six years, for supporting me and funding the work presented in this thesis. I would like to extend particular thanks to Dr. Kenneth G.W. Inn for his kind and thoughtful guidance.

I am also grateful for my good friends Ken Walter and Gretchen Gunn, who were my partners in crime at CSU from 2006-2008 (particularly in stats class).

I will be forever indebted to Dr. Cailin Wilke for encouraging me to actually finish this thesis – and for reminding me to always be chasing the sun.

Finally, I would like to thank the band Jimmy Eat World, whose songs *Let It Happen*, *Work*, *Damage*, *Big Casino*, and *Cautioners* carried me through the final slog of completing this thesis.

"It's wanting to know that makes us matter."
Hannah Jarvis, Tom Stoppard's *Arcadia*

"Some questions remain long after their owners have died.
Lingering like ghosts. Looking for the answers they never found in life."
Margrethe Bohr, Michael Frayn's *Copenhagen*

"How the world must have been changing while I was holding it still."
Alexander Bakunin, Tom Stoppard's *The Coast of Utopia: Voyage*

DEDICATION

This dissertation is dedicated to the ABDs: you are not forgotten.

TABLE OF CONTENTS

LIST OF TABLES

LIST OF FIGURES

CHAPTER 1. INTRODUCTION

1.1 Bioassay screening during radiological emergencies

Human exposure to radiation can be either external – i.e. from exposure to a source of radioactive material outside the body – or internal; i.e. from exposure to radioactive decay via the ingestion of radioactive isotopes. The dose from external exposure is relatively trivial to assess as long as the source attributes (such as the isotope and the amount of activity present), distance of exposure, and length of exposure are all known. However, the dose from internal exposure can be significantly more difficult to measure, as in most situations, the amount of intake of radioactive material is not known, and must be determined through secondary measurements.

Screening urine for the presence of radionuclides has been shown to be a suitable means to assess both radiation worker internal dose due to possible intake and public internal dose in the event of a radiological emergency.[1,2] Multiple determination methods have been explored, some specifically for urine/biological samples, others for generic matrices. Each method requires a varying degree of chemistry knowledge and labor.[1-13] As a general rule, the higher the number of different radionuclides that are present in a sample, the more chemical separation steps (and thus more time and labor) are required to process the sample for proper counting and determination. Thus, if a method could be developed which reduces the number of necessary chemistry steps, or reduces the amount of time each step takes, or both, this method would be better suited to use in emergency response conditions. However, the response time of current methods is limited by resin column chemistry (currently the fastest method available).[9,10,13] These methods are currently capable of returning full radiochemical determinations in just over 5

hr per sample.[10] In a large-scale emergency scenario, this timescale is clearly unworkable. Maxwell & Culligan have succeeded in increasing throughput at the chemical through use of their vacuum box & stacked resin cartridge system (currently, 10 samples at a time plus a control)[10]; however, the chemistry is only half of the picture: their method requires multiple (at least 3) 1-hour alpha counts per sample. Thus, the number of available alpha detectors must be triple the number of samples in order to maintain high throughput – an eventuality which is extremely unlikely. In reality, even with 48 alpha detectors available (roughly the number available to the Radioactivity Group at the National Institute of Standards and Technology in Gaithersburg, MD), throughput is limited to just 16 samples per hour. This throughput also assumes available labor (in the form of trained radiochemist technicians) is sufficient to keep up with chemical processing of samples. At 16 samples per hour, assuming round-the-clock shifts, 384 samples can be analyzed per day and it would take just over 3.5 years to process the samples from half a million citizens (roughly the population of the Washington, DC area, or one of its suburban counties). Obviously, this is not nearly soon enough for proper triage (separating out the truly contaminated from the "walking well") and treatment (chelation therapy, bone marrow transplants, etc) of the contaminated individuals – typically, treatment should be given as soon as possible, preferably within a matter of hours.

1.2 High-priority isotopes

The International Atomic Energy Agency (IAEA) provides a list[14] of the most relevant isotopic sources with common industrial uses. It divides these sources into three categories,[14] with category 1 sources being of the highest activity, causing imminent death within minutes, down to category 3 sources with less activity but still sufficient to cause permanent injury and possible fatality within a few hours of exposure. There are 25 isotopes on this list. However, 10

of these isotopes are "very unlikely to be used in individual radioactive sources with activity levels [sufficient] to place them within Categories 1, 2 or 3",[14] leaving 15 isotopes, as shown in Table 1.1.

1.3 Research Objectives

This research aims to overcome the deficiencies described in 1.1 above by development of a rapid screening method. Five of these isotopes have been selected for analysis in this study: Co-60, Sr-90, Cs-137, Pu-238, and Am-241. These isotopes have been selected to give a wide variation of decay types (including alpha, beta, and gamma). Additionally, the overlapping alpha energies of Am-241 and Pu-238 – and the similar maximum beta energies of Cs-137 and Sr-90 – allowed for a thorough study of the effects of the presence of each of these isotopes on the measurement uncertainties of each other.

The objective of this work was to determine the feasibility of quantitatively measuring the activity from multiple isotopes present in the same sample without performing chemical separations. There is, at present, a dearth of information regarding the effects of these types of interferences on measurement uncertainties in the scientific body of knowledge in this field. It is this gap that this dissertation intends to begin to fill.

Table 1.1 IAEA list of isotopes of concern

Alpha-emitters

Element	Isotope	t1/2 (a)	Highest-abundance alpha energy (keV)	Highest-abundance γ energy (keV)	γ abundance
Am	241	4.32E+02	5486	59.5	36%
Cf	252	2.65E+00	6118	n/a	0%
Cm	244	1.81E+01	5805	n/a	0%
Pu	238	8.77E+01	5499	n/a	0%
Pu	239	2.41E+04	5157	n/a	0%
Ra	226	1.60E+03	4784	186	4%

Beta emitters

Element	Isotope	t1/2 (a)	Highest-abundance beta max energy (keV)	Highest-abundance γ energy (keV)	γ abundance
Co	60	5.27E+00	318	1333	100%
Cs	137	3.01E+01	514	662	85%
Ir	192	2.02E-01	675	317	83%
Pm	147	2.62E+00	224	n/a	0%
Sr	90	2.88E+01	546	n/a	0%
Tm	170	3.52E-01	968	84.3	3%

Electron capture isotopes

Element	Isotope	t1/2 (a)	Highest-abundance γ energy (keV)	γ abundance
Gd	153	6.58E-01	97	29%
Se	75	3.28E-01	265	59%
Yb	169	8.77E-02	63	44%

CHAPTER 2. PRELIMINARY STUDIES AND RESULTS

2.1 Single-isotope urine screening via Liquid Scintillation Counting

Since May 2005, work has been done by members of the Radioactivity Group at the National Institute for Standards and Technology (NIST) in Gaithersburg, Maryland to develop a quantitative, rapid screening method to determine Sr-90 contamination in human urine.[a,b] The method that was developed uses activated carbon (AC) filtration to remove color (and other organic contaminants)[2] and liquid scintillation counting (LSC)[2] to detect the β^- particles. The method has produced remarkable results for Sr-90/Y-90, Sr-89, Sr-89 mixed with Sr-90/Y-90, and Ni-63. Quantification limits of ~0.1 Bq/ml for Sr-90/Y-90 have been achieved (using the Currie method).[15] Under realistic conditions, the method takes less than five minutes from receipt of a raw urine sample to the end of counting. Thus, the method is portable, accurate, and rapid. However, the method's robustness is limited to the following conditions: that the radioisotope contaminants present in the urine sample are known to be only Sr-90/Y-90, Sr-89, and/or Ni-63; and that none of the radioisotopes is organically bound (as they would then be adsorbed to the AC and thus not detected).[a] These assumptions are appropriate for conditions such as the detonation of an RDD contaminated with one of these isotopes, the poisoning of a water supply with one of these isotopes, the accidental ingestion of a source of one of these isotopes, etc.

Previous work has been done by Crawford et al. to support these findings.[a,c] Figure 2.1 shows the liquid scintillation counting efficiency of Nickel-63 in three different media:

---

[a] E. B. Crawford, J. La Rosa, S. Lederer, K. G. W. Inn, unpublished results

[b] Partially funded by the National Science Foundation (NSF) through the auspices of the NIST Summer Undergraduate Research Fellowship (SURF) program

[c] Crawford et al. unpublished results, presented at RRMC 2005, 2006, 2007, 2010, 2012, HPS 2007

Uncolored Synthetic Urine (SU), Synthetic Urine colored with Tea (ST), and Real Urine (RU). The blue bars show the Ni-63 counting efficiency in spiked samples of these three media which have not been treated with AC, while the purple bars show the counting efficiency in samples which have been treated with AC. As can be seen in Figure 2.1, counting efficiency falls from ~59% in untreated, uncolored synthetic urine to ~30% in untreated real urine. However, when the samples are treated with AC, efficiency for both ST and RU is ~58%, well within the ~1% standard deviation uncertainty (not shown on graph) of the 59% efficiency of untreated SU. The AC treatment, by removing colorants and other organics,[2] effectively removes the relevant quenching factors from the liquid scintillation counting systems while it appears to have no affinity for the radionuclide.

Figure 2.2 shows the relationship between Ni-63 efficiency and the molarity and type of acid used to acidify the urine sample upon receipt.[d] Nitric acid stabilizes the sample better at lower molarities; however at higher molarities the efficiency decreases (likely due to the oxidation of the organic compounds in the LS cocktail). Thus, 1M HCl is preferable assuming all radionuclides of interest are easily soluble in hydrochloric acid.

Liquid scintillation was selected as the counting method of choice for a number of reasons. First, it is a counting method with well-known efficiency (nearly 100%)[23] for all isotopes of concern in 4π geometry. Second, it yields spectra depicting the energy of the detected decay particles, which provide data that can be analyzed in more detail than a simple raw count. Third, since urine is already a liquid, minimal source preparation steps are required other than the aforementioned AC treatment which is performed using a syringe filtration system for both ease and speed.

[d] Crawford et al. unpublished results, presented at RRMC 2005, 2006, 2007, 2010, 2012, HPS 2007

Figure 2.3[e] depicts an LSC spectrum from a sample with unknown levels of activity from three radionuclides of differing maximum beta energies (depicted by dashed lines on graph): Sr-90, Sr-89, and Y-90.[e] Through spectral deconvolution techniques,[17] the spectrum can be analyzed accordingly as long as the radioisotopes present and their maximum beta energies are known.

Table 2.1 demonstrates the results of the deconvolution of this particular spectrum.[e] It is noted that the error associated with the Sr-89 calculation is somewhat high. However, the Sr-89 activity present is only roughly three times over background, which could explain the relatively high measurement bias.

In order to test the accuracy and precision of the method, a single operator test was performed. This test examined the method's speed, accuracy and precision given the following conditions: 1) that the only radionuclide present was Sr-90 (with possibly some Y-90 present; equilibrium not assumed), 2) a one-minute count time, 3) one available chemist/technician to perform all necessary steps. Each sample took an average of 3 minutes and 45 seconds from receipt of sample to return of results. The results of the single operator test are depicted in Table 2.2 and Figure 2.4.

The uncertainty bars in Figure 2.4 represent one standard deviation from the mean. In the event of a large-scale radiological emergency involving the possible release of and exposure to Sr-90, the expected intervention levels would be within an order of magnitude of **10 kBq/ml**.[18] Thus, extremely conservatively, the method should be precise and accurate at **100 Bq/ml**, roughly the activity present in sample 4. Given that the bias at this level – indeed, every activity level tested other than the absolute lowest (the quantification limit) – is less than the 1σ

[e] Crawford et al. unpublished results, presented at RRMC 2005, 2006, 2007, 2010, 2012, HPS 2007

uncertainty, which is less than 1%, the method's accuracy and precision need not be questioned further.

This method could, in theory, be deployed immediately if necessary in the event of a radiological incident that met the conditions stated above. Given one chemist and one LS counter, at 3.75 minutes per sample, the method is already capable of producing results at the same 384-sample-per-day maximum rate achievable by Maxwell and Culligan.[5,6,9,10] However, given access to multiple chemists (NIST has at least 10+ qualified and available) (or alternatively, automation of the AC procedure) and multiple LS counters, this rate rapidly multiplies – indeed, the logjam becomes not sample preparation, but count time. Given count times of 1 minute per sample, and throughput from 10 LS counters each in 10 different laboratories (or any other easily conceivable combination of 100 LS counters, the samples from a population of 500,000 could be analyzed in under 3.5 days – a vast improvement over the 3.5+ years it would take given Maxwell and Culligan's method.

2.2 Activated carbon filtration

Filtration with activated carbon powder is known to remove (via adsorption) organic materials from aqueous solutions.[19] Activated carbon (AC) powder also has some affinity for the adsorption of inorganic materials, as well. [19,20] However, AC powder has been shown to have little to no affinity for strontium and cesium. [20] This combination of properties makes AC powder an excellent material to use to filter urine samples prior to measuring these samples using liquid scintillation counting.

The work performed in this project demonstrated that AC powder filtration removes all measurable quenching effects from urine samples in liquid scintillation counting, making them indistinguishable (with respect to the quench indicating parameters on the Quantulus liquid

scintillation counter, as well as the isotopic counting efficiencies) from samples consisting of only spiked acidified water. Additionally, the work performed herein demonstrated that AC powder shows no affinity for any of the five isotopes studied (nor for Sr-90's daughter Y-90).

2.3 Gamma-decay measurements

Three of the five isotopes studied in this project have significant (i.e. >25%) gamma ray emissions: Co-60 at approximately 1173 and 1332 keV (100% abundance for each), Cs-137 at approximately 662 keV (85% abundance), and Am-241 at approximately 60 keV (30% abundance). Therefore, when these isotopes are individually present in a sample, their measurement and quantification is trivial in known, calibrated geometries. Limits of detection and quantification, as well as the overall uncertainty on the measurements, are all simple statistical calculations.[15]

However, when more than one gamma-emitting isotope is present in a sample, the Compton spectrum from the isotope with a higher-energy gamma emission can interfere with the measurement of the photopeak of the lower-energy gamma emission. In these cases, the uncertainties associated with the measurement of the lower-energy photopeak are related to the amount of activity present from the isotope with the higher-energy gamma emission, as well as the relative magnitude of the Compton spectrum in the vicinity of the lower-energy photopeak. The effect of Co-60 activity on the measurement of Cs-137 and Am-241, as well as the effect of Cs-137 activity on the measurement of Am-241, was carefully studied to quantify these effects, as described in Chapter 3. Additionally, the Bremsstrahlung spectrum from the Sr-90/Y-90 system can interfere with the measurement of Am-241; this effect, too, was carefully quantified, as described in Chapter 3.

High-purity germanium (HPGe) gamma detectors were used for all gamma measurements in this project.

2.4 Liquid scintillation measurements

Liquid scintillation counting (LSC) is capable of detecting both alpha and beta radioactive decay emissions. With 4π geometry, the efficiency of alpha counting using LSC is essentially 100%. The efficiency of beta counting depends on a number of factors, including the maximum beta decay energy of an isotope. However, the efficiency for beta counting is reproducible from one sample to the next, assuming each sample's quench is similar.

Alpha events produce Gaussian peaks in liquid scintillation spectra, because they are mono-energetic. These peaks can be fitted using a least-squares approach, which provides an accurate mathematical description of the spectral shape.

While each of the beta-emitting isotopes studied in this project has a single primary maximum beta emission energy, the spectra produced by beta emissions are *not* Gaussian: as beta emissions are accompanied by neutrinos, with the total maximum energy split between the two particles, the energy carried by the beta particle varies widely. The resulting beta curve runs from zero keV to the maximum beta energy, and these curves do not follow simple mathematical formulas, so cannot be easily fitted.

A Quantulus 1220 ("Quantulus") low-level liquid scintillation counter was used for all LSC measurements in this project. The Quantulus detector has a very low background count rate, which is achieved by the use of a significant amount of lead shielding around the detector cavity, as well as a guard detector surrounding the main photomultiplier tubes (PMTs). The anticoincidence circuitry linked to the guard detector greatly reduces the cosmic background seen by the main liquid scintillation detector within the Quantulus. This instrument is one of a

number of LS counters with the ability to perform pulse-shape analysis on the light pulses produced from individual decay events.[21] Beta events excite primarily singlet states in the solvent in the cocktail, while alpha events tend to excite a higher fraction of triplet states in the solvent. Triplet states take longer to transfer their energy to the fluor; accordingly, the light pulse from alpha events and their resulting triplet states has a longer decay time than the light pulse from beta events. By measuring the decay time of these light pulses, it is possible to discriminate between alpha and beta decay events within a sample being measured by the Quantulus. Separating the beta and alpha pulses using pulse-shape analysis allows for very weak alpha signals – which would usually be indistinguishable from the beta spectra when the beta/alpha activity ratio is high – to be quantitatively analyzed.[23]

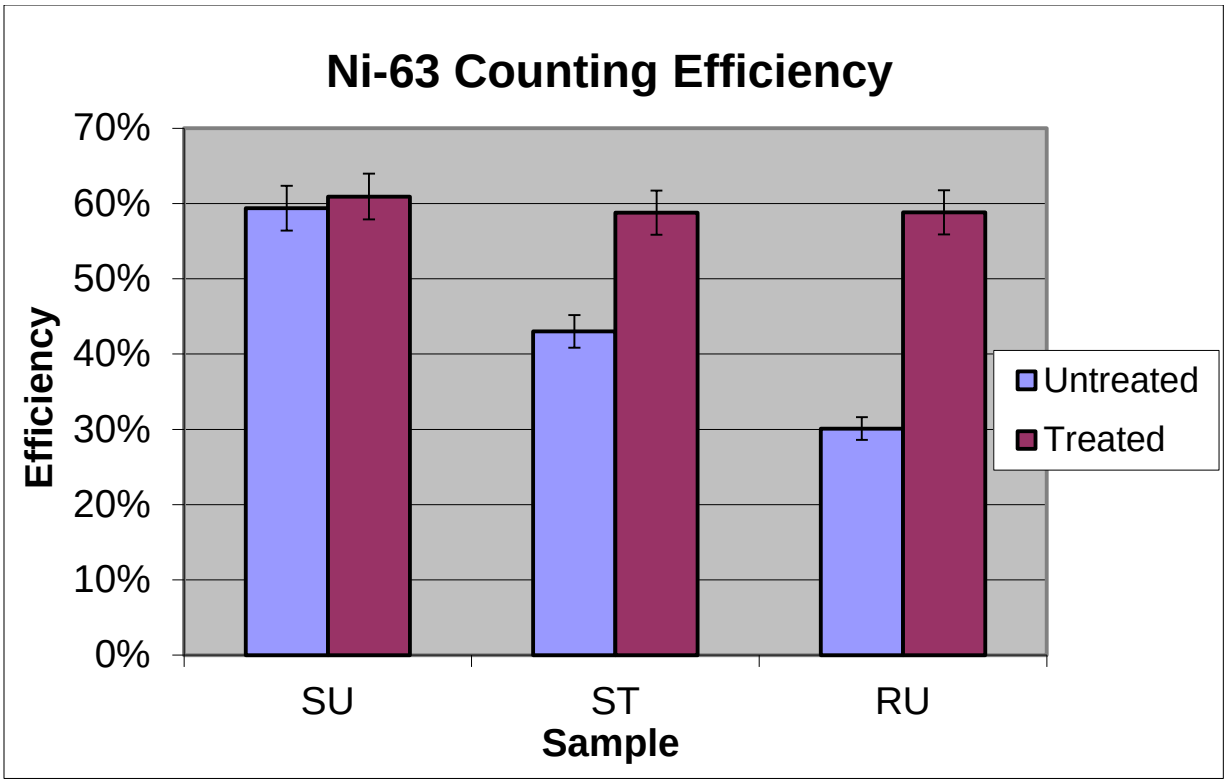

Figure 2.1: Effect of AC filtration on counting efficiency – Synthetic Urine (SU), Synthetic Urine stained with Tea (ST), Real Urine (RU)

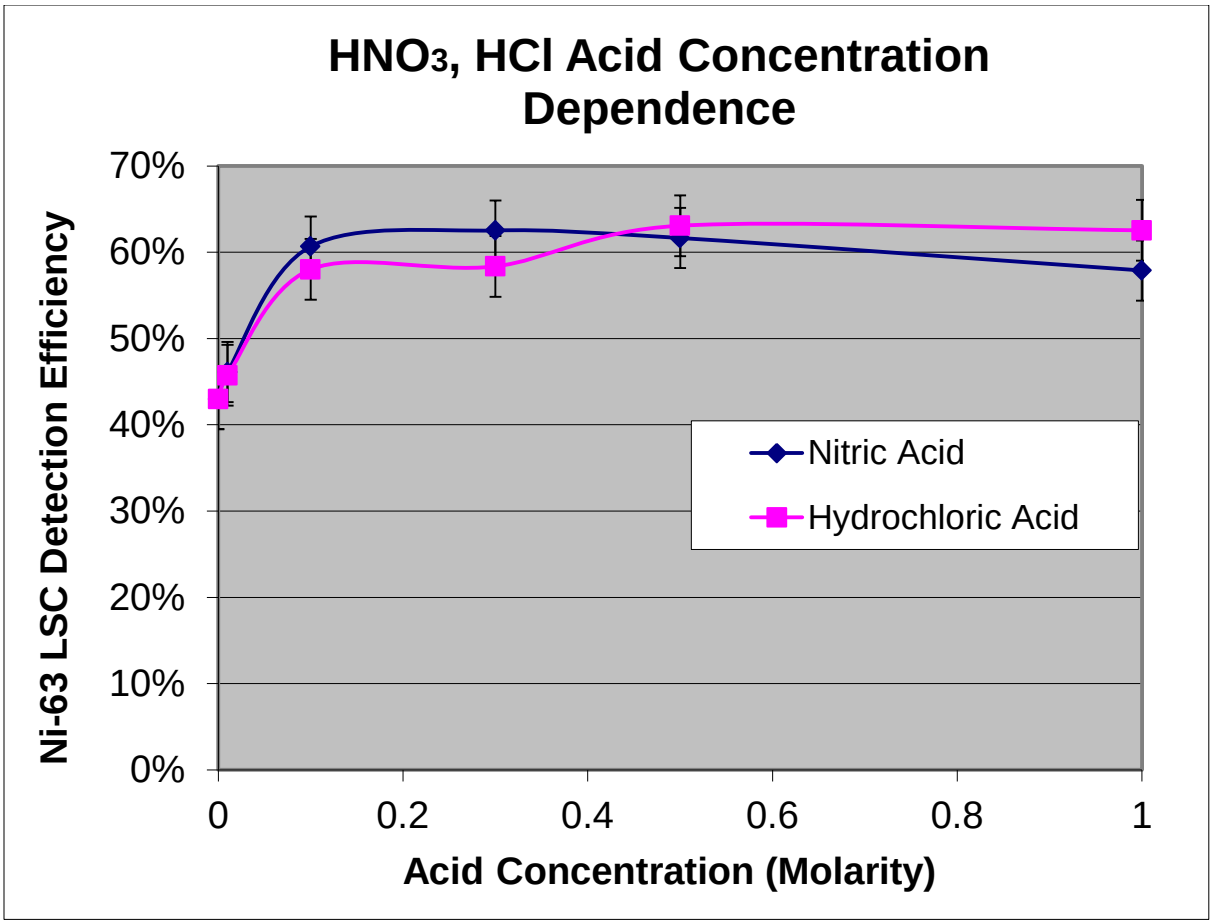

Figure 2.2 Efficiency Dependence upon Acid Concentration

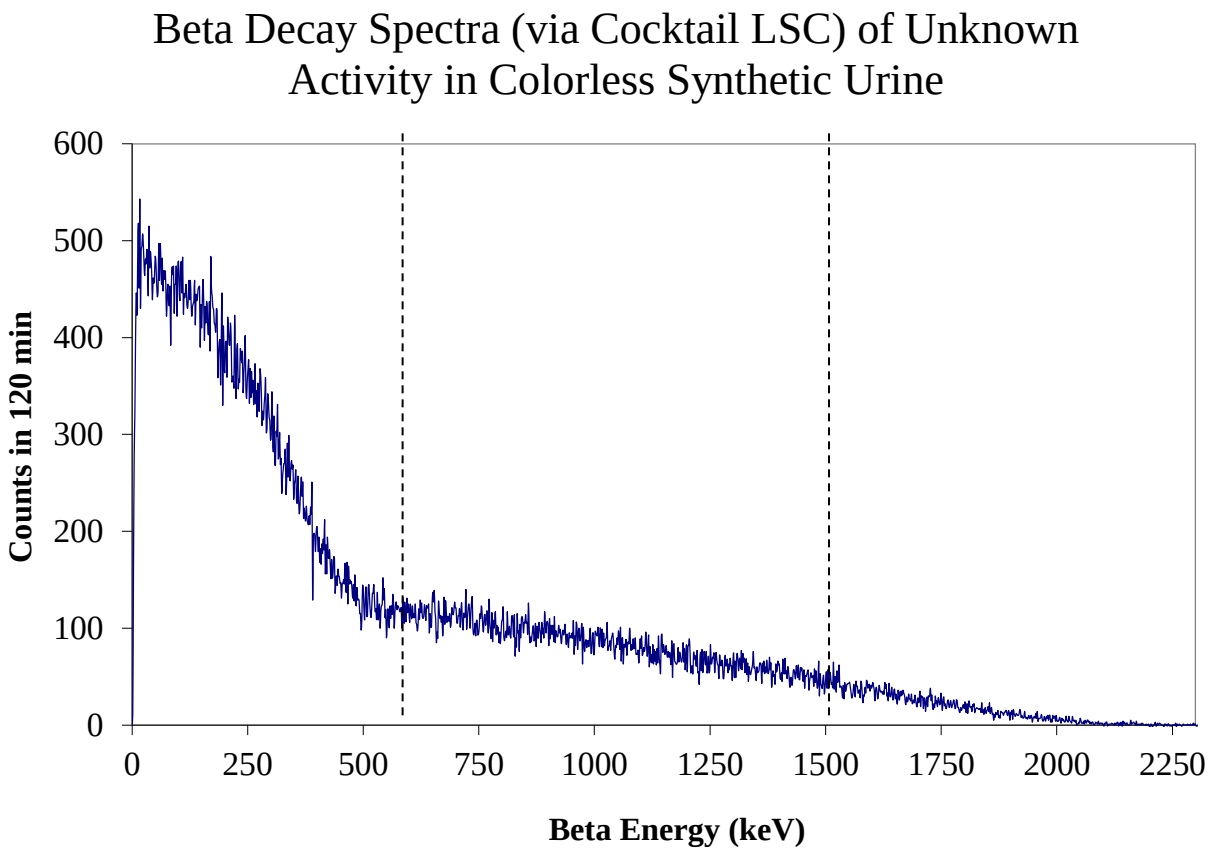

Figure 2.3 Beta spectrum energy windows

Table 2.1 Results of Figure 2.3 Spectral Deconvolution

	Calculated:	**Expected:**	**Bias:**
Sr-89:	1.26	1.69	-25.44%
Sr-90:	19.56	19.04	2.73%
Y-90:	21.07	21.45	-1.77%

Table 2.2 Single Operator Test for Sr-90

Test Level	Expected Sr-90 (Bq/ml)	Measured Sr-90 (Bq/ml)	1σ	1σ %	Bias %
Blank	**0.00**	**0.00**	**n/a**	**n/a**	**n/a**
1	**0.14**	**0.12**	**0.02**	**13.92%**	**-18.01%**
2	**2.11**	**2.12**	**0.05**	**2.22%**	**0.72%**
3	**13.84**	**13.75**	**0.15**	**1.11%**	**-0.63%**
4	**97.43**	**98.08**	**0.82**	**0.83%**	**0.67%**
5	**703.8**	**706.1**	**5.6**	**0.79%**	**0.32%**
6	**6328**	**6293**	**49**	**0.78%**	**-0.55%**

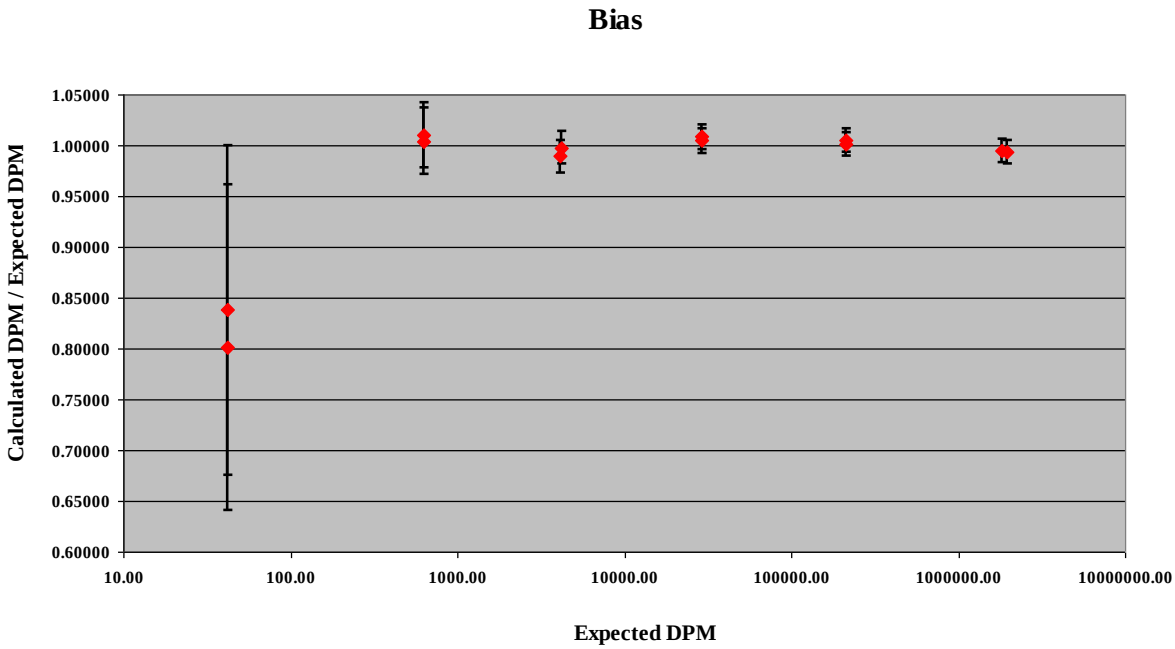

Figure 2.4 Single Operator Test for Sr-90

CHAPTER 3. DEVELOPMENT OF RAPID SCREENING METHOD

3.1 Introduction

The target activities for each isotope studied in this method were determined from an unpublished Centers for Disease Control and Prevention (CDC) chart[18] (Table 6.1 in the Appendix) which uses dose coefficients and excretion coefficients from the ICRP in order to calculate the amount of activity of each isotope of concern that would be present in an exposed person's 24-hour urine sample post-single-event-exposure. Excretion coefficients are given for F, M, and S-class solubility for each isotope. The solubility classes refer to Fast (F), Medium (M), and Slow (S) solubility for the varying chemical forms of each isotope.[22] This study assumed F-class solubility for all isotopes, as it is likely that four out of the five isotopes studied (Co-60, Sr-90, Cs-137, Am-241) would be present in F-class solubility in the environment given their valences. Pu-238 has a much more complicated chemistry and variable oxidation states, and can behave very unpredictably in the human body regardless of its solubility/oxidation state.[23,24] Regardless, it is possible that any of the isotopes could be present in the environment after a dispersal incident in some combination of solubility classes, which would greatly complicate the dose reconstruction.[25] The primary goal of this work was to develop a screening method and determine its minimum detectable activity (MDA) and minimum quantifiable activity (MQA) for each isotope of concern. Once the MDA and MQA were calculated, the method's suitability for each specific isotopic solubility could be assessed.

3.1.1 Review of Previously-Developed Methods

The methods used in this work build on and extrapolate from methods developed by others in the field over the past few decades. The use of the Quantulus 1220 and other liquid

scintillation counters for gross alpha/beta measurements is well-established – including the use of its pulse-shape discrimination capabilities to determine separate gross alpha and gross beta activities,[7,26,27,28,29,30,31] its calibration and use for the quantification of the activity of individual isotopes,[32,33,34,35,36] as well as its calibration and use for the quantification of the activity of multiple alpha emitters counted simultaneously.[37,38,39,40]

Recent developments in spectral deconvolution and unfolding[41,42,43,44] have made possible the fitting of peaks from individual isotopes given sufficient counting statistics and isotopic activity ratios relatively close to 1. Very recently, the use of the Quantulus 1220 for gross alpha and beta activity analysis in urine samples (using Sr-90 and Am-241) has been explored.[45] The experiments performed for this dissertation build in particular on this work.

Optimization of the Quantulus 1220's pulse-shape analyzer (PSA) setting has been calculated by maximizing the ratio of alpha efficiency to beta cross-talk in the Quantulus 1220's alpha spectrum.[28,38,39,45] However, the optimizations performed in these papers assume relatively similar alpha and beta activities, and do not take into account the vast differences in the orders of magnitude (as many as 5-6 orders of magnitude) between the activity of beta emitters and alpha emitters at their respective intervention levels, which necessitates more heavily weighting the rejection of beta pulses when calculating the optimal PSA setting. The work performed in this dissertation determines the optimal PSA settings for specific mixtures of alpha and beta emitters given these constraints.

The use of extractive scintillators with the Quantulus 1220 detector has also been shown to be effective for improving alpha efficiency and reducing beta cross-talk.[16,34]

The use of HPGe gamma detectors to quantify the activity of gamma-emitting isotopes has been well-established.[46]

The calibration and reproducibility of a liquid scintillation detector's per-isotope efficiency has previously been published.[47] The calibration of radioactivity measurements between a gamma detector and the Quantulus 1220 for a single isotope has also been explored.[48] At least one other study[49] suggests the use of multiple detectors to determine the activity from multiple isotopes present in a urine sample. The author of this dissertation (and his collaborators) had previously explored multi-detector calibration with other isotopes.[50] The work performed in this dissertation determines the calibration of radioactivity measurements between a gamma detector and the Quantulus 1220 for multiple isotopes, and traces the resulting uncertainty.

Many organic components – as well as the presence of oxygen in a sample – have been shown to affect not only the general quench of a sample in a liquid scintillation counter such as the Quantulus 1220, but also to reduce the efficacy of pulse-shape discrimination.[16,51] Therefore, the minimization / complete removal of quenching components from all samples was a priority in the work performed for this dissertation. However, an oxygen-purging step was not used due to the additional time required, as well as the complicated laboratory set-up required.

Filtration of urine samples with activated carbon powder has been demonstrated to remove organic components as well as coloration of the urine, and to reduce or eliminate the quenching effects of these components in LS counting.[2,33,52] Maintaining consistent sample volumes also reduces quench.[53] The measurements performed for this dissertation relied upon the use of activated carbon to remove chemical and color quenching effects in the urine samples.

3.1.2 Sample Preparation

All samples were prepared using urine collected from volunteers in the Radioactivity Group of the Physical Measurements Laboratory at the National Institute of Standards and Technology in Gaithersburg, MD. Urine from both male and female volunteers was collected.

The urine collected was often (though not always) pooled, so that many of the individual samples were prepared from urine from multiple volunteers. After collection, all urine specimens were acidified to 1M HCl using analytical-grade reagents.

Liquid scintillation (LS) vials were labeled and weighed prior to the addition of acidified urine. 5 ml of acidified urine was then added volumetrically to each LS vial. The vials were again weighed in order to gravimetrically confirm the amount of urine added.

The LS vials containing acidified urine were then spiked with 0.1-0.25 g of acidified solution containing the radioactive isotope of interest. The sources used for spiking were NIST Standard Reference Materials (SRMs),[54] or gravimetric dilutions thereof. The spiking was performed using a pycnometer, which was weighed before and after the addition of the radioactive solution to each LS vial. A pycnometer is a plastic pipette which has been heated over a flame and had its neck stretched out to make it quite long and narrow in order to both reduce evaporation of the solution inside and allow for very small drops (on the order of 0.015 g) to be dispensed. The gravimetric spiking of the samples provided for high accuracy and precision of the amount of each isotope that was added to each LS vial.

Norit SX Ultra (Sigma-Aldrich, St. Louis, MO) powdered activated carbon (AC) was weighed out in 0.1-gram aliquots. After the LS vials containing acidified urine were spiked with the relevant isotopes, a 0.1-gram aliquot of powdered AC was added to each vial. Each vial was then vigorously shaken for approximately 10 seconds, resulting in an opaque suspension of the powdered AC in the aqueous solution.

The contents of each vial was then transferred via pipette to a 10-ml plastic syringe with a 0.45-μm Millipore two-stage (glass fiber / polyethylene) syringe filter attached to it. The solution

was pushed through the syringe & filter into another (labeled) LS vial, which was weighed both before and after, in order to gravimetrically determine the recovery of the aqueous fraction.

Approximately 5.5 ml of Insta-Gel Plus liquid scintillator cocktail (manufactured by PerkinElmer, Waltham, MA) was then added to each LS vial. Each vial was once again weighed, both to gravimetrically determine the amount of Insta-Gel Plus added to each vial and to calculate the aqueous fraction of each vial. The aqueous fractions were kept just under 50% in order to ensure that they remained within the published acceptable limits for Insta-Gel Plus.

All uncertainties related to spiking samples were traced through each step. Gravimetric spiking measurements generally had an associated uncertainty of 0.00005 g per measurement, while measurements of more massive items (such as LS vials, AC, and bulk liquids including acidified urine and liquid scintillation cocktail) generally had an associated uncertainty of 0.01 g per measurement. When differences between masses are calculated, all gravimetric uncertainties can be combined using the square root of the sum of the squares of the uncertainty of each measurement:

$$\Delta(x+y) = \sqrt{\delta x^2 + \delta y^2} \tag{3.1}$$

The activity of each isotope used for spiking was corrected for its decay since certification date:

$$A(t) = A_0 e^{-\lambda(t-t_0)} \tag{3.2}$$

The uncertainty for the decay calculation was calculated as follows (any uncertainty associated with the certification time t_0 was incorporated into the uncertainty on the activity A_0):

$$\Delta A(t) = \sqrt{(\delta A_0 e^{-\lambda(t-t_0)})^2 + (-\delta\lambda A_0 (t-t_0) e^{-\lambda(t-t_0)})^2 + (-\delta t \lambda A_0 e^{-\lambda(t-t_0)})^2} \tag{3.3}$$

All other uncertainties were calculated using the first-order partial derivative for each variable in the relevant equations. These equations will be included herein as necessary.

3.2 High-purity germanium (HPGe) detector counting

After preparation, each sample was counted on at least an HPGe detector. (Information on the HPGe detector used is shown in Figure A4.1 in the Appendix.) The detectors were energy-calibrated using isotopes with well-known energies, including Am-241, Cs-137, Co-60, and K-40. Each LS vial was placed directly on the detector endcap to maximize the solid angle between the sample and the detector and therefore maximize the detector efficiency. Reproducible geometry was assured by using identical LS vials, equal volumes for each sample, and identical sample placement on top of the detector. Samples were counted for varying times to ensure reproducible statistics.

3.3 Quantitative analysis of HPGe spectra – single isotopes

The activity from gamma-emitting isotopes can be readily quantified using the signal count rate from their mono-energetic gamma emissions with known abundances. Each individual spectrum was analyzed in Microsoft Excel. The gamma emissions corresponding to each mono-energetic gamma line produce a Gaussian peak around that peak energy in the HPGe spectra.[17] The Gaussian peaks were fitted after first removing any interfering background and/or Compton spectra.[17] All fits were performed by taking the natural log of the count rate and applying either a linear least-squares fit (for background / Compton counts) or a quadratic least-squares fit (for each Gaussian peak).

The quadratic fits take the generic form:

$$g(x) = Ax^2 + Bx + C \tag{3.4}$$

After the fits were calculated using the natural log of the count rate, the fits could be mapped to the actual count rate by raising *e* to the exponent consisting of the quadratic fit:

$$f(x) = e^{g(x)},$$

(3.5)

or

$$f(x) = e^{Ax^2+Bx+C}$$

(3.6)

A Gaussian function can be described by only two components: its mean value, or **μ**, and its standard deviation, or **σ**, which can be used to define the function's full width at half maximum (FWHM):[55]

$$FWHM = 2\sqrt{2\ln 2}\,\sigma$$

(3.7)

The equation for a Gaussian function can also be written as

$$f(x) = a * e^{\frac{-(x-b)^2}{2c^2}}$$

(3.8)

where

$$a = \frac{1}{\sigma\sqrt{2\pi}}$$

(3.9)

for a distribution with an integral summing to 1, or

$$a = f(\mu)$$

(3.10)

i.e. the maximum value in the peak channel;

$$b = \mu \tag{3.11}$$

and

$$c = \sigma \tag{3.12}$$

If the two equations for Gaussian functions established herein are set equal to each other, the relationships between the associated constants therein can be solved, as follows:

$$A = \frac{-1}{2\sigma^2} \tag{3.13}$$

$$B = \frac{\mu}{\sigma^2} \tag{3.14}$$

$$C = \frac{-\mu^2 - 2\sigma^2 \ln\left(\frac{1}{\sigma\sqrt{2\pi}}\right)}{2\sigma^2} \tag{3.15}$$

These relationships mean that the quadratic fit for a Gaussian function can be approximated by simply determining the peak channel – or the mean value μ - and the FWHM of the distribution; accordingly, it is also trivial to solve for the mean value μ and the standard deviation σ of a distribution if it has been fitted using a least-squares quadratic fit.

Co-60 was quantified using its 1332.5-keV gamma emission, Cs-137 was quantified using its 661.7-keV gamma emission, and Am-241 was quantified using its 59.5-keV gamma emission. The 1172-keV photopeak for Co-60 was not used for any calculations, as it has some interference from the low-energy tail of the 1332.5-keV photopeak.

A 1.3-Ms background count was used to background-correct each sample count. Backgrounds under each peak were accounted for by applying a linear least-squares fit to the natural log of the count rate in the vicinity of the peak, but excluding other natural background peaks in the area. For Am-241, the channels used to calculate this background fit were those corresponding to 48.2-51.2 keV, 54.5-61.1 keV, and 64.5-71.2 keV. For Cs-137, channels used to fit the background were those corresponding to 631.1-657.8 keV and 666.5-693.1 keV. For Co-60, channels used to fit the background were those corresponding to 1251.2-1362.8 keV. The equations produced from these least-squares fits were in the form of

$$f(x) = e^{ax+b} \tag{3.16}$$

The background counts were subtracted from each spectrum in the region of each photopeak using these equations.

The location of the peak produced by each gamma in the HPGe spectrum was determined from the energy calibration of the detector. The curve produced by the additional counts in between the Compton edge and the photopeak – referred to as the "low-energy tail" – were also fitted with linear least-squares fits of the natural log of the count rates in these tails. For Am-241, the channels used to calculate the fit for the low-energy tail were those corresponding to 29.6-44.5 keV, 47.6-47.9 keV, 50.2-50.9 keV, and 53.3-54.4 keV. For Cs-137, the channels used to calculate the fit for the low-energy tail were those corresponding to 643.5-655.9 keV. For Co-60, the channels used to calculate the fit for the low-energy tail were those corresponding to 1326.3-1328.1 keV.

The equations for these fits took the same form as equation 3.16 above. The count rate for each of these tails was subtracted from the spectrum under the lower-energy side of the

photopeak; i.e. from every channel less than or equal to those corresponding to the center of the peak. After subtracting the background and the low-energy tail, the remaining count rate produced a Gaussian curve representing the photopeak.

The Gaussian curve formed by each photopeak was fitted in Microsoft Excel using a quadratic least-squares fit of the natural log of the count rate. The channels used to perform the least-squares fit corresponded to the FWHM of each photopeak. For Am-241, these channels corresponded to 58.9-59.9 keV; for Cs-137, these channels corresponded to 661.0-662.5 keV; for Co-60, these channels corresponded to 1331.7-1333.7 keV.

Once each photopeak was fitted, the sum of the count rate under the channels representing the FWHM (listed above) was divided by the activity that was known to have been added to each sample in order to determine the counting efficiency for each isotope within the FWHM of its respective photopeak:

$$efficiency_{isotope} = \frac{count\ rate\ within\ FWHM_{isotope} * cps}{total\ spiked\ activity_{isotope} * Bq} \tag{3.17}$$

$$Activity_{isotope}(Bq) = \frac{count\ rate\ within\ FWHM_{isotope}(cps)}{eficiency_{isotope}\left(\frac{cps}{Bq}\right)} \tag{3.18}$$

The units for the detector's counting efficiency are cps · Bq^{-1}.

All uncertainties involving count rates were calculated by multiplying the count rate by the count time to determine the total counts observed, taking the square root of these counts, and dividing by the count time:

$$\Delta(count\ rate) = \frac{\sqrt{count\ rate * count\ time}}{count\ time}$$

(3.19)

The uncertainty for the efficiency was calculated from the general form of the first-order partial derivative for a division equation:

$$\Delta\left(\frac{x}{y}\right) = \sqrt{\left(\frac{\partial x}{y}\right)^2 + \left(\frac{\partial y * x}{y^2}\right)^2}$$

(3.20)

This calculated efficiency – and the associated uncertainty – can be used to determine the activity for any of these individual isotopes if present in an identical geometry; i.e. a well-mixed liquid scintillation vial containing 10 ml of solution and centered on top of the detector.

Once the background count rate and the efficiency have been determined, the minimum detectable activity (MDA) and the minimum quantifiable activity (MQA) for each individual isotope on the HPGe detector can be calculated using the following formulas:[15]

$$L_D(counts) = 2.71 + 3.29\sqrt{\mu_B}$$

(3.21)

This expression gives the limit of detection L_D[15] in units of total counts during a given count time. The total background counts during this counting period are represented by μ_B.

The equation can be rearranged to calculate the MDA as follows:

$$MDA(Bq) = \frac{\frac{L_D}{t}}{eff_{isotope}}$$

(3.22)

where *t* represents the count time.

We can also define μ_B as the count rate c multiplied by the count time:

$$\mu_B = c * t \tag{3.23}$$

The equation for MDA therefore becomes:

$$MDA(Bq) = \frac{\frac{2.71 + 3.29\sqrt{c * t}}{t}}{eff_{isotope}} \tag{3.24}$$

The uncertainty for the MDA (the length of the count time is assumed to be well-known and thus have no uncertainty) is defined by:

$$\Delta MDA = \sqrt{\left(\delta c \frac{1.645}{eff_{isotope}\sqrt{c * t}}\right)^2 + \left(\delta eff_{isotope} \frac{-3.29(\sqrt{c * t} + .8237)}{{eff_{isotope}}^2 * t}\right)^2} \tag{3.25}$$

The MQA for an individual isotope on the can be calculated from the following expression:[15]

$$L_Q(counts) = 50\left(1 + \sqrt{1 + \frac{\mu_B}{25}}\right) \tag{3.26}$$

By manipulating this equation in a manner similar to the one used with the L_D equation above, we can define the MQA for a given count time as follows:

$$MQA(Bq) = \frac{\frac{50\left(1 + \sqrt{1 + \frac{c * t}{25}}\right)}{t}}{eff_{isotope}} \tag{3.27}$$

The uncertainty for the MQA is defined by:

$$\Delta MQA = \sqrt{\left(\delta c \frac{5}{eff_{isotope}\sqrt{c*t+25}}\right)^2 + \left(\delta eff_{isotope} \frac{-10\left(\sqrt{c*t+25}+5\right)}{{eff_{isotope}}^2 * t}\right)^2} \quad (3.28)$$

These equations can be used to determine the appropriate count times for each isotope at any given activity; for example, the intervention level.

3.4 Quantulus LS counting

After preparation, each sample was counted on a Quantulus 1220 liquid scintillation counter (manufactured by PerkinElmer, Waltham, MA). The counter was set to record counts in both the "beta" (which the Quantulus software refers to as spectrum 11) and "alpha" (referred to as spectrum 12) windows. The pulse shape analyzer (PSA) setting, which measures the decay time of each light pulse produced by radiation interacting with the scintillator fluid (and ranges from 0 to 255 – a unitless time scale), was varied from approximately 30 to 60 in order to determine the optimal setting for discrimination between beta pulses and alpha pulses. The selection of this setting will be discussed further in section 3.8.

Samples were counted with ~10 ml of liquid volume in a 20-ml LS vial.

3.5 Quantitative analysis of LS spectra – single isotopes

The resulting Quantulus spectra from counting alpha- and beta-emitting isotopes are analyzed very differently. Alpha-emitting isotopes produce monoenergetic pulses, much like gamma photopeaks on an HPGe detector. Consequently, they, too, produce Gaussian peaks in the aforementioned "alpha" window. The fitting of these peaks can be performed in the same manner as previously discussed in section 3.3.

The theoretical efficiency of the Quantulus detector for alpha emissions is ~100%.[16] However, since the Quantulus detector divides pulses into separate "alpha" and "beta" windows,

and this division is not perfect; i.e. some alpha pulses are counted as beta pulses and vice versa (depending on the PSA setting), calibration samples were counted at varying PSA settings – again, from approximately 30 to 60 – in order to determine the counting efficiency for each alpha isotope at each PSA setting.

Beta-emitting isotopes produce complex spectra[41,42,43,56] that are not trivial to describe mathematically. However, this method takes advantage of the fact that the activated carbon filtration step described in section 3.1.2 removes the color and organics from the sample. As a result, there is very little inter-sample variation in quenching, and all samples have a quench indicating parameter that is functionally equivalent to acidified water. Therefore, the energy calibration for a beta spectrum produced from one sample with a specific isotope in it will be comparable to another sample's energy calibration.

Accordingly, rather than mathematically fitting the entire beta spectrum for each isotope, the spectra are analyzed empirically. Single isotopes are analyzed on a full-spectrum basis, with efficiencies calculated for PSAs ranging from 30-60.

The only significant complication for single-isotope Quantulus spectrum analysis is Sr-90 (beta max 546 keV, half-life 28.78 years), which has a Y-90 daughter (beta max 2280 keV, half-life 64 hrs). If the parent and daughter are in equilibrium, the efficiency calculation is trivial. However, it is unlikely[57,58,59] that Sr-90 and Y-90 would *exit* the body through the urine pathway in equilibrium, even if they entered the body in equilibrium (which is also not necessarily likely). Therefore, equilibrium cannot be assumed. In order to calculate the Sr-90 fraction – which, as the longer-lived parent radionuclide, is of greater concern – the Y-90 contribution to the spectrum must be removed. This is achieved by determining the efficiency for Y-90 in the Quantulus detector at energies above the 546-keV Sr-90 beta max, as well as below it. The Y-90 counts

above the Sr-90 beta max can then be used to extrapolate the Y-90 counts that appear within the Sr-90 portion of the spectrum. These counts can then be subtracted from the spectrum, leaving only counts representing the Sr-90 activity.[f]

The Quantulus detector uses a logarithmic energy scale on its "channels" axis. In order to determine the cut-off between the Sr-90 signal and the Y-90 signal, the energy calibration for a ~50% aqueous solution in InstaGel Plus in the Quantulus was determined by selecting the beta endpoints and/or other characteristic markers for a few isotopes. The energies chosen were the 318-keV beta max for Co-60 at channel 567, the 624-keV and 656-keV conversion electrons from Cs-137 at channels 675 and 690, respectively,[60] the 1175.6-keV beta max for Cs-137 at channel 790, and the 2280-keV beta max for Y-90 at channel 900. These points were fitted a logarithmic least-squares equation; the R^2 value for the fit was greater than 0.999. This fit was used to determine the channel that represented the Sr-90 beta maximum energy of 546 keV; this channel was determined to be channel 657.

For Sr-90/Y-90 samples, all counts above channel 657 are considered to come from Y-90, while all counts below channel 657 are considered to come from a combination of Sr-90 and Y-90. The efficiencies for Y-90 above channel 657 ($eff_{Y\text{-}90\ High}$), Y-90 below channel 658 ($eff_{Y\text{-}90\ Low}$), and Sr-90 ($eff_{Sr\text{-}90}$) were each determined by measuring a Sr-90 calibration standard sample in the Quantulus. The units on these efficiencies are cps · Bq^{-1}.

The Sr-90 activity can be determined from the following equation:

$$A_{Sr} = \frac{cps_{low} - cps_{high}\frac{eff_{Y-90\ low}}{eff_{Y-90\ high}}}{eff_{Sr-90}} \tag{3.29}$$

[f] Crawford et al. unpublished results, presented at RRMC 2005, 2006, 2007, 2010, 2012, HPS 2007

where cps_{high} is defined as the net count rate (after background subtraction) in channels 658-1024, and cps_{low} is defined as the net count rate in channels 1-657.

The uncertainty for the Sr-90 activity is defined by:

$$\Delta A_{Sr} = \left[\left(\frac{\delta cps_{low}}{eff_{Sr-90}}\right)^2 + \left(\frac{-\delta cps_{high} * eff_{Y-90\ low}}{eff_{Sr-90} * eff_{Y-90\ high}}\right)^2 + \left(\frac{-\delta eff_{Y-90\ low} * cps_{high}}{eff_{Sr-90} * eff_{Y-90\ high}}\right)^2 + \left(\frac{-\delta eff_{Y-90\ high} * eff_{Y-90\ low} * cps_{high}}{eff_{Sr-90} * eff_{Y-90\ high}^{\ 2}}\right)^2\right]^{\frac{1}{2}} \quad (3.30)$$

Because of the Y-90 ingrowth, the MDA and MQA calculations for Sr-90 has the potential to be a bit more complicated: the MDA and MQA are dependent upon the background count rate; the "background" rate below the Sr-90 counts is related to the Y-90 activity, and as the Y-90 activity grows into equilibrium, it becomes dependent upon the Sr-90 activity. This complication creates a circular calculation. However, for the practical purposes of this method, since it's a rapid screening method, we can simply set the Y-90 activity equivalent to the Sr-90 intervention level, since Y-90 activity any higher than that would indicate the potential presence of Sr-90 at the intervention level or greater, and hence would trigger further medical intervention anyway.

When calculating the Sr-90 MDA and MQA, μ_B is defined by:

$$\mu_B = cps_{high}\frac{eff_{Y-90\ low}}{eff_{Y-90\ high}} * t \quad (3.31)$$

If we set the Y-90 activity to be equivalent to the Sr-90 activity at the intervention level, cps_{high} becomes a constant, and as $eff_{Y\text{-}90\ Low}$ and $eff_{Y\text{-}90\ High}$ are also constants, we can define $cps_{Y\text{-}90\ Low}$ as:

$$cps_{Y-90\ Low} = cps_{high}\frac{eff_{Y-90\ low}}{eff_{Y-90\ high}}$$

(3.32)

In turn, the equation for μ_B becomes:

$$\mu_B = cps_{Y-90\ Low} * t$$

(3.33)

The uncertainty associated with μ_B is calculated from the general form of the first-order partial derivative for a division equation (eqn. 3.20) and the general form of the first-order partial derivative for a multiplication equation:

$$\Delta(x * y) = \sqrt{(\delta x * y)^2 + (\delta y * x)^2}$$

(3.34)

Therefore, the equation for Sr-90 MDA is:

$$MDA_{Sr-90} = \frac{\frac{2.71 + 4.65\sqrt{cps_{Y-90\ Low} * t}}{t}}{eff_{Sr-90}}$$

(3.35)

The uncertainty associated with the Sr-90 MDA calculation is defined by:

$$\Delta MDA_{Sr-90}$$

$$= \sqrt{\left(\frac{\delta c * 2.325}{eff_{Sr-90} * \sqrt{cps_{Y-90\ Low} * t}}\right)^2 + \left(\delta eff_{Sr-90}\frac{-4.65(\sqrt{cps_{Y-90\ Low} * t} + .5828)}{{eff_{Sr-90}}^2 * t}\right)^2}$$

(3.36)

The MQA for Sr-90 measurements in the Quantulus is defined by:

$$MQA_{Sr-90} = \frac{\dfrac{50\left(1+\sqrt{1+\dfrac{cps_{Y-90\ Low} * t}{12.5}}\right)}{t}}{eff_{Sr-90}} \tag{3.37}$$

The uncertainty associated with the Sr-90 MQA calculation is defined by:

$$\Delta MQA_{Sr-90} = \left[\left(\frac{\delta cps_{Y-90\ Low} * 5\sqrt{2}}{eff_{Sr-90}\sqrt{cps_{Y-90\ Low} * t + 12.5}}\right)^2 + \left(\delta eff_{Sr-90}\frac{-10\sqrt{2} * \left(\sqrt{cps_{Y-90\ Low} * t + 12.5} + 2.5\sqrt{2}\right)}{{eff_{Sr-90}}^2 * t}\right)^2\right]^{\frac{1}{2}} \tag{3.38}$$

MDAs and MQAs for various count times for Sr-90 appear in Chapter 4.

The alpha emitters – Pu-238 and Am-241 – are relatively easy to detect and quantify on the Quantulus detector when one of them is the only isotope in the sample. Their monoenergetic alpha emissions produce Gaussian peaks, whose FWHM channels are 609-646 in the alpha window.

The counting efficiency of each alpha-emitting isotope within its FWHM channels is determined by dividing the count rate in these channels by the activity known to have been spiked into the samples. The MDA and MQA for Pu-238 or Am-241 on the Quantulus detector are calculated in the exact same manner as those for individual isotopes on the HPGe detector, as described in section 3.3.

3.6 Linkage of HPGe spectra to Quantulus LS spectra

Since gamma-emitting isotopes produce mono-energetic photopeaks that can be easily quantified, the gamma-emitting isotopes studied in this project (Co-60, Cs-137, Am-241) were

each quantifiably measured on the HPGe gamma detector. However, a crucial aspect of this work is that these measurements can be directly linked to the same isotopes' measurements on the Quantulus detector.

Due to the use of activated carbon (AC) powder – described above in section 3.1 – to remove all color and organic contaminants from the acidified urine samples, the quench indicating parameter for all samples is functionally equivalent, as previously discussed in section 3.5. Therefore, the energy calibration for the detector is identical for all samples. Accordingly, individual per-sample energy calibrations are irrelevant and unnecessary: one sample of a particular isotope produces the same (relative) spectrum as another sample of the same isotope.

Therefore, a calibration factor for each isotope in the Quantulus detector can be calculated: for each isotope, it is known exactly what spectrum – i.e. how many counts per channel – is produced by a unit of radioactivity from that isotope in the sample.

By quantifying the activity of a particular isotope in a particular sample via its gamma emission on the HPGe detector, it is therefore possible to predict the exact spectrum that that isotope will produce in that sample when it's counted on the Quantulus detector.

The uncertainties for this spectral linkage have been carefully traced for each isotope, and can be calculated for any sample / isotope / count time combination. The values calculated in these experiments are presented in Chapter 4.

3.7 Quantitative analysis of HPGe spectra – multiple isotopes

It is possible to quantify the activity of multiple gamma-emitting isotopes, even if present together in a single sample, via counting that sample on the HPGe detector. The unique monoenergetic peaks produce "signature" gamma lines, so isotopic identification is facile. Once the isotopes present have been identified, it is possible to fit the Gaussian peaks, similarly to the

method described in section 2.3 above. However, complications arise & additional uncertainty is added to each gamma photopeak in the spectrum with a lower energy than the most-energetic peak: the Compton spectrum from the more-energetic peaks produces an additional background signal below the lower-energy peaks.

Even in mixed-isotope samples, Co-60 can always be quantified on an HPGe detector by its 1332-keV gamma emission. None of the isotopes involved in this study interfere with this measurement in any way. As previously mentioned, for high-activity samples, quantitative dilutions of the sample may be recommended in order to reduce detector dead time.

Cs-137 can also be quantified on an HPGe detector by its 662-keV gamma emission. However, if it is in a mixed sample whose isotopes include Co-60, there will be interference from Co-60's Compton spectrum. Accordingly, the Cs-137 MDA and MQA are dependent upon the Co-60 activity present in the sample.

Since the Cs-137 activity is quantified from the channels corresponding to its FWHM (channels 5341-5353), μ_B is calculated from the Co-60 counting efficiency in these channels, or $eff_{Co\text{-}60(Cs\text{-}137)}$, multiplied by the Co-60 activity in the sample (which is determined from its 1332-keV gamma emission), $A_{Co\text{-}60}$:

$$\mu_B = eff_{Co-60(Cs-137)} * A_{Co-60} * t \tag{3.39}$$

Therefore, the equation for Cs-137 MDA is:

$$MDA_{Cs-137} = \frac{\frac{2.71 + 4.65\sqrt{eff_{Co-60(Cs-137)} * A_{Co-60} * t}}{t}}{eff_{Cs-137}} \tag{3.40}$$

The uncertainty associated with the Cs-137 MDA calculation is defined by:

$$\Delta MDA_{Cs-137} = \left[\left(\frac{\delta eff_{Co-60(Cs-137)} * 2.325 * A_{Co-60}}{eff_{Cs-137} * \sqrt{eff_{Co-60(Cs-137)} * A_{Co-60} * t}}\right)^2 + \left(\frac{\delta A_{Co-60} * 2.325 * eff_{Co-60(Cs-137)}}{eff_{Cs-137} * \sqrt{eff_{Co-60(Cs-137)} * A_{Co-60} * t}}\right)^2 + \left(\delta eff_{Cs-137} \frac{-4.65(\sqrt{eff_{Co-60(Cs-137)} * A_{Co-60} * t} + .5828)}{{eff_{Cs-137}}^2 * t}\right)^2\right]^{\frac{1}{2}}$$

(3.41)

The MQA for Cs-137 measurements on the HPGe detector (with Co-60 present) is defined by:

$$MQA_{Cs-137} = \frac{\frac{50\left(1 + \sqrt{1 + \frac{eff_{Co-60(Cs-137)} * A_{Co-60} * t}{12.5}}\right)}{t}}{eff_{Cs-137}}$$

(3.42)

The uncertainty associated with the Cs-137 MQA calculation is defined by:

$$\Delta MQA_{Cs-137} = \left[\left(\frac{\delta eff_{Co-60(Cs-137)} * A_{Co-60} * 5\sqrt{2}}{eff_{Cs-137}\sqrt{eff_{Co-60(Cs-137)} * A_{Co-60} * t + 12.5}}\right)^2 + \left(\frac{\delta A_{Co-60} * eff_{Co-60(Cs-137)} * 5\sqrt{2}}{eff_{Cs-137}\sqrt{eff_{Co-60(Cs-137)} * A_{Co-60} * t + 12.5}}\right)^2 + \left(\delta eff_{Cs-137} \frac{-10\sqrt{2} * \left(\sqrt{eff_{Co-60(Cs-137)} * A_{Co-60} * t + 12.5} + 2.5\sqrt{2}\right)}{{eff_{Cs-137}}^2 * t}\right)^2\right]^{\frac{1}{2}}$$

(3.43)

Am-241 can be quantified by counting on an HPGe detector by its 59.5-keV gamma emission. However, if Am-241 is present in a sample with activity from Co-60, Cs-137, and/or Sr-90, significant interferences from these other isotopes can arise in the FWHM of the Am-241 peak.

Since the Am-241 activity is quantified from the channels corresponding to its FWHM (channels 486-494), $A_{(Am\text{-}241)}$ is calculated from the Co-60 counting efficiency in these channels, or $eff_{Co\text{-}60(Am\text{-}241)}$, multiplied by the Co-60 activity in the sample (which is determined from its 1332-keV gamma emission), $A_{Co\text{-}60}$; the Cs-137 counting efficiency in these channels, or $eff_{Cs\text{-}137(Am\text{-}241)}$, multiplied by the Cs-137 activity in the sample (which is determined from its 662-keV gamma emission), $A_{Cs\text{-}137}$; and the count rate of Bremsstrahlung radiation from Y-90 in these channels, or $eff_{Y\text{-}90(Am\text{-}241)}$, multiplied by the Y-90 activity in the sample (which is determined from the Quantulus measurement), $A_{Y\text{-}90}$:

$$A_{Am-241} = \frac{cps_{Am-241}}{eff_{Am-241}} - \frac{\left(eff_{Co-60(Am-241)} * A_{Co-60} + eff_{Cs-137(Am-241)} * A_{Cs-137} + eff_{Y-90(Am-241)} * A_{Y-90}\right)}{eff_{Am-241}} \tag{3.44}$$

$\mu_{B(Am\text{-}241)}$ is calculated as follows:

$$\mu_{B(Am-241)} = \left(eff_{Co-60(Am-241)} * A_{Co-60} + eff_{Cs-137(Am-241)} * A_{Cs-137} + eff_{Y-90(Am-241)} * A_{Y-90}\right) * t \tag{3.45}$$

The uncertainty for μ_B is determined from:

$$\Delta\mu_{B(Am-241)} = \Big[\left(\delta eff_{Co-60(Am-241)} * A_{Co-60} * t\right)^2 + \left(\delta A_{Co-60} * eff_{Co-60(Am-241)} * t\right)^2 + \left(\delta eff_{Cs-137(Am-241)} * A_{Cs-137} * t\right)^2 + \left(\delta A_{Cs-137} * eff_{Cs-137(Am-241)} * t\right)^2 + \left(\delta eff_{Y-90(Am-241)} * A_{Y-90} * t\right)^2 + \left(\delta A_{Y-90} * eff_{Y-90(Am-241)} * t\right)^2\Big]^{\frac{1}{2}} \tag{3.46}$$

The MDA for Am-241 on the HPGe detector is defined by:

$$MDA_{Am-241} = \frac{\frac{2.71 + 4.65\sqrt{\mu_{B(Am-241)}}}{t}}{eff_{Am-241}} \tag{3.47}$$

The uncertainty associated with the Am-241 MDA calculation is defined by:

$$\Delta MDA_{Am-241} = \sqrt{\left(\frac{\delta\mu_{B(Am-241)} * 2.325}{eff_{Am-241} * \sqrt{\mu_{B(Am-241)}} * t}\right)^2 + \left(\delta eff_{Am-241} \frac{-4.65\left(\sqrt{\mu_{B(Am-241)}} + .5828\right)}{{eff_{Am-241}}^2 * t}\right)^2} \tag{3.48}$$

The MQA for Am-241 on the HPGe detector is defined by:

$$MQA_{Am-241} = \frac{\frac{50\left(1 + \sqrt{1 + \frac{\mu_{B(Am-241)}}{12.5}}\right)}{t}}{eff_{Am-241}} \tag{3.49}$$

The uncertainty associated with the Am-241 MQA calculation is defined by:

$$\Delta MQA_{Am-241} = \left[\left(\frac{\delta\mu_{B(Am-241)} * 5\sqrt{2}}{eff_{Am-241}\sqrt{\mu_{B(Am-241)} + 12.5} * t}\right)^2 + \left(\delta eff_{Am-241} \frac{-10\sqrt{2} * \left(\sqrt{\mu_{B(Am-241)} + 12.5} + 2.5\sqrt{2}\right)}{{eff_{Am-241}}^2 * t}\right)^2\right]^{\frac{1}{2}} \tag{3.50}$$

The MDA and MQA for Am-241 given a range of count times and interfering-isotope activities has been calculated and is presented in the "results" section.

3.8 Quantitative analysis of Quantulus spectra – multiple isotopes

When multiple beta-emitting isotopes are present in a sample it is still possible to quantify the activity of each isotope by counting the sample on both the HPGe detector and on the Quantulus detector. The HPGe detector can be used to quantify the activity from Co-60, Cs-137, and possibly Am-241 (if the interfering activities are low enough and/or if the count time is long enough). The Quantulus detector can be used to quantify the Sr-90 activity, and either the Pu-238 activity or the gross alpha activity from Pu-238 and Am-241 (depending on whether or not the Am-241 activity was quantified from counting on the HPGe detector).

Sr-90 activity can be quantified by subtracting the background, Co-60 contribution, Cs-137 contribution, and Y-90 contribution to channels 1-657 in the beta window of the Quantulus.

The contribution from each interfering component was calculated by dividing the spectrum into "low" (channels 1-657) and "high" (channels 658-1024) sections, with the dividing point being the channel representing the Sr-90 beta maximum energy as previously determined. Net counting efficiencies for each isotope in each of the two sections ($eff_{isotope(low)}$ and $eff_{isotope(high)}$) were calculated by counting individual isotope counting standards and dividing the net count rate in each section by the known spike activity added to each sample. The data from these calculations can be seen in the "results" section.

The Co-60 activity ($A_{Co\text{-}60}$) and the Cs-137 activity ($A_{Cs\text{-}137}$) are calculated from counting the sample on the HPGe detector.

The Sr-90 activity can be calculated as follows:

$$A_{Sr-90}$$

$$= \frac{cps_{low} - eff_{Co-60(low)} * A_{Co-60} - eff_{Cs-137(low)} * A_{Cs-137}}{eff_{Sr-90}}$$

$$- \frac{\left[\left(cps_{high} - eff_{Co-60(high)} * A_{Co-60} - eff_{Cs-137(high)} * A_{Cs-137}\right) * \frac{eff_{Y-90\ low}}{eff_{Y-90\ high}}\right]}{eff_{Sr-90}}$$

(3.51)

The uncertainty equation for this calculation is extraordinarily complex, so in practice, the equation was broken down into multiple steps, and the uncertainty for each step was calculated and carried forward to the next step. The uncertainty equations used took the general forms of the first-order partial derivative for division, multiplication, and addition/subtraction equations, as discussed previously.

The MDA and MQA for Sr-90 can also be calculated; once again, the "background" rate below the Sr-90 counts is related to the Y-90 activity, and as the Y-90 activity grows into equilibrium, it becomes dependent upon the Sr-90 activity. This complication creates a circular calculation. However, for the practical purposes of this method, since it's a rapid screening method, we can simply set the Y-90 activity equivalent to the Sr-90 intervention level, since Y-90 activity any higher than that would indicate the potential presence of Sr-90 at the intervention level or greater, and hence would trigger further medical intervention anyway. To calculate the MDA and MQA for Sr-90 in a mixed-isotope sample, μ_B can be defined as:

$$\mu_{B(Sr-90)} = t * \left(eff_{Co-60(low)} * A_{Co-60} + eff_{Cs-137(low)} * A_{Cs-137} + \left[\left(cps_{high} - eff_{Co-60(high)} * A_{Co-60} - eff_{Cs-137(high)} * A_{Cs-137} \right) * \frac{eff_{Y-90\ low}}{eff_{Y-90\ high}} \right] \right)$$

(3.52)

The uncertainty for μ_B can be defined as:

$$\Delta\mu_{B(Sr-90)} = \Bigg[\left(\delta eff_{Co-60(low)} * A_{Co-60} * t\right)^2 + \left(\delta A_{Co-60} * \frac{\left(eff_{Y-90(high)} * eff_{Co-60(low)} - eff_{Y-90(low)} * eff_{Co-60(high)}\right) * t}{eff_{Y-90(high)}}\right)^2 + \left(\delta eff_{Cs-137(low)} * A_{Cs-137} * t\right)^2 + \left(\delta A_{Cs-137} * \frac{\left(eff_{Y-90(high)} * eff_{Cs-137(low)} - eff_{Y-90(low)} * eff_{Cs-137(high)}\right) * t}{eff_{Y-90(high)}}\right)^2 + \left(\delta cps_{high} * \frac{eff_{Y-90(low)} * t}{eff_{Y-90(high)}}\right)^2 + \left(\delta eff_{Co-60(high)} * \frac{A_{Co-60} * eff_{Y-90(low)} * t}{eff_{Y-90(high)}}\right)^2 + \left(\delta eff_{Cs-137(high)} * \frac{A_{Cs-137} * eff_{Y-90(low)} * t}{eff_{Y-90(high)}}\right)^2 + \left(\delta eff_{Y-90(low)} * \frac{\left(cps_{high} - eff_{Co-60(high)} * A_{Co-60} - eff_{Cs-137(high)} * A_{Cs-137}\right) * t}{eff_{Y-90(high)}}\right)^2 + \left(\delta eff_{Y-90(high)} * eff_{Y-90\ low} * \frac{\left(eff_{Co-60(high)} * A_{Co-60} + eff_{Cs-137(high)} * A_{Cs-137} - cps_{high}\right) * t}{eff_{Y-90(high)}^{\ 2}}\right)^2\Bigg]^{\frac{1}{2}} \quad (3.53)$$

The MDA, MQA, and their related uncertainties for Sr-90 are calculated using the exact same equations as those used for Am-241 (eqn.s 3.47, 3.48, 3.49, and 3.50).

When quantifying alpha activity in the Quantulus detector, it is useful to take advantage of the pulse-shape analyzer, which measures the decay time of each light pulse produced by an interaction within the LS cocktail. The longer a pulse's decay time, the more likely the pulse

came from an alpha emitter.[16,28,38,39,45] By setting the pulse shape analyzer (PSA) at a level that minimizes the beta counts that are improperly classified as alpha counts while maximizing the alpha counts that are properly classified as such, the relative figure of merit for detecting alpha emitters can be maximized.

For these measurements, the PSA setting was optimized by counting the single-isotope standard calibration samples at every three PSA settings from 38-59, determining the count rate for each isotope in the alpha peak FWHM channels (609-646), and modeling the data for each isotope by fitting a quadratic least-squares curve to them.

The alpha activity A_{alpha} can be calculated as follows:

$$A_{alpha} = \frac{cps_{alpha} - \left(eff_{Co-60(alpha)} * A_{Co-60} + eff_{Cs-137(alpha)} * A_{Cs-137} + eff_{Sr-90(alpha)} * A_{Sr-90}\right)}{eff_{alpha}} \tag{3.54}$$

where cps_{alpha} is the gross count rate in the alpha peak FWHM channels, $eff_{isotope(alpha)}$ is the efficiency of each isotope in these channels, $A_{isotope}$ is the activity of each isotope as previously calculated from the HPGe and/or Quantulus measurements of that sample, and eff_{alpha} is the counting efficiency of each alpha isotope in the alpha peak FWHM channels.

To calculate the MDA and MQA for alpha emitters in a mixed-isotope sample, μ_B can be defined as:

$$\mu_{B(alpha)} = \left(eff_{Co-60(alpha)} * A_{Co-60} + eff_{Cs-137(alpha)} * A_{Cs-137} + eff_{Sr-90(alpha)} * A_{Sr-90}\right) * t \tag{3.55}$$

The uncertainty for μ_B can be defined as:

$$\Delta\mu_{B(alpha)} = \Big[\left(\delta eff_{Co-60(alpha)} * A_{Co-60} * t\right)^2 + \left(\delta A_{Co-60} * eff_{Co-60(alpha)} * t\right)^2 + \left(\delta eff_{Cs-137(alpha)} * A_{Cs-137} * t\right)^2 + \left(\delta A_{Cs-137} * eff_{Cs-137(alpha)} * t\right)^2 + \left(\delta eff_{Sr-90(alpha)} * A_{Y-90} * t\right)^2 + \left(\delta A_{Sr-90} * eff_{Y-90(alpha)} * t\right)^2\Big]^{\frac{1}{2}}$$

(3.56)

The MDA for an alpha emitter on the Quantulus detector is defined by:

$$MDA_{alpha} = \frac{\frac{2.71 + 4.65\sqrt{\mu_{B(alpha)}}}{t}}{eff_{alpha}}$$

(3.57)

The uncertainty associated with the alpha MDA calculation is defined by:

$$\Delta MDA_{alpha} = \sqrt{\left(\frac{\delta\mu_{B(alpha)} * 6.30075}{eff_{alpha} * \sqrt{\mu_{B(alpha)}} * t}\right)^2 + \left(\delta eff_{alpha}\frac{-12.6015(\sqrt{\mu_{B(alpha)}})}{eff_{alpha}{}^2 * t}\right)^2}$$

(3.58)

The MQA for alpha emitters on the Quantulus detector is defined by:

$$MQA_{alpha} = \frac{\frac{50\left(1 + \sqrt{1 + \frac{\mu_{B(alpha)}}{12.5}}\right)}{t}}{eff_{alpha}}$$

(3.59)

The uncertainty associated with the alpha MQA calculation is defined by:

$$\Delta MQA_{alpha} = \left[\left(\frac{\delta \mu_{B(alpha)} * 5\sqrt{2}}{eff_{alpha}\sqrt{\mu_{B(alpha)} + 12.5} * t} \right)^2 + \left(\delta eff_{alpha} \frac{-10\sqrt{2} * \left(\sqrt{\mu_{B(alpha)} + 12.5} + 2.5\sqrt{2} \right)}{{eff_{alpha}}^2 * t} \right)^2 \right]^{\frac{1}{2}} \quad (3.60)$$

These equations were used to calculate the MDA and MQA at a range of different activity levels for every PSA setting from 30-60 (using the efficiency curves fitted as described above), for each of Pu-238 and Am-241, individually. Tables showing the results of these calculations appear in the "results" section. PSA 53 was chosen as the optimal PSA setting for minimizing the alpha-emitter MDA and MQA.

If the Am-241 activity was quantified on the HPGe detector, the Pu-238 activity can be determined by simply subtracting the Am-241 activity as calculated by the HPGe measurement from the total alpha activity calculated from the Quantulus measurement:

$$A_{Pu-238} = \frac{cps_{alpha} - (A_{Am-241} * eff_{Am-241})}{eff_{Pu-238}} \quad (3.61)$$

The MDA and MQA for Pu-238 are, accordingly, dependent upon the activity of *all four of the other isotopes* used in this work. Additionally, given the extremely low activity required to trigger the intervention level for Pu-238 (0.0288 Bq per 5 ml urine sample), and as can be seen from the tables in the "results" section, it is extraordinarily difficult (if not impossible) to detect Pu-238 at the intervention level in a mixed-isotope sample if activity equivalent to just 1% of the intervention level for each of the three beta/gamma emitters is present in the sample.

In these cases, and when the Am-241 gamma emission is not quantifiable in the HPGe spectrum above the counts from other isotopes, one further step is required to quantify the Pu-238 (and possibly Am-241) activity.

3.9 Use of extractive scintillators for extraction of actinides

If the Am-241 gamma emission is not visible in the HPGe spectrum above Compton spectra of other isotopes given a reasonable count time, and/or if there is too much beta/gamma activity present in the sample to quantify any potential contamination with Pu-238 at the intervention level, liquid-liquid extraction can be used to both preconcentrate alpha activity *and* get it away from beta/gamma isotopes.

The Photon-Electron Rejecting Alpha Liquid Scintillation (PERALS) system[16] uses extractive scintillators in combination with a highly customized liquid scintillation counter to achieve optimal alpha/beta discrimination (using pulse-shape analysis) and optimal alpha energy resolution. While this system is quite sophisticated, it has significant limitations, including the limited maximum sample volume (~1 ml), the use of culture tubes instead of LS vials, the lack of an automated sample changer, etc. However, extractive scintillators can also be used with the Quantulus detector.

An extractive scintillator is a fully-organic liquid scintillation cocktail with no detergent to form emulsions, and which contains an extractant compound – such as HDEHP, TOPO, or one of many other compounds – targeted for a specific isotope or set of isotopes. The extractive scintillator is mixed with an aqueous sample to extract the isotopes of interest, centrifuged to improve the phase separation between the aqueous and organic fractions, and then drawn off of the top of the aqueous fraction with a pipette. It is then added to a liquid scintillation vial, topped

off to 10 ml volume with NONEX scintillator fluid, and counted on the HPGe and Quantulus detectors.

If the extraction is quantitative, 45 ml of an aqueous acidified urine sample can be combined with 5 ml of the extractive scintillator in a 50-ml centrifuge tube, allowing for the preconcentration of approximately 9x the 5-ml urine sample intervention level of alpha activity. Additionally, the extraction should not extract any significant amount of the beta/gamma emitters involved in this experiment.

For the experiments herein, Eichrom's DIPEX extractant (manufactured by Eichrom, Lisle, IL) was dissolved into toluene and combined with NONEX scintillator (manufactured by ETRAC Laboratories, Oak Ridge, TN) at a concentration of 5 mg DIPEX per ml of total solution. Approximately 100 ml of acidified urine was spiked with activity concentrations for each of the five isotopes roughly equivalent to the intervention level, with the exception of Co-60, which was at approximately 10% of the intervention level due to the lack of available spiking activity. 2 g of AC powder was mixed into the spiked acidified urine, which was then shaken, and then filtered (via vacuum filtration) through a glass fiber filter and a 0.45-µm polyethylene filter. The resulting solution was clear and colorless. This solution was split into two fractions. 0.25 g of Mohr's salt (a reducing agent) was added to each fraction. Each was shaken for 2 minutes, and then centrifuged. 5 ml of the DIPEX in toluene / NONEX solution was added to each fraction; each was shaken for 5 minutes, then centrifuged for 5 minutes. A cloudy substance at the aqueous/organic interface was observed in both samples; both were re-shaken for 10 seconds and then re-centrifigued for 5 minutes. After this second centrifuge step, the cloudy substance had disappeared, and a clear aqueous/organic interface was observed. 4.25 ml of each organic fraction was removed with a pipette and added to LS vials; 4.4 ml of each aqueous

fraction was added to LS vials. The LS vials containing the organic fractions were topped off to 10 ml total volume with additional NONEX scintillator; those containing the aqueous fractions were topped off to 10 ml total volume with InstaGel Plus. All LS samples were shaken to ensure complete mixing (for reproducible HPGe detector geometry). The samples were massed at every step to keep track of the gravimetric recoveries.

All samples were counted on both the HPGe detector and the Quantulus detector to calculate the recoveries; the PSA was set to PSA 50.

Am-241 activity was determined by the background-corrected count rate within the Am-241 photopeak FWHM on the HPGe detector. Gaussian curves were fitted to the peaks that appeared in the alpha window on the Quantulus (it appears that Pu-238 extracted in the DIPEX+NONEX scintillator produces two Gaussian alpha peaks in the Quantulus detector; this feature was not explored in this work) in order to determine total alpha activity; the calculated Am-241 activity was subtracted from this activity to determine the Pu-238 activity. The calculated Am-241 and Pu-238 activities were divided by the known spike activities in order to determine the recovery of each isotope using the DIPEX extractant.

These results – and a discussion thereof – are presented in the "results" section.

3.10 Summary of method

Upon receipt of a urine sample, it is acidified to 1M HCl. 5 ml (preferably measured both volumetrically and gravimetrically, to determine recoveries) of the total volume is taken to make a sample for counting. 0.1 g of AC powder is added to the 5 ml sample; this mixture is shaken for approximately 10 seconds. The resulting suspension is passed through a syringe with a glass fiber / 0.45-μm polyethylene syringe filter into an LS vial. Approximately 5.5 ml of InstaGel Plus LS cocktail is added to the solution. The mixture is shaken to ensure complete mixing. The

sample is then counted on both the HPGe detector and the Quantulus detector for count times appropriate to detect each isotope (these count times can be determined from the MDA and MQA tables in the "results" section). If the gamma activity present in the sample results in high dead time on the HPGe detector, another 5-ml sample can be produced as described above from a gravimetric dilution of the original urine sample. If the beta/gamma activity is significant enough that detecting Pu-238 at its intervention level would require a prohibitively long count time (again, see tables in "results" section to make this determination), proceed to perform a liquid-liquid extraction using an extractive scintillator (such as DIPEX in toluene/NONEX), and count the resulting sample to determine the Pu-238 and Am-241 activity concentration within it.

CHAPTER 4. RESULTS

4.1 Introduction

All HPGe data were collected via measurements on a Canberra model GR7023 HPGe detector, with a crystal diameter of 74.5 mm and a length of 66.5 mm. Further information on the HPGe detector can be seen in Figure A4.1 in the Appendix.

All Quantulus data were collected via measurements on a Quantulus 1220 detector.

All samples were spiked with radioactivity gravimetrically. The actual spike activity for most samples at a specific time can be found in Table 5.2 in the Appendix.

4.2 Quantitative analysis of HPGe spectra – single isotopes

The activity from samples containing individual gamma-emitting isotopes – Co-60, Cs-137, and Am-241 – was quantified by counting these samples on the HPGe detector as described in Chapter 3, sections 3.2 and 3.3. The channels representing the full width at half max (FWHM) for each isotope's characteristic gamma emission, as well as the counting efficiencies and background count rate for each isotope within the FWHM of its peak, are presented in Tables 4.1, 4.2, and 4.3.

The minimum detectable activity (MDA) and minimum quantifiable activity (MQA) for each isotope were calculated as described in Chapter 3, section 3.3, and are presented in Tables 4.4, 4.5, and 4.6, and Figures 4.1, 4.2, 4.3, 4.4, 4.5, and 4.6.

4.3 Quantitative analysis of Quantulus spectra – single isotopes

The activity from samples containing individual isotopes – Co-60, Sr-90, Cs-137, Pu-238, and Am-241 – was quantified by counting these samples on the Quantulus detector as described in Chapter 3, sections 3.4 and 3.5. For the beta emitters Co-60 and Cs-137, counting efficiencies

were determined over the entire beta spectrum. For Sr-90, the beta spectrum was split into two sections at the channel representing the 546-keV maximum beta energy for Sr-90 in order to calculate the individual counting efficiencies in each section from Sr-90 and its Y-90 daughter. For the alpha emitters Pu-238 and Am-241, a Gaussian curve was fitted to the peaks in the alpha spectrum produced by their mono-energetic alpha emissions. Counting efficiencies were calculated for the FWHM of these curves. All measurements were made with the pulse shape analyzer (PSA) set to 53.

Efficiencies for the beta-emitting isotopes Co-60, Sr-90, and Cs-137 are shown in Tables 4.7, 4.8, and 4.9. Net beta efficiency refers to the net counting efficiency in the beta window; net alpha efficiency refers to the net counting efficiency in the alpha window. These numbers are presented to demonstrate the alpha/beta discrimination at PSA 53. As discussed in Chapter 3, section 3.5, the efficiency numbers for Sr-90 are reproducible when Y-90 is present in equilibrium with its Sr-90 parent. However, if equilibrium cannot be assumed, individual efficiencies must be calculated for the parent and daughter isotopes.

Since the Quantulus uses a logarithmic energy scale, a beta energy calibration was performed as described in Chapter 3, section 3.5. The energies used for this energy calibration are shown in Table 4.10, and the calculated least-squares fit for the energy calibration is shown in Figure 4.7.

The least-squares fit equation was used to calculate that the channel representing the 546-keV maximum beta energy for Sr-90 would be channel 657. The Y-90 efficiency for channels greater than and less than the Sr-90 maximum beta energy were calculated, as shown in Table 4.11. The calculated individual Sr-90 and Y-90 efficiencies are consistent with previous

measurements on a Packard Tri-Carb LSC,[g] calculated from samples produced after a chemical separation of Sr-90 and Y-90. The sum of these efficiencies (190.80% ± 3.30%) is also consistent with the observed equilibrium efficiency in the Quantulus of 190.83% ± 4.32%.

Tables for the alpha-emitting isotopes Pu-238 and Am-241 are shown in Tables 4.12 and 4.13. Net beta efficiency refers to the net counting efficiency in the beta window; net alpha efficiency refers to the net counting efficiency in the alpha window. These numbers are presented to demonstrate the alpha/beta discrimination at PSA 53. Additionally, tables for the net efficiencies in the alpha peak FWHM are included.

MDAs and MQAs for Co-60 and Cs-137 on the Quantulus detector were not calculated, as these isotopes can easily be quantified at activities well below their respective intervention levels via their HPGe counts. The MDAs and MQAs for Sr-90 and the alpha emitters Pu-238 and Am-241 are shown in Tables 4.14, 4.15, 4.16, 4.17, 4.18, and 4.19. As discussed in Chapter 3, section 3.5, when calculating the Sr-90 MDA and MQA, Y-90 is assumed to be present at the Sr-90 intervention level (since any more Y-90 activity than that would clearly trigger medical intervention anyway).

Sample spectra for each individual isotope on the Quantulus are shown in Figures 4.8, 4.9, 4.10, 4.11, and 4.12. In these figures, the blue line represents the counts in the beta window, while the red line represents counts in the alpha window.

4.4 Quantitative analysis of HPGe spectra – multiple isotopes

It is possible to quantify the activity of multiple gamma-emitting isotopes, even if present together in a single sample, via counting that sample on the HPGe detector, as described in Chapter 3, section 3.7.

[g] Crawford et al. unpublished results, presented at RRMC 2005, 2006, 2007, 2010, 2012, HPS 2007

Co-60 can always be quantified on an HPGe detector by its 1332-keV gamma emission. None of the isotopes involved in this study interfere with this measurement in any way. For high-activity samples, quantitative dilutions of the sample may be recommended in order to reduce detector dead time.

Cs-137 can also be quantified on an HPGe detector by its 662-keV gamma emission. However, if it is in a mixed sample whose isotopes include Co-60, there will be interference from Co-60's Compton spectrum, as Cs-137's photopeak falls on top of the Compton spectrum. This interference can be modeled by determining the count rate per unit activity in the Co-60 Compton spectrum, as described in Chapter 3, section 3.7, and is shown in Table 4.20.

Using the count rate observed in this work, the MDA and MQA for Cs-137 can be calculated for a specified count time over a range of Co-60 activities, and are shown in Tables 4.21 and 4.22.

Am-241 can be quantified by its gamma emission; however, in practice, doing so quickly becomes complicated in the presence of other isotopes, as the activity from the other gamma-emitting isotopes in this study – as well as from Sr-90/Y-90, due to Bremsstrahlung radiation – can quickly swamp its low-energy 60-keV peak.

The MDA and MQA for Am-241 are related to the combined activity of Co-60, Sr-90/Y-90, and Cs-137 in the sample. The Co-60 and Cs-137 activity in a mixed sample can be quantified by counting on the HPGe detector, as described above and in Chapter 3, section 3.7, but in order to then determine the Am-241 activity in a mixed-isotope sample, the Sr-90/Y-90 activity must first be calculated from a Quantulus measurement, as described in Chapter 3, section 3.8, and later on in this chapter.

Table 4.23 shows the MDA and MQA for various count times, from Chapter 3, section 3.7, assuming the presence of 1% of the intervention level activity for each of Co-60, Sr-90, and Cs-137.

Table 4.24 shows the MDA and MQA for various count times, from Chapter 3, section 3.7, assuming the presence of 10% of the intervention level activity for each of Co-60, Sr-90, and Cs-137.

4.5 Optimizing PSA setting for alpha/beta discrimination

Since no Pulse Shape Analyzer (PSA) setting exists which gives perfect discrimination between alpha and beta counts, this setting must be optimized to minimize the fraction of true beta events that are misclassified as alpha events in the alpha window, while simultaneously maximizing the efficiency of true alpha events in the alpha window. The equations used to perform this optimization are discussed in Chapter 3, section 3.8. Table 4.25 shows the isotopic counting efficiencies in the alpha peak FWHM at varying PSA setting. Figures 4.13, 4.14, 4.15, and 4.16 show the curves fitted to each isotope's efficiency data. The equations from the fits in Figures 4.13 through 4.16 were used to model the efficiency of each isotope at every PSA setting from 30-60, as shown in Table 4.26. Table 4.27 presents the MDA and MQA, calculated as described in Chapter 3, section 3.8, for a 5-minute count of a sample containing Co-60, Sr-90, and Cs-137 at 1% of the intervention level. Table 4.28 presents the MDA and MQA for 35-minute count of a sample containing Co-60, Sr-90, and Cs-137 at 10% of the intervention level.

4.6 Quantitative analysis of Quantulus spectra – multiple isotopes

As previously discussed, Co-60 and Cs-137 activities can be quantified from the HPGe detector measurements. However, Sr-90 can only be quantifiably detected on the Quantulus detector – where it will have significant interferences from the presence of Co-60 and Cs-137

activity. In this method, as described in Chapter 3, section 3.8, Sr-90 is detected (when in the presence of other isotopes) by measuring the sample first on the HPGe detector to quantify the Co-60 and Cs-137 activities, and then on the Quantulus. The Sr-90 activity is calculated by subtracting the contributions of Co-60 and Cs-137 to the overall Quantulus beta window spectrum, and then correcting for the presence of Y-90 activity, using the equations given in Chapter 3, section 3.8.

The MDA and MQA for Sr-90 are calculated by taking into account all of these variables. Tables 4.29 and 4.30 show the MDA and MQA for 20-minute counts over a couple of different interfering-activity ranges. In Table 4.29, the following assumptions are made: a 20-minute count time, the presence of Cs-137 at the intervention level, and the presence of Y-90 at the intervention level; the amount of Co-60 activity in the sample is varied to determine its effect on the MDA and MQA. In Table 4.30, the following assumptions are made: a 20-minute count time, the presence of Co-60 at the intervention level, and the presence of Y-90 at the intervention level; the amount of Cs-137 activity in the sample is varied to determine its effect on the MDA and MQA.

Am-241 can be quantified by its gamma emission; however, doing so quickly becomes complicated in the presence of other isotopes, as the activity from the other gamma-emitting isotopes in this study – as well as from Sr-90/Y-90's Bremsstrahlung radiation – can quickly swamp its low-energy 60-keV peak.

If the Am-241 activity can be quantified on the HPGe detector, the Pu-238 activity can be determined by simply subtracting the Am-241 activity as calculated by the HPGe measurement from the total alpha activity calculated from the Quantulus measurement, as described in Chapter 3, section 3.8. Tables 4.31 and 4.32 show the Pu-238 MDA and MQA given varying count times

and varying levels of interference from the beta/gamma emitters. If the Am-241 activity could not be quantified, gross alpha activity can be quantified given the quantification limits shown in Tables 4.27 and 4.28, or as otherwise calculated from the equations in Chapter 3, section 3.8, given a specific sample's other isotopic activities.

4.7 Proof-of-concept: Calculated activity in mixed-isotope samples

Seven samples – U1-U7 – containing mixed isotopes in differing ratios were produced in order to test the method outlined in Chapter 3. The spike activity added to these samples was targeted to be approximately equal to the values in Table 4.33.

After spiking, these samples were measured on the HPGe detector and then on the Quantulus detector for approximately 20 minutes each. The resulting spectra were analyzed as described in Chapter 3 in order to calculate the activity of each isotope in the sample. Table 4.34 shows the resulting calculated activities and associated biases. These results will be discussed further in Chapter 5.

4.8 Use of extractive scintillators for extraction of actinides

Since the count times required for quantifying Am-241 by its gamma emission on the HPGe detector – and Pu-238 by its alpha emission on the Quantulus detector – become prohibitively long as the activity from the other beta/gamma-emitting isotopes in the sample increases, liquid-liquid extraction becomes an attractive option to both preconcentrate alpha activity *and* get it away from beta/gamma isotopes. The extractant and extracting procedure used are described in Chapter 3, section 3.9.

A single ~100-ml spiked sample was split into two fractions, labeled UD1 and UD2. The alpha activity spiked into each of these samples is shown in Table 4.35. Given the 85% organic phase recovery (Chapter 3, section 3.9), if the extraction was quantitative, Table 4.36 shows the

activities that should have been extracted. The actual alpha activity calculated to be in each sample (from counting on the Quantulus) is shown in Table 4.37. The organic phases were counted on the HPGe detector determine the extracted beta/gamma activity, which is shown in Tables 4.38 and 4.39. The aqueous phase from UD2 was counted for an extended period on the HPGe detector in order to determine how much, if any, Am-241 remained in the aqueous phase. The Am-241 activity calculated to be remaining in UD2 Aq was:

$$0.2152 \text{ +/- } 0.0353 \text{ Bq } (16.4\% \text{ uncertainty at } 1\sigma)$$

If no Am-241 activity had been extracted by the DIPEX extractant, the expected Am-241 activity remaining in UD2 Aq would be:

$$0.2237 \pm 0.0010 \text{ Bq } (0.45\% \text{ uncertainty at } 1\sigma)$$

Therefore, 96.2% ± 15.8% of the Am-241 was not extracted by the DIPEX extractant and remained in the aqueous phase.

Additional calculations based on the beta window of the Quantulus measurements of the organic phases showed that only approximately 0.49% of the Y-90 activity was extracted into the DIPEX. Y-90 is trivalent, like Am-241, and should therefore behave chemically similarly to Am-241.

These results will be discussed further in Chapter 5.

Table 4.1 Am-241 on HPGe Detector "A"

Detector A - LS Vial - FWHM	cps/Bq	1σ uncert	uncert %	<--FWHM channels:
Am-241 Photopeak Efficiency	5.160%	0.075%	1.45%	<--Channels 486-494

Det A BKG rate 486-494	cps	1σ uncert	uncert %
From BKG measurement	0.003905	0.000056	1.43%

Table 4.2 Cs-137 on HPGe Detector "A"

Detector A - LS Vial - FWHM	cps/Bq	1σ uncert	uncert %	<--FWHM channels:
Cs-137 Photopeak Efficiency	3.307%	0.013%	0.39%	<--Channels 5341-5353

Det A BKG rate 5341-5353	cps	1σ uncert	uncert %
From BKG measurement	0.00119	0.00003	2.57%

Table 4.3 Co-60 on HPGe Detector "A"

Detector A - LS Vial - FWHM	cps/Bq	1σ uncert	uncert %	<--FWHM channels
Co-60 Photopeak Efficiency	1.912%	0.005%	0.26%	<--Channels 10749-10765

Det A BKG rate 10749-10765	cps	1σ uncert	uncert %
From BKG measurement	0.000557	0.000031	5.56%

Table 4.4 Am-241 MDA and MQA on HPGe Detector "A"

count time (min)	MDA (Bq)	1σ uncert	uncert %	MQA (Bq)	1σ uncert	uncert %
1	1.390	0.020	0.015	32.37	0.47	0.01
2	0.801	0.012	0.015	16.22	0.24	0.01
3	0.589	0.009	0.015	10.84	0.16	0.01
4	0.476	0.007	0.015	8.15	0.12	0.01
5	0.405	0.006	0.015	6.53	0.09	0.01
6	0.356	0.005	0.015	5.46	0.08	0.01
7	0.319	0.005	0.015	4.69	0.07	0.01
8	0.291	0.004	0.015	4.11	0.06	0.01
9	0.269	0.004	0.015	3.66	0.05	0.01
10	0.250	0.004	0.015	3.30	0.05	0.01
20	0.159	0.002	0.015	1.69	0.02	0.01
30	0.123	0.002	0.015	1.15	0.02	0.01
40	0.103	0.002	0.016	0.88	0.01	0.01
50	0.090	0.001	0.016	0.71	0.01	0.01
60	0.081	0.001	0.016	0.61	0.01	0.01
70	0.074	0.001	0.016	0.53	0.01	0.01
80	0.068	0.001	0.016	0.47	0.01	0.01
90	0.064	0.001	0.016	0.42	0.01	0.01
100	0.060	0.001	0.016	0.39	0.01	0.01
200	0.041	0.001	0.016	0.22	0.00	0.01
300	0.033	0.001	0.016	0.16	0.00	0.01
400	0.028	0.000	0.016	0.13	0.00	0.02
500	0.025	0.000	0.016	0.11	0.00	0.02
600	0.022	0.000	0.016	0.10	0.00	0.02
700	0.021	0.000	0.016	0.09	0.00	0.02
800	0.019	0.000	0.016	0.08	0.00	0.02
900	0.018	0.000	0.016	0.07	0.00	0.02
1000	0.017	0.000	0.016	0.07	0.00	0.02

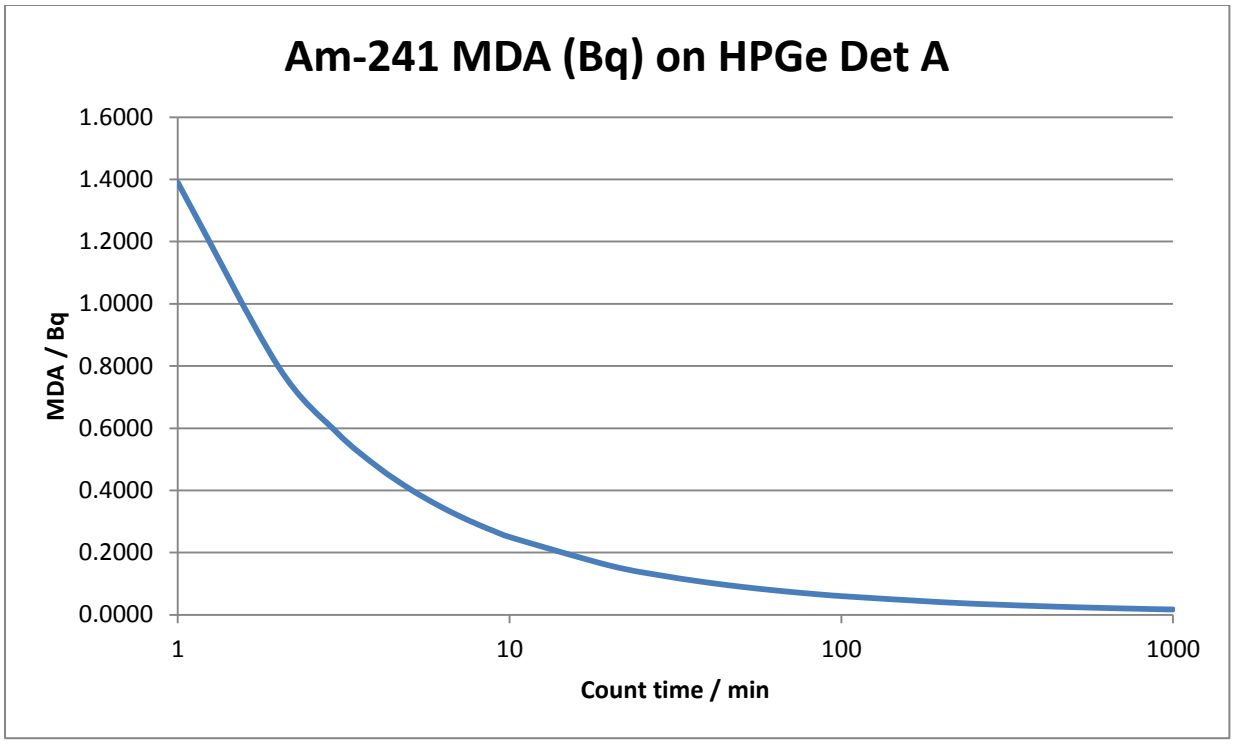

Figure 4.1 Am-241 MDA on HPGe Detector "A"

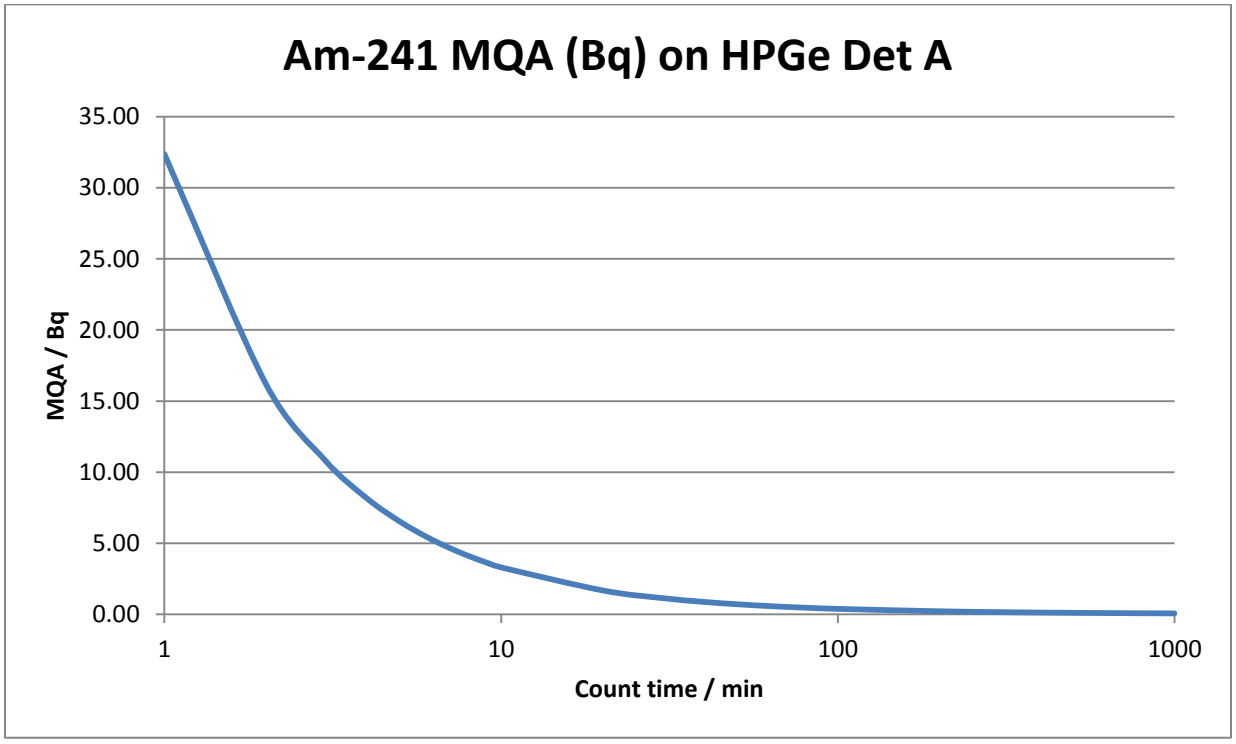

Figure 4.2 Am-241 MQA on HPGe Detector "A"

Table 4.5 Cs-137 MDA and MQA on HPGe Detector "A"

count time (min)	MDA (Bq)	1σ uncert	uncert %	MQA (Bq)	1σ uncert	uncert %
1	1.808	0.009	0.005	50.44	0.19	0.00
2	0.996	0.006	0.006	25.24	0.10	0.00
3	0.711	0.004	0.006	16.84	0.06	0.00
4	0.563	0.004	0.006	12.64	0.05	0.00
5	0.471	0.003	0.007	10.12	0.04	0.00
6	0.408	0.003	0.007	8.44	0.03	0.00
7	0.362	0.003	0.007	7.24	0.03	0.00
8	0.327	0.002	0.007	6.34	0.02	0.00
9	0.299	0.002	0.007	5.64	0.02	0.00
10	0.277	0.002	0.008	5.08	0.02	0.00
20	0.167	0.001	0.009	2.56	0.01	0.00
30	0.126	0.001	0.009	1.72	0.01	0.00
40	0.104	0.001	0.009	1.29	0.01	0.00
50	0.090	0.001	0.010	1.04	0.00	0.00
60	0.080	0.001	0.010	0.87	0.00	0.00
70	0.072	0.001	0.010	0.75	0.00	0.00
80	0.067	0.001	0.010	0.66	0.00	0.00
90	0.062	0.001	0.010	0.59	0.00	0.00
100	0.058	0.001	0.011	0.54	0.00	0.00
200	0.038	0.000	0.011	0.28	0.00	0.00
300	0.030	0.000	0.012	0.20	0.00	0.01
400	0.026	0.000	0.012	0.16	0.00	0.01
500	0.023	0.000	0.012	0.13	0.00	0.01
600	0.020	0.000	0.012	0.11	0.00	0.01
700	0.019	0.000	0.012	0.10	0.00	0.01
800	0.017	0.000	0.012	0.09	0.00	0.01
900	0.016	0.000	0.012	0.08	0.00	0.01
1000	0.015	0.000	0.012	0.07	0.00	0.01

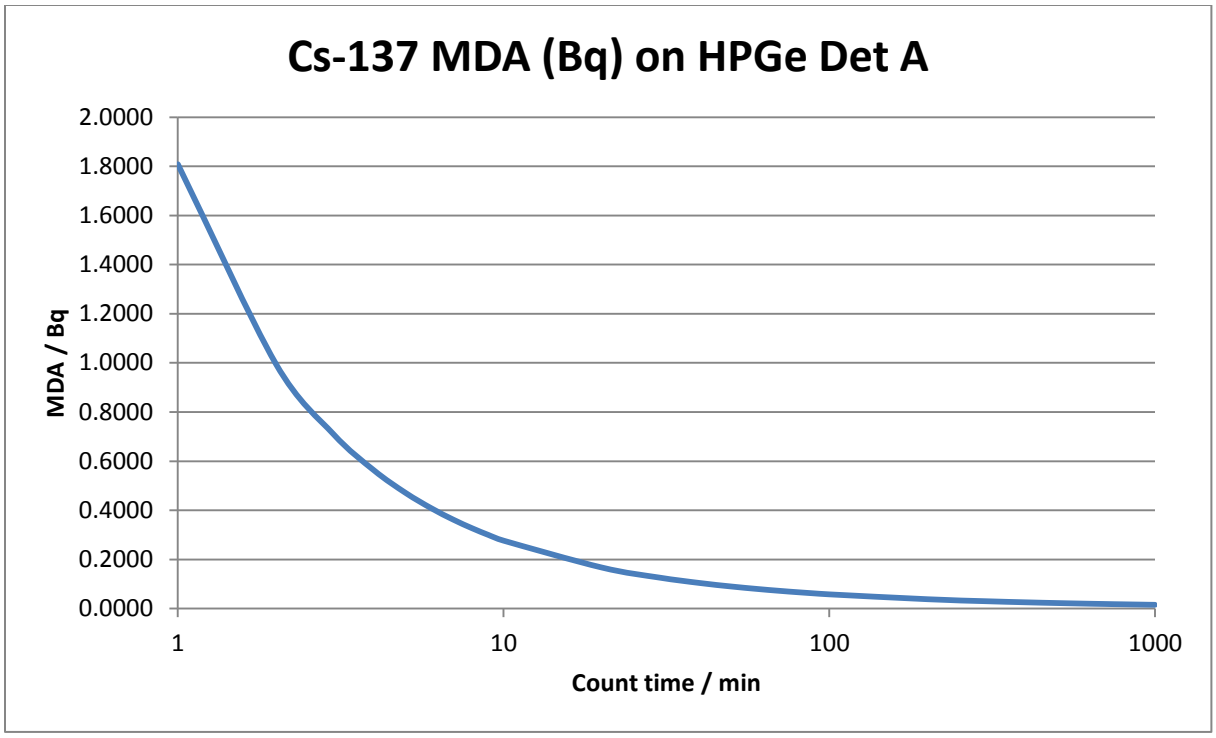

Figure 4.3 Cs-137 MDA on HPGe Detector "A"

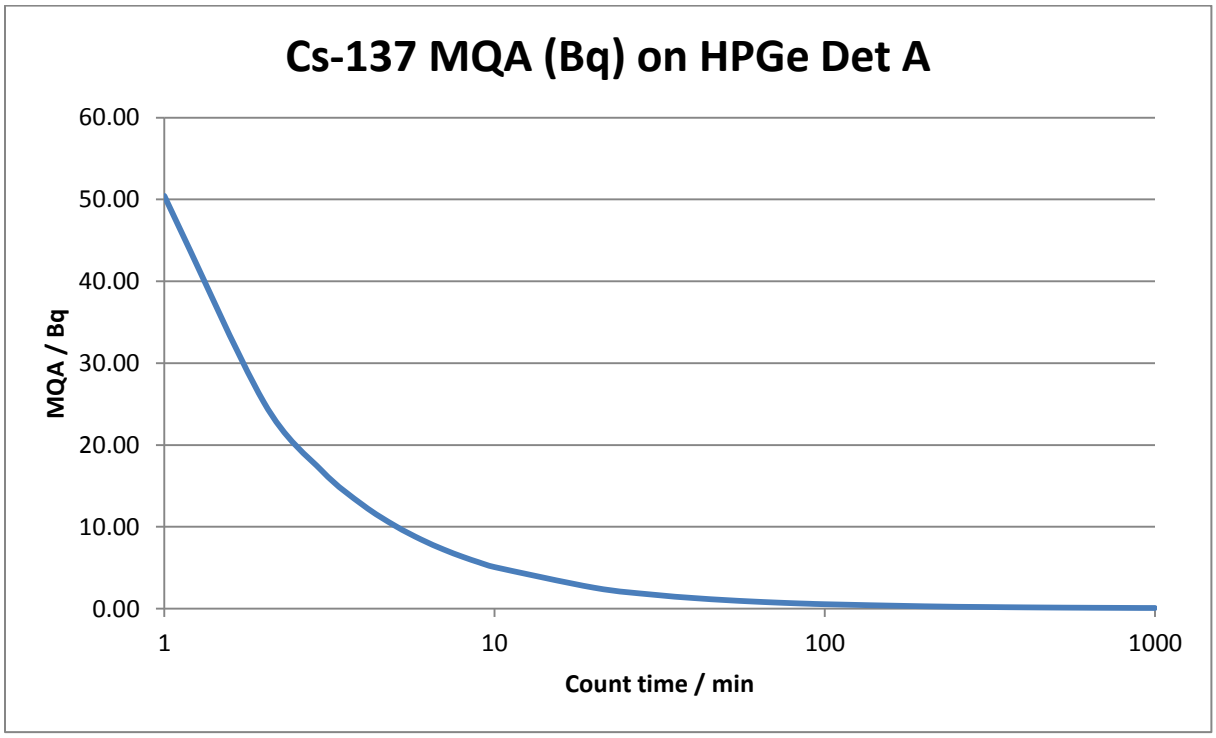

Figure 4.4 Cs-137 MQA on HPGe Detector "A"

Table 4.6 Co-60 MDA and MQA on HPGe Detector "A"

count time (min)	MDA (Bq)	1σ uncert	uncert %	MQA (Bq)	1σ uncert	uncert %
1	2.887	0.016	0.006	87.20	0.23	0.00
2	1.552	0.011	0.007	43.61	0.11	0.00
3	1.090	0.009	0.008	29.08	0.08	0.00
4	0.853	0.008	0.009	21.82	0.06	0.00
5	0.707	0.007	0.010	17.46	0.05	0.00
6	0.608	0.006	0.010	14.56	0.04	0.00
7	0.536	0.006	0.011	12.48	0.03	0.00
8	0.481	0.005	0.011	10.92	0.03	0.00
9	0.437	0.005	0.011	9.71	0.03	0.00
10	0.402	0.005	0.012	8.75	0.02	0.00
20	0.235	0.003	0.014	4.39	0.01	0.00
30	0.175	0.003	0.015	2.93	0.01	0.00
40	0.142	0.002	0.016	2.21	0.01	0.00
50	0.121	0.002	0.017	1.77	0.00	0.00
60	0.107	0.002	0.018	1.48	0.00	0.00
70	0.096	0.002	0.018	1.27	0.00	0.00
80	0.088	0.002	0.019	1.12	0.00	0.00
90	0.082	0.002	0.019	1.00	0.00	0.00
100	0.076	0.001	0.019	0.90	0.00	0.00
200	0.049	0.001	0.021	0.46	0.00	0.00
300	0.038	0.001	0.022	0.32	0.00	0.01
400	0.032	0.001	0.023	0.24	0.00	0.01
500	0.028	0.001	0.023	0.20	0.00	0.01
600	0.025	0.001	0.024	0.17	0.00	0.01
700	0.023	0.001	0.024	0.15	0.00	0.01
800	0.021	0.001	0.024	0.13	0.00	0.01
900	0.020	0.000	0.024	0.12	0.00	0.01
1000	0.019	0.000	0.024	0.11	0.00	0.01

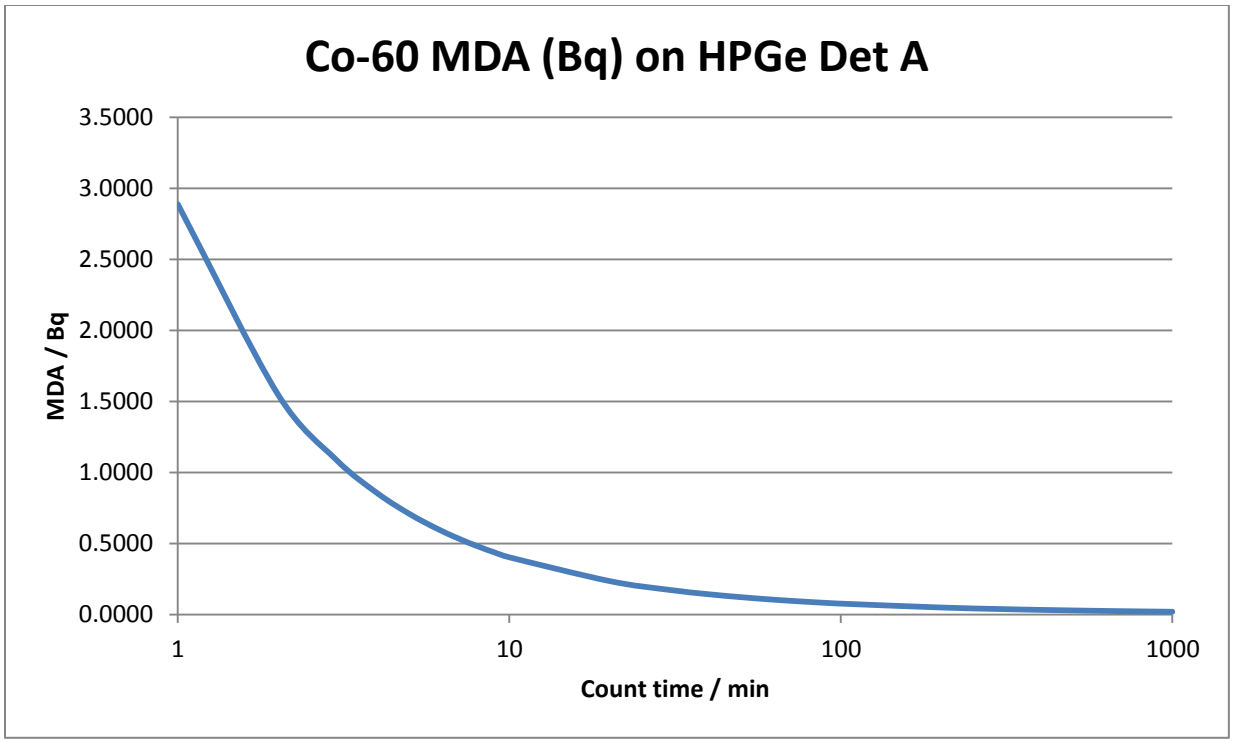

Figure 4.5 Co-60 MDA on HPGe Detector "A"

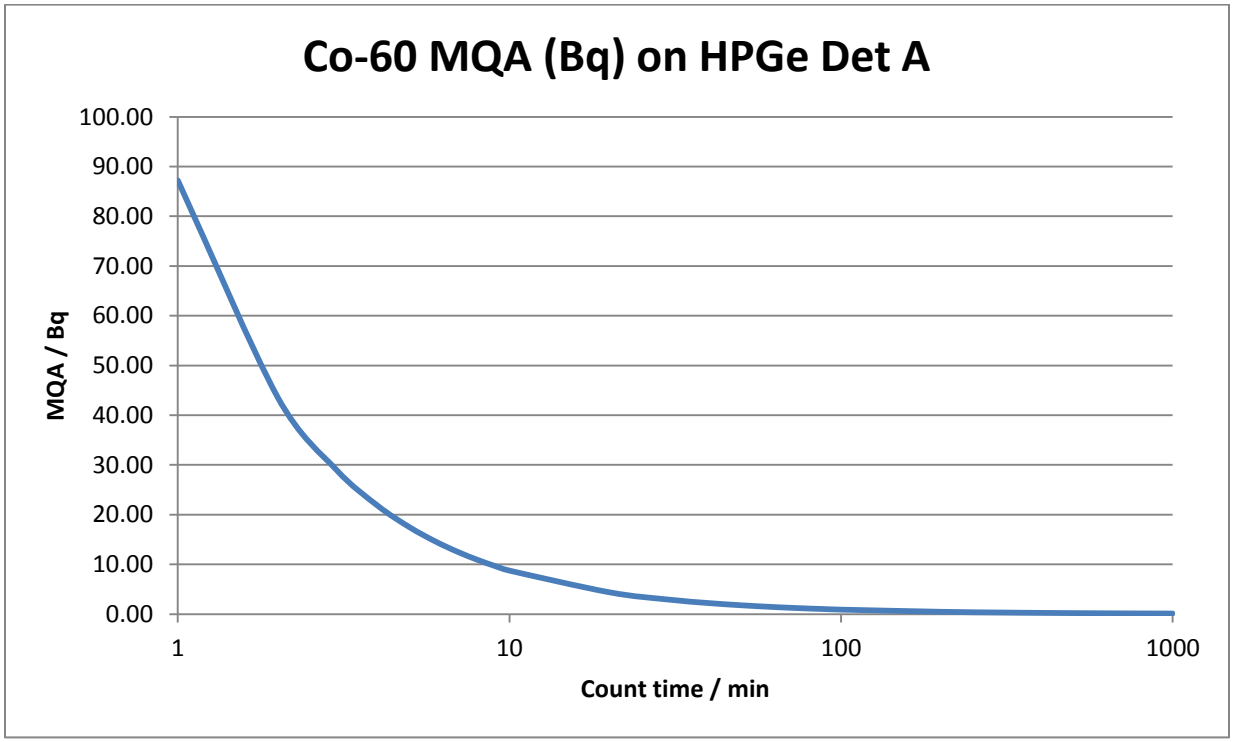

Figure 4.6 Co-60 MQA on HPGe Detector "A"

Table 4.7 Co-60 efficiency on the Quantulus detector

	cps/Bq	1σ uncert	uncert %
Net beta eff	53.28%	1.21%	2.28%
Net alpha eff	1.74%	0.04%	2.28%

Table 4.8 Cs-137 efficiency on the Quantulus detector

	cps/Bq	1σ uncert	uncert %
Net beta eff	103.98%	2.37%	2.28%
Net alpha eff	2.41%	0.06%	2.28%

Table 4.9 Sr-90 efficiency on the Quantulus detector

	cps/Bq	1σ uncert	uncert %
Net beta eff	190.83%	4.32%	2.26%
Net alpha eff	3.913%	0.089%	2.27%

Table 4.10 Quantulus beta energy calibration

beta energy (keV)	channel
656	690
2280	900
624	675
1175.63	790
318	567

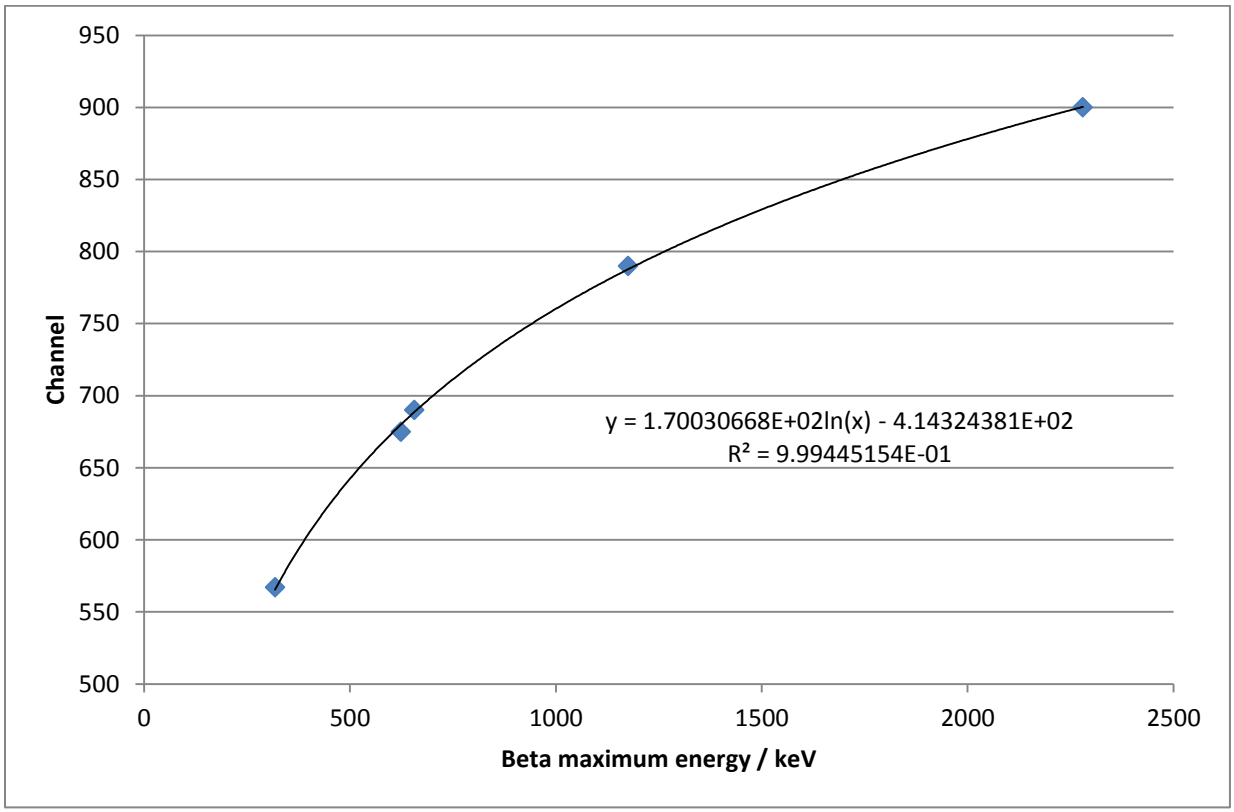

Figure 4.7 Quantulus beta energy calibration

Table 4.11 Sr-90 and Y-90 efficiencies on the Quantulus detector

Y-90 cps frac above Sr-90 (chn 658++)		1σ uncert	uncert %
	58.43%	1.32%	2.26%
Sr-90 eff		1σ uncert	uncert %
	93.50%	2.38%	2.54%
Y-90 cps frac below Sr-90 (chn 0-657)		1σ uncert	uncert %
	38.87%	1.86%	4.79%
Total Y-90 eff		1σ uncert	uncert %
	97.30%	2.28%	2.35%
Total Sr-90 + Y-90 eff		1σ uncert	uncert %
	190.80%	3.30%	1.73%

Table 4.12 Pu-238 efficiencies on the Quantulus detector

	cps/Bq	1σ uncert	uncert %
Net beta eff	37.49%	1.68%	4.48%
Net alpha eff	65.42%	1.91%	2.92%
Pu-238 eff, alpha FWHM, chn 609-646	39.21%	0.88%	2.24%

Table 4.13 Am-241 efficiencies on the Quantulus detector

	cps/Bq	1σ uncert	uncert %
Net beta eff	22.44%	0.68%	3.03%
Net alpha eff	80.46%	1.94%	2.41%
Am-241 eff, alpha FWHM, chn 609-646	50.14%	0.51%	1.02%

Table 4.14 Sr-90 MDA on Quantulus

count time (min)	MDA (Bq)	1σ uncert
1	23.9	0.6096
2	16.9	0.4303
3	13.8	0.3511
4	11.9	0.3039
5	10.7	0.2718
6	9.7	0.2481
7	9.0	0.2296
8	8.4	0.2148
9	8.0	0.2025
10	7.5	0.1921
20	5.3	0.1358
30	4.4	0.1109
40	3.8	0.0960
50	3.4	0.0859
60	3.1	0.0784
70	2.9	0.0726
80	2.7	0.0679
90	2.5	0.0640
100	2.4	0.0607
200	1.7	0.0429
300	1.4	0.0350
400	1.2	0.0303
500	1.1	0.0271
600	1.0	0.0248
700	0.9	0.0229
800	0.8	0.0215
900	0.8	0.0202
1000	0.8	0.0192

Table 4.15 Sr-90 MQA on Quantulus

count time (min)	MQA (Bq)	1σ uncert
1	73.44	1.87
2	51.74	1.32
3	42.18	1.07
4	36.49	0.93
5	32.62	0.83
6	29.76	0.76
7	27.55	0.70
8	25.76	0.66
9	24.28	0.62
10	23.03	0.59
20	16.27	0.41
30	13.27	0.34
40	11.49	0.29
50	10.28	0.26
60	9.38	0.24
70	8.68	0.22
80	8.12	0.21
90	7.66	0.19
100	7.26	0.18
200	5.13	0.13
300	4.19	0.11
400	3.63	0.09
500	3.25	0.08
600	2.96	0.08
700	2.74	0.07
800	2.57	0.07
900	2.42	0.06
1000	2.29	0.06

Table 4.16 Pu-238 MDA on Quantulus

count time (min)	MDA (Bq)	1σ uncert
1	0.152	0.099
2	0.083	0.049
3	0.059	0.033
4	0.047	0.025
5	0.039	0.020
6	0.034	0.016
7	0.030	0.014
8	0.027	0.012
9	0.025	0.011
10	0.023	0.010
20	0.014	0.005
30	0.011	0.003
40	0.009	0.002
50	0.007	0.002
60	0.007	0.002
70	0.006	0.001
80	0.006	0.001
90	0.005	0.001
100	0.005	0.001
200	0.003	0.000
300	0.002	0.000
400	0.002	0.000
500	0.002	0.000
600	0.002	0.000
700	0.002	0.000
800	0.001	0.000
900	0.001	0.000
1000	0.001	0.000

Table 4.17 Pu-238 MQA on Quantulus

count time (min)	MQA (Bq)	1σ uncert
1	4.253	0.096
2	2.128	0.049
3	1.420	0.033
4	1.066	0.025
5	0.853	0.020
6	0.711	0.017
7	0.610	0.015
8	0.534	0.013
9	0.475	0.012
10	0.428	0.011
20	0.215	0.006
30	0.145	0.004
40	0.109	0.003
50	0.088	0.003
60	0.074	0.002
70	0.063	0.002
80	0.056	0.002
90	0.050	0.002
100	0.045	0.002
200	0.024	0.001
300	0.017	0.001
400	0.013	0.001
500	0.011	0.001
600	0.009	0.000
700	0.008	0.000
800	0.007	0.000
900	0.007	0.000
1000	0.006	0.000

Table 4.18 Am-241 MDA on Quantulus

count time (min)	MDA (Bq)	1σ uncert
1	0.119	0.077
2	0.065	0.039
3	0.047	0.026
4	0.037	0.019
5	0.031	0.015
6	0.027	0.013
7	0.024	0.011
8	0.021	0.010
9	0.020	0.009
10	0.018	0.008
20	0.011	0.004
30	0.008	0.003
40	0.007	0.002
50	0.006	0.002
60	0.005	0.001
70	0.005	0.001
80	0.004	0.001
90	0.004	0.001
100	0.004	0.001
200	0.002	0.000
300	0.002	0.000
400	0.002	0.000
500	0.001	0.000
600	0.001	0.000
700	0.001	0.000
800	0.001	0.000
900	0.001	0.000
1000	0.001	0.000

Table 4.19 Am-241 MQA on Quantulus

count time (min)	MQA (Bq)	1σ uncert
1	3.326	0.036
2	1.664	0.019
3	1.110	0.013
4	0.833	0.010
5	0.667	0.009
6	0.556	0.008
7	0.477	0.007
8	0.418	0.006
9	0.372	0.006
10	0.335	0.005
20	0.168	0.003
30	0.113	0.002
40	0.085	0.002
50	0.069	0.002
60	0.058	0.002
70	0.050	0.001
80	0.044	0.001
90	0.039	0.001
100	0.035	0.001
200	0.019	0.001
300	0.013	0.001
400	0.010	0.000
500	0.008	0.000
600	0.007	0.000
700	0.006	0.000
800	0.006	0.000
900	0.005	0.000
1000	0.005	0.000

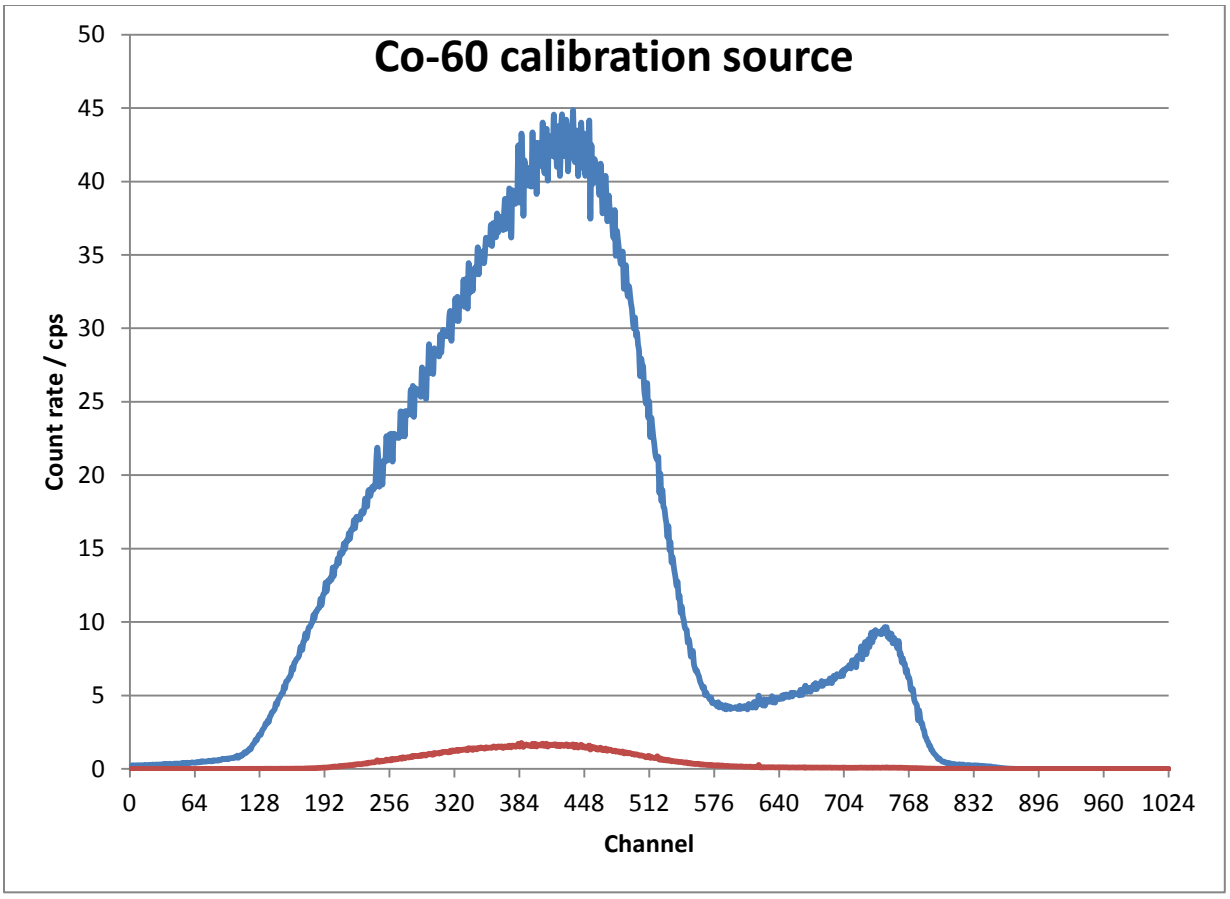

Figure 4.8 Co-60 spectrum on the Quantulus

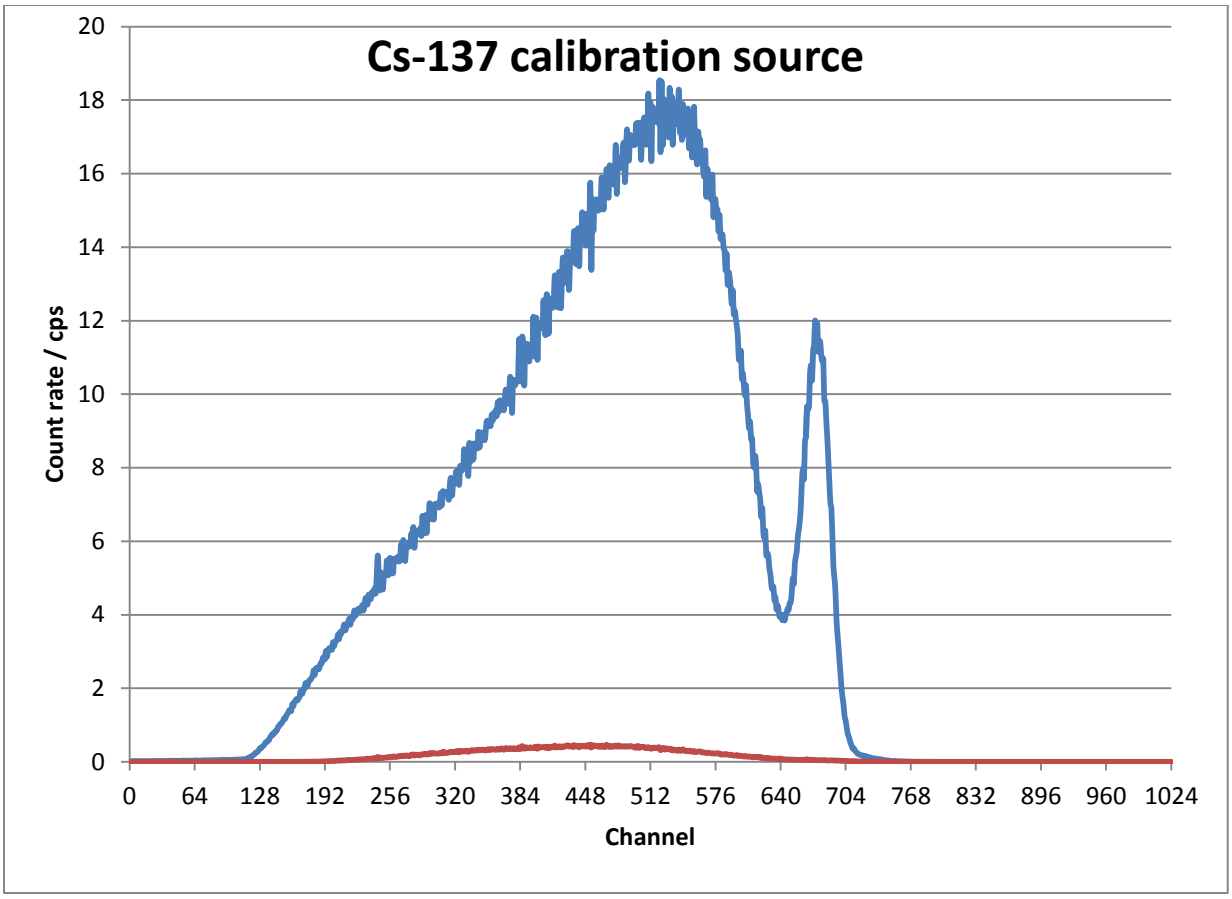

Figure 4.9 Cs-137 spectrum on the Quantulus

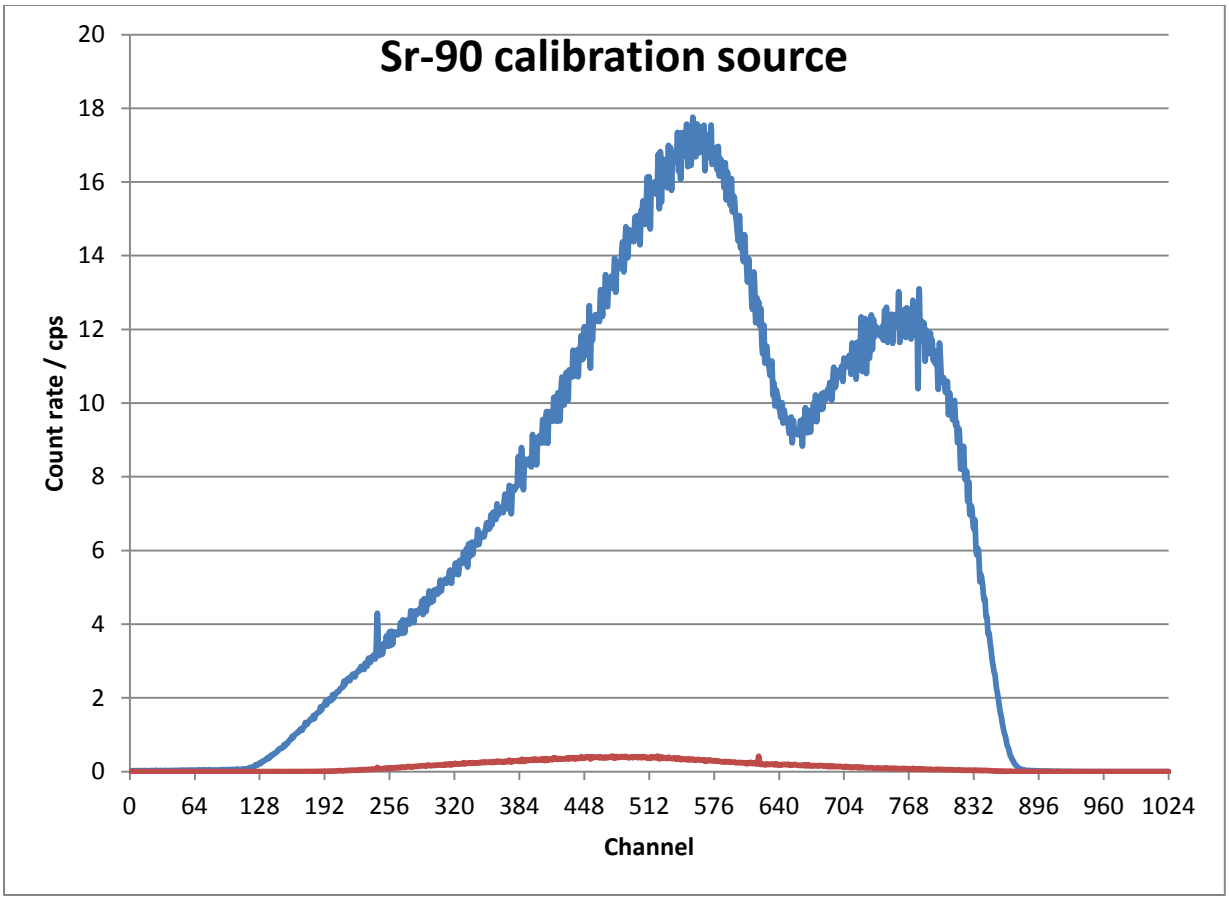

Figure 4.10 Sr-90/Y-90 spectrum on the Quantulus

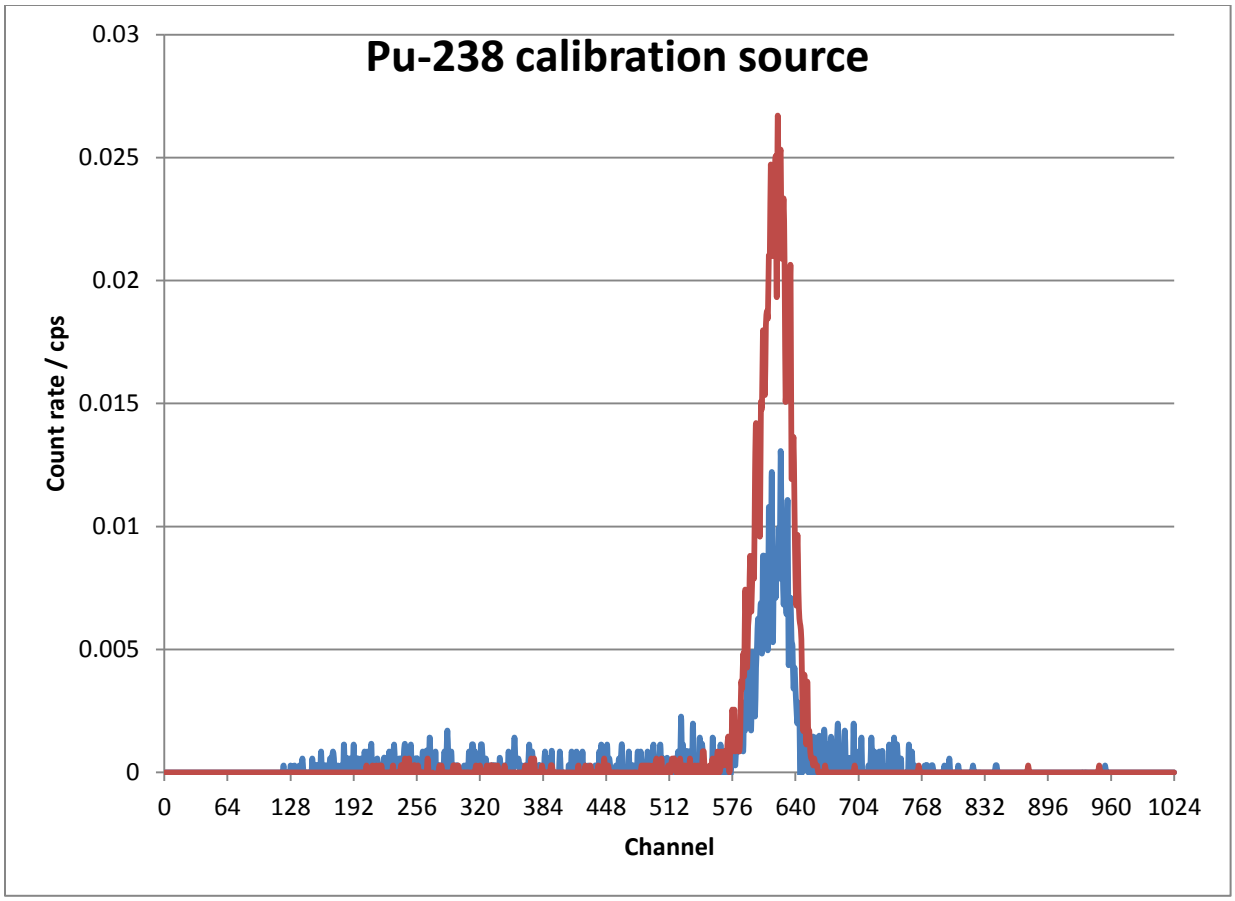

Figure 4.11 Pu-238 spectrum on the Quantulus

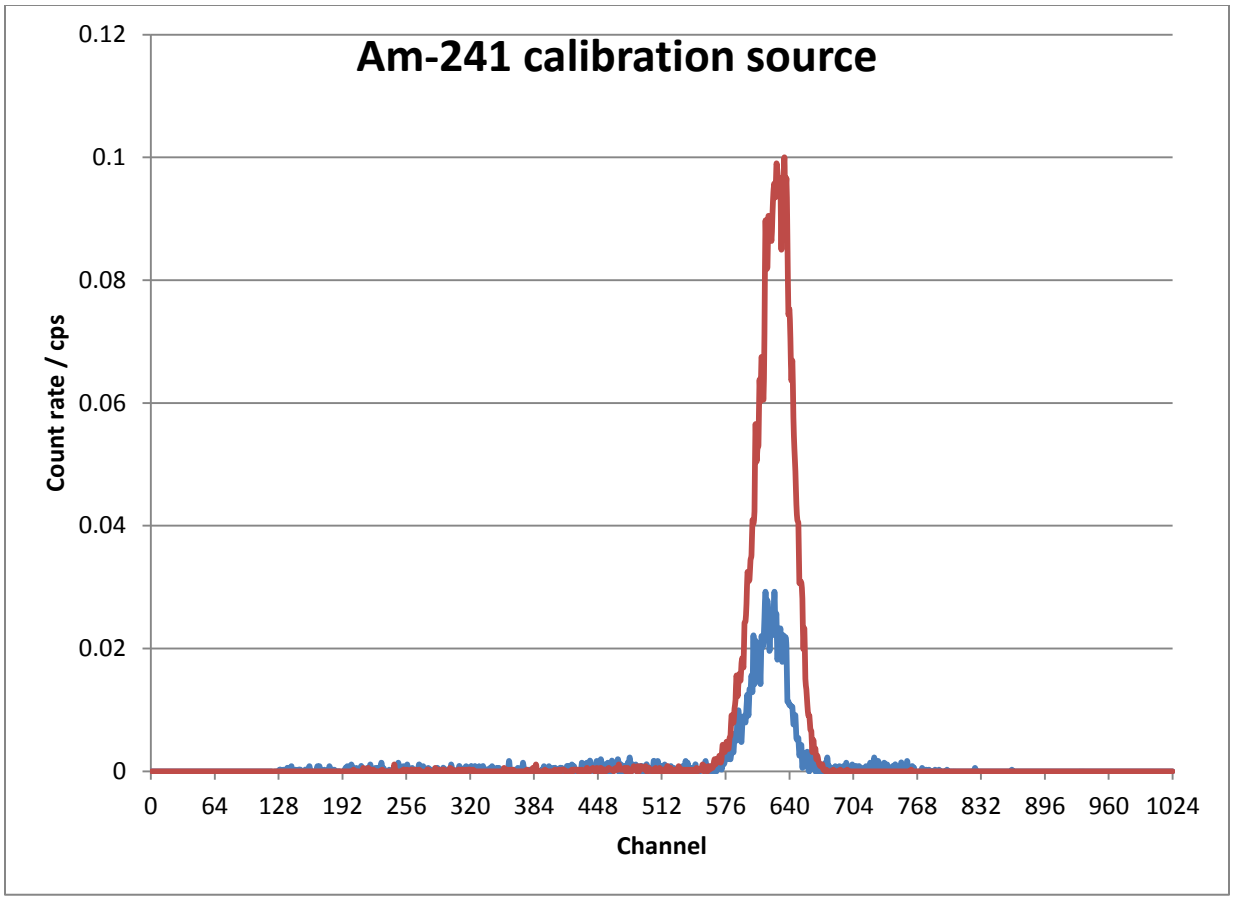

Figure 4.12 Am-241 spectrum on the Quantulus

Table 4.20 Co-60 interference in Cs-137 FWHM on HPGe detector

Co-60 cps/Bq in Cs-137 FWHM	1σ uncert	uncert %	
0.000229	0.000009	3.73%	<--Channels 5341-5353

Table 4.21 Cs-137 MDA, 5-min count

Co-60 int lvl %	MDA (Bq)	1σ uncert	uncert %
0.0%	0.55	0.23	42.39%
0.1%	0.93	0.23	25.13%
0.2%	1.16	0.23	20.16%
0.3%	1.34	0.23	17.43%
0.4%	1.50	0.23	15.63%
0.5%	1.64	0.23	14.32%
0.6%	1.76	0.23	13.30%
0.7%	1.88	0.23	12.49%
0.8%	1.99	0.23	11.81%
0.9%	2.09	0.23	11.24%
1.0%	2.18	0.23	10.75%
2%	2.96	0.23	7.93%
3%	3.56	0.23	6.60%
4%	4.06	0.23	5.79%
5%	4.50	0.24	5.22%
6%	4.91	0.24	4.79%
7%	5.28	0.24	4.46%
8%	5.62	0.24	4.19%
9%	5.95	0.24	3.96%
10%	6.25	0.24	3.77%
20%	8.72	0.24	2.71%
30%	10.62	0.24	2.24%
40%	12.22	0.24	1.96%
50%	13.63	0.24	1.76%
60%	14.90	0.24	1.62%
70%	16.07	0.24	1.51%
80%	17.17	0.24	1.42%
90%	18.19	0.24	1.34%
100%	19.16	0.25	1.28%
200%	26.98	0.26	0.95%
300%	32.98	0.27	0.81%
400%	38.04	0.28	0.73%
500%	42.50	0.29	0.67%

Table 4.22 Cs-137 MQA, 5-min count

Co-60 int lvl %	MQA (Bq)	1σ uncert	uncert %
0.0%	10.15	0.12	1.23%
0.1%	10.46	0.27	2.55%
0.2%	10.76	0.34	3.16%
0.3%	11.04	0.39	3.53%
0.4%	11.31	0.43	3.77%
0.5%	11.57	0.46	3.93%
0.6%	11.82	0.48	4.05%
0.7%	12.06	0.50	4.13%
0.8%	12.29	0.51	4.19%
0.9%	12.51	0.53	4.22%
1.0%	12.73	0.54	4.25%
2%	14.64	0.61	4.16%
3%	16.22	0.64	3.94%
4%	17.61	0.66	3.73%
5%	18.86	0.67	3.54%
6%	20.01	0.68	3.38%
7%	21.07	0.68	3.23%
8%	22.07	0.69	3.11%
9%	23.01	0.69	3.00%
10%	23.91	0.69	2.90%
20%	31.23	0.71	2.27%
30%	36.91	0.72	1.95%
40%	41.72	0.72	1.74%
50%	45.97	0.73	1.59%
60%	49.82	0.73	1.47%
70%	53.36	0.74	1.38%
80%	56.66	0.74	1.31%
90%	59.76	0.75	1.25%
100%	62.70	0.75	1.20%
200%	86.42	0.79	0.91%
300%	104.65	0.82	0.78%
400%	120.02	0.85	0.71%
500%	133.56	0.88	0.66%

Table 4.23 Am-241 MDA, MQA on HPGe, 1% int. level Co-60, Sr-90, Cs-137

count time (min)	MDA (Bq)	1σ uncert	MQA (Bq)	1σ uncert
1	3.39	0.76	34.02	1.1
2	2.22	0.38	17.79	0.7
3	1.74	0.25	12.35	0.5
4	1.48	0.19	9.60	0.4
5	1.30	0.15	7.94	0.4
6	1.17	0.13	6.82	0.3
7	1.08	0.11	6.01	0.3
8	1.00	0.10	5.39	0.2
9	0.94	0.08	4.91	0.2
10	0.88	0.08	4.52	0.2
20	0.61	0.04	2.70	0.1
30	0.49	0.03	2.04	0.1
40	0.42	0.02	1.68	0.1
50	0.37	0.02	1.45	0.0
60	0.34	0.01	1.29	0.0
70	0.31	0.01	1.17	0.0
80	0.29	0.01	1.08	0.0
90	0.27	0.01	1.01	0.0
100	0.26	0.01	0.94	0.0
200	0.18	0.00	0.63	0.0
300	0.15	0.00	0.50	0.0
400	0.13	0.00	0.43	0.0
500	0.11	0.00	0.38	0.0
600	0.10	0.00	0.34	0.0
700	0.10	0.00	0.31	0.0
800	0.09	0.00	0.29	0.0
900	0.08	0.00	0.27	0.0
1000	0.08	0.00	0.26	0.0

Table 4.24 Am-241 MDA, MQA on HPGe, 10% int. level Co-60, Sr-90, Cs-137

count time (min)	MDA (Bq)	1σ uncert	MQA (Bq)	1σ uncert
1	8.53	0.77	44.48	2.0
2	5.85	0.39	26.40	1.1
3	4.71	0.26	19.86	0.8
4	4.04	0.20	16.35	0.6
5	3.60	0.16	14.13	0.5
6	3.27	0.13	12.57	0.4
7	3.02	0.12	11.40	0.4
8	2.81	0.10	10.49	0.3
9	2.65	0.09	9.76	0.3
10	2.51	0.08	9.15	0.3
20	1.75	0.05	6.07	0.1
30	1.43	0.03	4.82	0.1
40	1.23	0.03	4.11	0.1
50	1.10	0.02	3.63	0.1
60	1.00	0.02	3.29	0.1
70	0.93	0.02	3.02	0.1
80	0.87	0.02	2.81	0.0
90	0.82	0.01	2.64	0.0
100	0.77	0.01	2.49	0.0
200	0.55	0.01	1.73	0.0
300	0.44	0.01	1.40	0.0
400	0.38	0.01	1.20	0.0
500	0.34	0.01	1.07	0.0
600	0.31	0.00	0.98	0.0
700	0.29	0.00	0.90	0.0
800	0.27	0.00	0.84	0.0
900	0.26	0.00	0.79	0.0
1000	0.24	0.00	0.75	0.0

Table 4.25 Counting efficiencies in alpha FWHM vs. PSA setting

Co-60	PSA	eff. in α FWHM	1σ uncert
U8c	38	0.0539%	0.0003%
U8c	41	0.0401%	0.0003%
U8c	44	0.0306%	0.0002%
U8c	47	0.0241%	0.0002%
U8c	53	0.0161%	0.0002%
U8c	56	0.0151%	0.0001%
U8c	59	0.0151%	0.0001%
Sr-90			
U9c	38	0.7200%	0.0029%
U9c	41	0.5169%	0.0024%
U9c	44	0.3745%	0.0019%
U9c	47	0.2919%	0.0017%
U9c	53	0.2092%	0.0014%
U9c	56	0.1883%	0.0013%
U9c	59	0.1737%	0.0012%
Cs-137			
U10c	38	0.2284%	0.0013%
U10c	41	0.1643%	0.0011%
U10c	44	0.1210%	0.0009%
U10c	47	0.0935%	0.0008%
U10c	53	0.0659%	0.0006%
U10c	56	0.0584%	0.0006%
U10c	59	0.0539%	0.0006%
Am-241			
U12c	38	61.03%	0.57%
U12c	41	58.91%	0.56%
U12c	44	56.22%	0.54%
U12c	47	55.22%	0.54%
U12c	53	50.14%	0.51%
U12c	56	47.21%	0.49%
U12c	59	44.13%	0.47%

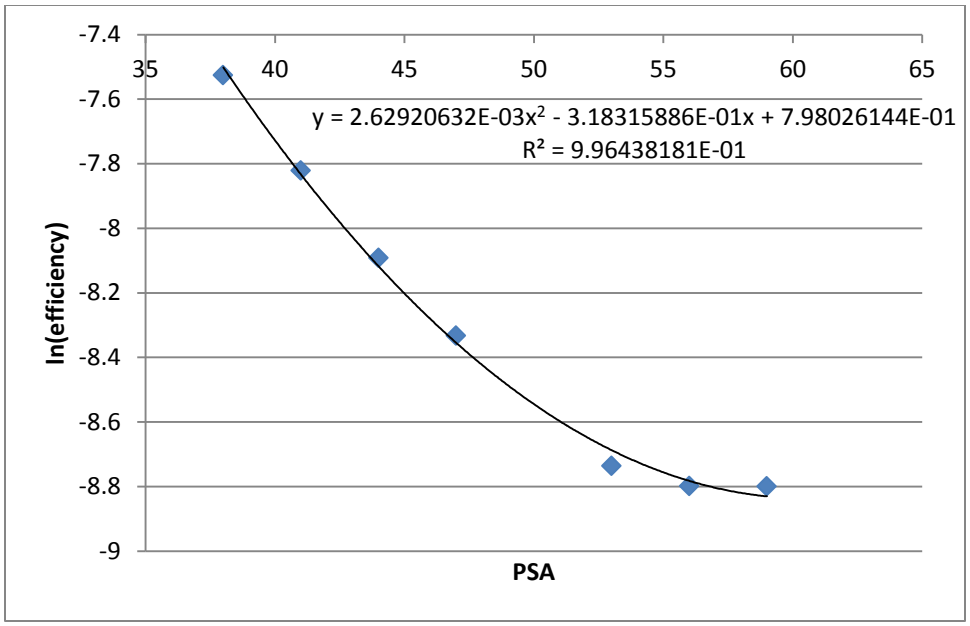

Figure 4.13 Co-60 efficiency/PSA curve fit

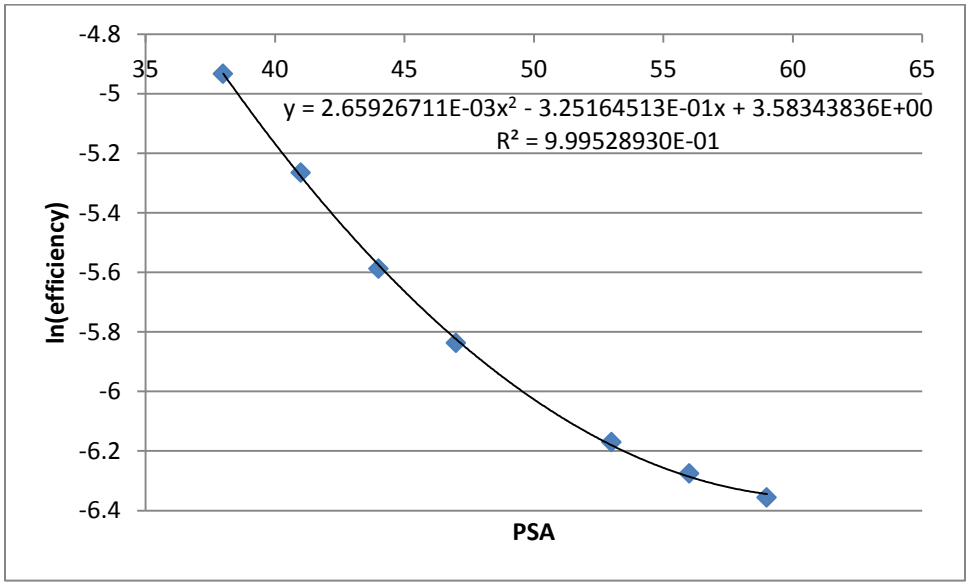

Figure 4.14 Sr-90 efficiency/PSA curve fit

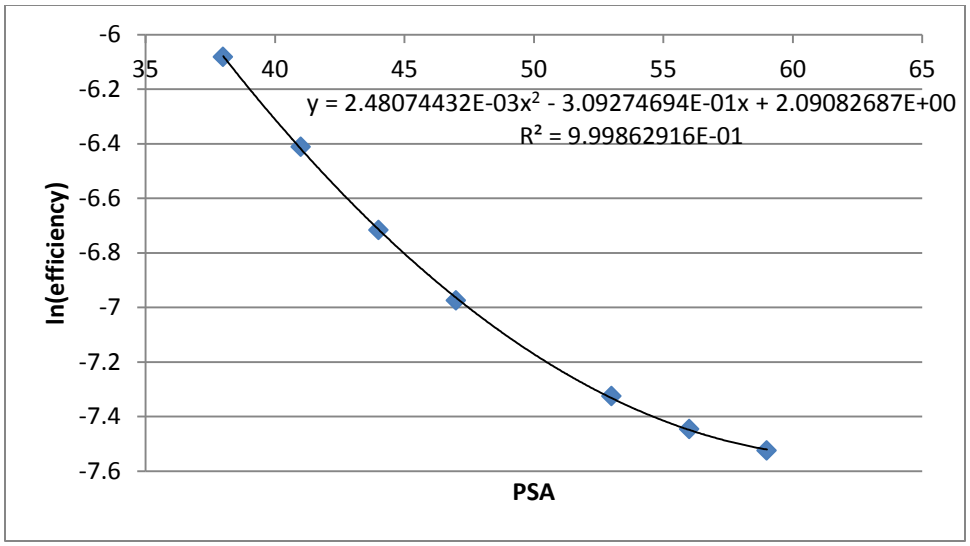

Figure 4.15 Cs-137 efficiency/PSA curve fit

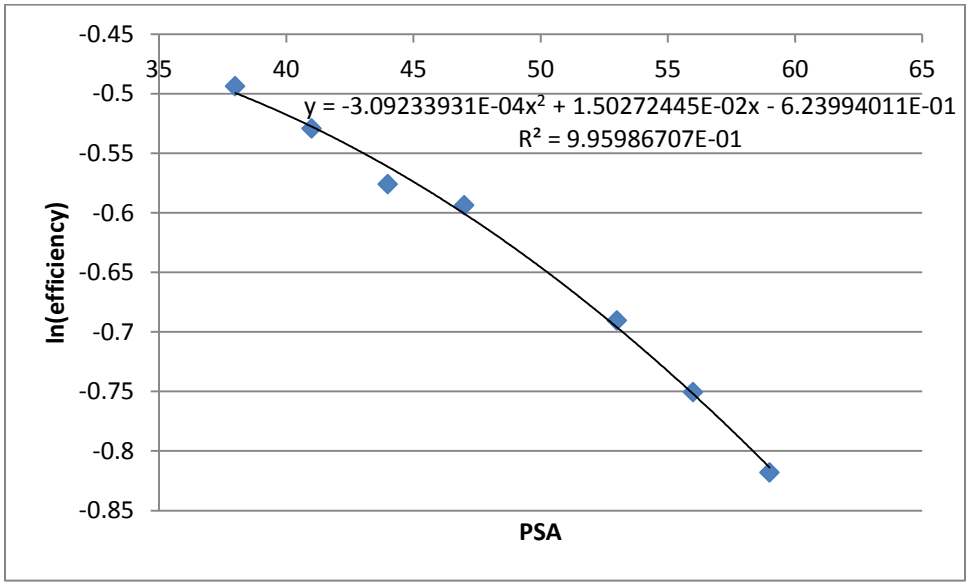

Figure 4.16 Am-241 efficiency/PSA curve fit

Table 4.26 Modeled counting efficiencies, alpha FWHM, Quantulus

	Co-60	Sr-90	Cs-137	Am-241
PSA	% in alpha peak	% in alpha peak	% in alpha peak	% in alpha peak
30	0.17%	2.29%	0.70%	63.67%
31	0.14%	1.94%	0.60%	63.42%
32	0.12%	1.66%	0.52%	63.14%
33	0.11%	1.42%	0.45%	62.82%
34	0.09%	1.23%	0.39%	62.47%
35	0.08%	1.07%	0.34%	62.07%
36	0.07%	0.93%	0.29%	61.64%
37	0.06%	0.82%	0.26%	61.18%
38	0.06%	0.72%	0.23%	60.68%
39	0.05%	0.64%	0.20%	60.15%
40	0.04%	0.57%	0.18%	59.59%
41	0.04%	0.51%	0.16%	59.00%
42	0.04%	0.46%	0.15%	58.37%
43	0.03%	0.42%	0.13%	57.72%
44	0.03%	0.38%	0.12%	57.04%
45	0.03%	0.35%	0.11%	56.33%
46	0.03%	0.32%	0.10%	55.59%
47	0.02%	0.30%	0.09%	54.84%
48	0.02%	0.27%	0.09%	54.06%
49	0.02%	0.26%	0.08%	53.25%
50	0.02%	0.24%	0.08%	52.43%
51	0.02%	0.23%	0.07%	51.59%
52	0.02%	0.22%	0.07%	50.73%
53	0.02%	0.21%	0.07%	49.85%
54	0.02%	0.20%	0.06%	48.96%
55	0.02%	0.19%	0.06%	48.05%
56	0.02%	0.19%	0.06%	47.13%
57	0.02%	0.18%	0.06%	46.20%
58	0.01%	0.18%	0.06%	45.26%
59	0.01%	0.18%	0.05%	44.32%
60	0.01%	0.17%	0.05%	43.36%

Table 4.27 Alpha MDA, MQA on Quantulus, 5 min, 1% int. level beta

PSA	MDA(alpha) (Bq)	MQA(alpha) (Bq)
30	0.502	1.770
31	0.466	1.663
32	0.435	1.569
33	0.406	1.486
34	0.381	1.413
35	0.358	1.348
36	0.338	1.291
37	0.320	1.241
38	0.305	1.197
39	0.290	1.159
40	0.278	1.126
41	0.267	1.097
42	0.257	1.073
43	0.248	1.052
44	0.240	1.035
45	0.234	1.021
46	0.228	1.010
47	0.223	1.002
48	0.219	0.996
49	0.215	0.993
50	0.213	0.992
51	0.211	0.994
52	0.210	0.998
53	0.209	1.004
54	0.209	1.012
55	0.209	1.023
56	0.211	1.035
57	0.213	1.050
58	0.215	1.067
59	0.218	1.086
60	0.222	1.108

Table 4.28 Alpha MDA, MQA on Quantulus, 35 min, 10% int. level beta

PSA	MDA(alpha) (Bq)	MQA(alpha) (Bq)
30	0.586	1.813
31	0.543	1.682
32	0.504	1.566
33	0.470	1.462
34	0.440	1.371
35	0.413	1.289
36	0.389	1.216
37	0.367	1.151
38	0.348	1.093
39	0.331	1.041
40	0.316	0.995
41	0.303	0.955
42	0.291	0.919
43	0.280	0.887
44	0.271	0.859
45	0.262	0.834
46	0.255	0.813
47	0.249	0.795
48	0.244	0.780
49	0.240	0.768
50	0.236	0.758
51	0.234	0.750
52	0.232	0.745
53	0.231	0.743
54	0.230	0.742
55	0.231	0.744
56	0.232	0.749
57	0.234	0.755
58	0.236	0.764
59	0.240	0.776
60	0.244	0.790

Table 4.29 Sr-90 MDA, MQA, 20-min count, int. level Cs-137 and Y-90

Co-60 int. lv. %	Sr-90 MDA (Bq)	1σ uncert	Sr-90 MQA (Bq)	1σ uncert
0.0%	8.10	0.25	24.66	0.77
0.1%	8.11	0.25	24.70	0.77
0.2%	8.13	0.25	24.75	0.77
0.3%	8.14	0.25	24.79	0.77
0.4%	8.15	0.25	24.84	0.77
0.5%	8.17	0.25	24.88	0.78
0.6%	8.18	0.26	24.93	0.78
0.7%	8.20	0.26	24.97	0.78
0.8%	8.21	0.26	25.02	0.78
0.9%	8.23	0.26	25.06	0.78
1%	8.24	0.26	25.11	0.78
2%	8.39	0.26	25.55	0.79
3%	8.53	0.26	25.98	0.80
4%	8.67	0.27	26.40	0.81
5%	8.81	0.27	26.82	0.82
6%	8.94	0.27	27.23	0.83
7%	9.08	0.28	27.64	0.84
8%	9.21	0.28	28.04	0.85
9%	9.34	0.28	28.43	0.86
10%	9.46	0.29	28.82	0.87
20%	10.66	0.32	32.45	0.96
30%	11.73	0.34	35.72	1.05
40%	12.72	0.37	38.71	1.13
50%	13.63	0.39	41.48	1.20
60%	14.48	0.42	44.09	1.27
70%	15.29	0.44	46.54	1.34
80%	16.06	0.46	48.87	1.40
90%	16.79	0.48	51.10	1.46
100%	17.49	0.50	53.23	1.52
200%	23.37	0.66	71.12	2.01
300%	28.05	0.79	85.33	2.41
400%	32.05	0.90	97.50	2.75
500%	35.60	1.00	108.30	3.05

Table 4.30 Sr-90 MDA, MQA, 20-min count, int. level Co-60 and Y-90

Cs-137 int. lv. %	Sr-90 MDA (Bq)	1σ uncert	Sr-90 MQA (Bq)	1σ uncert
0.0%	16.40	0.47	49.90	1.43
0.1%	16.40	0.47	49.91	1.43
0.2%	16.40	0.47	49.91	1.43
0.3%	16.40	0.47	49.91	1.43
0.4%	16.40	0.47	49.92	1.43
0.5%	16.40	0.47	49.92	1.43
0.6%	16.40	0.47	49.92	1.43
0.7%	16.40	0.47	49.93	1.43
0.8%	16.41	0.47	49.93	1.43
0.9%	16.41	0.47	49.93	1.43
1%	16.41	0.47	49.94	1.43
2%	16.42	0.47	49.97	1.43
3%	16.43	0.47	50.01	1.43
4%	16.44	0.47	50.04	1.43
5%	16.45	0.47	50.08	1.43
6%	16.46	0.47	50.11	1.43
7%	16.48	0.47	50.14	1.43
8%	16.49	0.47	50.18	1.44
9%	16.50	0.47	50.21	1.44
10%	16.51	0.47	50.25	1.44
20%	16.62	0.48	50.59	1.45
30%	16.73	0.48	50.92	1.46
40%	16.84	0.48	51.26	1.47
50%	16.95	0.49	51.59	1.48
60%	17.06	0.49	51.93	1.49
70%	17.17	0.49	52.25	1.50
80%	17.28	0.50	52.58	1.52
90%	17.38	0.50	52.91	1.53
100%	17.49	0.51	53.23	1.54
200%	18.52	0.54	56.36	1.64
300%	19.49	0.57	59.33	1.74
400%	20.42	0.60	62.15	1.83
500%	21.31	0.63	64.85	1.92

Table 4.31 Pu-238 MDA, MQA, 60-min count, 1% int. level beta

PSA	MDA(alpha) (Bq)	MQA(alpha) (Bq)
30	0.152	0.483
31	0.141	0.449
32	0.131	0.418
33	0.122	0.392
34	0.114	0.368
35	0.107	0.348
36	0.101	0.330
37	0.096	0.314
38	0.092	0.300
39	0.088	0.288
40	0.084	0.278
41	0.081	0.269
42	0.078	0.262
43	0.076	0.255
44	0.074	0.250
45	0.073	0.246
46	0.072	0.243
47	0.071	0.241
48	0.070	0.240
49	0.070	0.240
50	0.070	0.241
51	0.070	0.243
52	0.070	0.245
53	0.071	0.249
54	0.072	0.254
55	0.074	0.259
56	0.076	0.266
57	0.078	0.274
58	0.080	0.283
59	0.083	0.294
60	0.087	0.306

Table 4.32 Pu-238 MDA, MQA, 360-min count, 1% int. level beta

PSA	MDA(alpha) (Bq)	MQA(alpha) (Bq)
30	0.0619	0.1915
31	0.0572	0.1773
32	0.0531	0.1649
33	0.0495	0.1539
34	0.0463	0.1443
35	0.0436	0.1359
36	0.0411	0.1284
37	0.0389	0.1219
38	0.0371	0.1162
39	0.0354	0.1112
40	0.0340	0.1069
41	0.0327	0.1031
42	0.0316	0.0999
43	0.0307	0.0972
44	0.0299	0.0950
45	0.0293	0.0932
46	0.0288	0.0918
47	0.0284	0.0907
48	0.0282	0.0901
49	0.0281	0.0898
50	0.0280	0.0898
51	0.0281	0.0903
52	0.0283	0.0910
53	0.0286	0.0922
54	0.0291	0.0937
55	0.0297	0.0957
56	0.0304	0.0980
57	0.0312	0.1008
58	0.0322	0.1041
59	0.0334	0.1080
60	0.0347	0.1124

Table 4.33 Mixed-isotope target spike levels

Sample / % Int. level	Co-60	Cs-137	Sr-90	Pu-238	Am-241
U1	100%	100%	100%	100%	100%
U2	100%	100%	100%	1000%	0%
U3	100%	100%	100%	0%	100%
U4	10%	10%	10%	1000%	1000%
U5	0%	0%	0%	1000%	1000%
U6	100%	10%	10%	0%	0%
U7	10%	100%	100%	0%	0%

Table 4.34 Calculated activities for mixed-isotope samples

U1	Spiked Bq	1σ uncert	uncert %	Calc'ed Bq	1σ uncert	uncert%	Bias	1σ uncert	uncert %
Co-60	25498	575	2.25%	22706	509	2.2%	-10.9%	2.8%	-26%
Sr-90	3225	72	2.23%	2835	294	10%	-12.1%	9.3%	-77%
Cs-137	2082	47	2.25%	1744	40	2.3%	-16.2%	2.7%	-17%
Pu-238	0.02618	0.00059	2.25%	18.47	2.45	13%	70442%	9507%	13%
Am-241	0.2009	0.0045	2.25%	20.02	1.41	7.0%	9864%	735%	7%

U2	Spiked Bq	1σ uncert	uncert %	Calc'ed Bq	1σ uncert	uncert%	Bias	1σ uncert	uncert %
Co-60	22685	513	2.26%	19867	447	2.2%	-12.4%	2.8%	-22%
Sr-90	3397	76	2.24%	2729	270	9.9%	-19.7%	8.1%	-41%
Cs-137	1767	40	2.26%	1495	35	2.3%	-15.4%	2.7%	-18%
Pu-238	0.27644	0.00626	2.26%	4.28	2.18	51%	1447%	790%	55%
Am-241				16.12	1.25	7.8%			

U3	Spiked Bq	1σ uncert	uncert %	Calc'ed Bq	1σ uncert	uncert%	Bias	1σ uncert	uncert %
Co-60	22474	511	2.28%	20041	453	2.3%	-11%	2.9%	-26%
Sr-90	2859	65	2.26%	2981	267	9.0%	4%	9.6%	227%
Cs-137	1688	38	2.28%	1427	33	2.3%	-15%	2.8%	-18%
Pu-238				2.36	2.17	92%			
Am-241	2.2490	0.0510	2.27%	16.78	1.25	7.5%	646%	58%	9%

U4	Spiked Bq	1σ uncert	uncert %	Calc'ed Bq	1σ uncert	uncert%	Bias	1σ uncert	uncert %
Co-60				0.2	0.0	23.6%			
Sr-90	294.6	6.9	2.33%	281.7	10.5	3.7%	-4.4%	4.2%	-96%
Cs-137	162.9	3.8	2.33%	163.5	4.0	2.4%	0.3%	3.4%	1008%
Pu-238	0.27628	0.00645	2.34%	0.08	0.19	257%	-73%	70.4%	-97%
Am-241	2.2918	0.0533	2.33%	2.64	0.13	5.1%	15%	6.5%	43%

U5	Spiked Bq	1σ uncert	uncert %	Calc'ed Bq	1σ uncert	uncert%	Bias	1σ uncert	uncert %
Co-60				0.1	0.1	70.7%			
Sr-90				0.6	0.0	5.6%			
Cs-137				0.0	0.0	-70.8%			
Pu-238	0.27227	0.00622	2.28%	0.13	0.26	199%	-52%	96%	-183%
Am-241	2.4018	0.0546	2.27%	2.74	0.20	7.2%	14%	9%	60%

U6	Spiked Bq	1σ uncert	uncert %	Calc'ed Bq	1σ uncert	uncert%	Bias	1σ uncert	uncert %
Co-60	23436	534	2.28%	21156.5	479	2.3%	-10%	2.9%	-30%
Sr-90	308	7	2.28%	187	257	137%	-39%	84%	-213%
Cs-137	151.3	3.5	2.28%	144.6	6.7	4.6%	-4.4%	4.9%	-112%
Pu-238				-17.96	2.13	-12%			
Am-241				15.96	1.22	8%			

Table 4.34, continued: Calculated activities for mixed-isotope samples

U7	Spiked Bq	1σ uncert	uncert %	Calc'ed Bq	1σ uncert	uncert%	Bias	1σ uncert	uncert %
Co-60	2273	51	2.25%	2273	52	2.3%	0.0%	3.2%	63163%
Sr-90	2901	65.3	2.25%	2518	103	4.1%	-13.2%	4.1%	-31%
Cs-137	1753	39.8	2.27%	1726	40	2.3%	-1.5%	3.2%	-206%
Pu-238				3.89	0.91	23.5%			
Am-241				1.50	0.55	36.8%			

Table 4.35 Spike activity in samples UD1 and UD2

UD1 activity		1σ uncert	
Co-60 Activity (Bq)	19133	72	0.38%
Sr-90 Activity (Bq)	3047.4	7.3	0.24%
Cs-137 Activity (Bq)	1677.3	6.0	0.36%
Pu-238 Activity (Bq)	0.2974	0.0011	0.36%
Am-241 Activity (Bq)	2.1850	0.0071	0.32%

UD2 activity		1σ uncert	
Co-60 Activity (Bq)	16761	64	0.38%
Sr-90 Activity (Bq)	2669.5	6.4	0.24%
Cs-137 Activity (Bq)	1469.3	5.3	0.36%
Pu-238 Activity (Bq)	0.26053	0.00093	0.36%
Am-241 Activity (Bq)	1.9141	0.0062	0.33%

Table 4.36 Theoretical activity to be extracted by DIPEX

	Bq	1σ uncert	uncert %
Pu-238 in UD1 Org	0.2528	0.0040	1.58%
Am-241 in(?) UD1 Org	1.857	0.029	1.58%
Pu-238 in UD2 Org	0.2214	0.0035	1.58%
Am-241 in(?) UD2 Org	1.6270	0.0257	1.58%

Table 4.37 Calculated alpha activity in UD1 org and UD2 org

Sample	Activity	Uncertainty
UD1 Org	0.2703 ± 0.0051 Bq	1.89% uncertainty at 1σ
UD2 Org	0.2520 ± 0.0049 Bq	1.94% uncertainty at 1σ

Table 4.38 UD1 Org calculated activities – HPGe

Calc'ed Co-60 activity (Bq)	1σ uncert	uncert %	Co-60 extracted fraction	1σ uncert	uncert %
0.226	0.101	44.72%	0.0014%	0.0006%	44.79%
Calc'ed Cs-137 activity (Bq)	1σ uncert	uncert %	Cs-137 extracted fraction	1σ uncert	uncert %
0.365	0.098	26.84%	0.0256%	0.0069%	26.95%
Calc'ed Am-241 activity (Bq)	1σ uncert	uncert %	Am-241 extracted fraction	1σ uncert	uncert %
0.047	0.054	113.3%	2.55%	2.89%	113.34%

Table 4.39 UD2 Org calculated activities – HPGe

Calc'ed Co-60 activity (Bq)	1σ uncert	uncert %	Co-60 extracted fraction	1σ uncert	uncert %
0.024	0.024	100.00%	0.0002%	0.0002%	100.03%
Calc'ed Cs-137 activity (Bq)	1σ uncert	uncert %	Cs-137 extracted fraction	1σ uncert	uncert %
0.240	0.058	24.27%	0.0192%	0.0047%	24.39%
Calc'ed Am-241 activity (Bq)	1σ uncert	uncert %	Am-241 extracted fraction	1σ uncert	uncert %
0.096	0.046	48.1%	5.91%	2.84%	48.13%

CHAPTER 5. SUMMARY, DISCUSSION, AND CONCLUSIONS

5.1 Summary and discussion of results

The work presented herein shows that a rapid method for detecting, and in many cases quantifying, the activity from five separate isotopes in a single 5-ml urine sample can be developed. The method developed in this work requires minimal sample preparation time – less than 5 minutes if no liquid-liquid separation is necessary; approximately 20 minutes per sample if a liquid-liquid separation is performed.

Using activated carbon (AC) powder filtration to remove organics from real urine samples produces a highly reproducible lack of any color or chemical quenching effect when the resulting solutions are measured on a liquid scintillation counter. As a result, the energies associated with individual channel regions in one measured spectrum directly correspond to the same equivalent energies in other spectra. Therefore, rather than energy-calibrating and fitting the data in each spectrum individually, all spectra can be mathematically treated the same way on a per-channel and per-channel-region basis. This allows for the use of an isotopic calibration standard to determine the per-channel count rate for a particular isotope in the Quantulus, regardless of the pre-AC-filtration coloration of each sample.

Measuring identical LS vials with essentially identical volumes of same-density liquids on the HPGe detector and always placing the sample in the exact same spot on top of the detector allow for reproducible geometry from one sample to the next. Therefore, the photopeak efficiency of each isotope remains the same from one sample measurement to the next.

The MDAs and MQAs associated with this method and determined in this work for Co-60, Sr-90, and Cs-137 are more than sufficient to detect and quantify activity levels well below

their associated intervention levels, even when in combination with each other, at very short count times: all three of these isotopes can be quantified at activities equivalent to 10% or less of their associated intervention levels in count times of 10 minutes or less.

High detector dead time distorts HPGe spectra and is the likely source of the significant and consistent negative bias for the calculated Co-60 and Cs-137 activities in samples U1, U2, U3, and U6. The biases for these isotopes are much lower in samples U4 and U7, which have no Co-60 activity and 10% of the Co-60 activity in the aforementioned samples, respectively. Dilution of samples with significant Co-60 activity (i.e. greater than 10% of the intervention level) is recommended in order to avoid these problems associated with detector dead time.

The bias associated with Sr-90 measurements fluctuated quite a bit in these experiments, and was usually negative. It is not entirely clear why this is the case; however, one possible explanation is that all efficiency calibration calculations were based on the measurements from a single calibration sample for each isotope. While multiple calibration samples would have been optimal, both time and resource constraints limited the available calibration samples to one per isotope.

Despite the biases associated with Sr-90 measurements calculated from this method, Sr-90 activity was still both detectable and quantifiable at or near its intervention level in all mixed-isotope samples. The maximum bias magnitude for any Sr-90 measurement was -39.2% in sample U6; however, Sr-90 was present at only ~10% of the intervention level in this sample. As this is a screening method, these biases are almost certainly acceptable, as the detected and quantified activity would still be sufficient to flag the sample for further analysis and to alert medical staff of the potential need to treat the exposed individual.

For Am-241 and Pu-238, the associated MDAs and MQAs only approach the intervention level for reasonable count times if the isotopes are present individually. Even with optimal alpha/beta discrimination at PSA setting 53, the bleed-over in the alpha spectrum from beta pulses improperly classified as alpha pulses is significant enough if activity from all three beta/gamma isotopes is present in a sample at even 1% of the isotopes' respective intervention levels to require prohibitively long count times to detect the alpha emitters at their intervention levels: in this situation, Am-241 can be detected, but not quantified, at its intervention level only after a ~2-hour count. Quantification of Am-241 activity at its associated intervention level in this situation would require more than 16 hours.

The Pu-238 and Am-241 activities calculated in samples U1, U2, and U3 are essentially entirely meaningless, because of the high levels of beta/gamma activity in these samples – though their associated calculated uncertainties do not necessarily belie such. That is why it is imperative to run the MDA and MQA calculations for Pu-238 and Am-241 when making these measurements: the MDA and MQA provide the best descriptions for the limitations of this method, and the MDA/MQA calculations for these samples would clearly show that there is no way to detect any alpha activity in these samples given reasonable count times.

Sample U4 provides a "best-case" scenario for detecting and quantifying alpha activity: the beta/gamma isotopes are present at 10% of their respective intervention levels, while the alpha isotopes are present at 10x their respective intervention levels. In this sample, the Am-241 activity was overestimated by 15.1%, which resulted in the underestimation of the Pu-238 activity by 72.6% - however, the calculated gross alpha activity of 2.72 Bq was not nearly as far off: given the total spiked activity of 2.57 Bq, the bias on the gross alpha activity calculation was

only 5.8%. A longer count time on the HPGe detector would likely have allowed for a more accurate Am-241 determination, and therefore a more accurate Pu-238 determination.

Given the constraints placed on the alpha MDA and MQA from even minimal beta/gamma activity, if beta/gamma activity is detected in a sample, a liquid-liquid separation using an all-organic extractive scintillator is recommended in order to improve the effective figure of merit for counting the alpha-emitting isotopes. The results from the DIPEX extraction experiments suggest that this additional step should allow for the detection and quantification of the alpha-emitting isotopes at their intervention levels, even if the original sample contains significant beta/gamma activity.

It is not entirely clear why the DIPEX extractant used in this research only extracted the Pu-238 and did not extract the Am-241 in any significant quantity, but it is very clear from the count rates on the respective detectors that that is what happened. It is also intriguing that the results indicate that the Mohr's salt added to the sample apparently did not reduce the Pu IV+ to Pu III+. If it had reduced the Pu, the Pu probably would not have been extracted, since the other trivalent radionuclides were not appreciably extracted. In addition to the lack of extraction of Am III+, the lack of extraction of any appreciable fraction of the Y III+ suggests that there is something in the acidified urine matrix that is either chemically or kinetically inhibiting DIPEX from extracting trivalent ions.

However, the fact that Pu (presumably IV+) was extracted and Am III+ was not does not discount the usefulness of DIPEX as an extractant to be used in extractive scintillators for a rapid screening method. Indeed, as Pu-238 is the most difficult isotope of all those studied in this work to quantify, and this extraction allowed for its extraordinarily accurate quantification with minimal count time, it could be argued that the extraction of Pu only is actually superior to the

extraction of both Pu and Am. While it makes the Am-241 more difficult to quantify, the fact remains that Am-241 can be detected – and eventually quantified, with a long enough count time – by its gamma emission. Alternatively, if the Pu-238 is quantitatively extracted, the Am-241 can also be quantified by counting the aqueous fraction on the Quantulus detector (since no Pu-238 would remain in the aqueous fraction). So, even if it is not extracted into the organic phase, the Am-241 activity present in a sample can still be calculated in a variety of ways – and the lack of interference from Am-241 makes quantification of Pu-238 both trivial and accurate. Of course, it would be optimal to find an extractant that extracted both Pu-238 and Am-241 (but still no significant fraction of the beta/gamma emitters), as the extraction of both of the alpha emitters would allow for the quickest and most accurate quantification thereof.

Additionally, the fact that a strong reducing agent such as Mohr's salt seemingly did not reduce Pu to Pu III+ in acidified urine may suggest that Pu in an acidified urine sample is likely to stay in its tetravalent oxidation state in this matrix, as it is unlikely that a reducing agent stronger than Mohr's salt would be naturally present either in the body or in the urine sample. Of course, our understanding of the complicated chemistry of radionuclides in this matrix is relatively poor.

While it would be optimal to determine the chemistry behind the apparent lack of trivalent ion extraction by the DIPEX in these experiments, both time and resource constraints limited the scope of this work.

It is also worth noting that spiking urine samples *ex vivo,* as was done in these experiments, does not necessarily produce samples that are entirely representative of the chemistry of real urine samples from individuals that have been exposed to internal contamination. However, it is possible that the rapid acidification of such samples would

solubilize the radionuclides of interest such that they would behave chemically similarly to the spiked radionuclides in these experiments.

An additional consideration is that the combined doses associated with each isotope present in a urine sample must be considered: if all five isotopes are present at the intervention level, this scenario would result in a 50-year committed effective dose of five times the 0.5-Sv 50-year committed effective dose limit that the intervention level represents. Accordingly, it is possible that all five isotopes could be present, each individually below the intervention level, but that their combined activity would result in a dose higher than the 0.5-Sv limit. In such a scenario, it is likely that medical intervention would be necessary in order to reduce the exposed individual's 50-year committed effective dose to below the 0.5-Sv limit.

5.2 Further research

The two areas of this work with the most room for further investigation are the calibration of the HPGe and Quantulus spectra, and the use of extractive scinitillators to perform liquid-liquid extractions of the alpha-emitting isotopes.

More calibration standards would allow for a more robust calibration of the individual detectors as well as of the link between them. Additionally, measurements of calibration standards over a wide range of activity levels could allow for the modeling of the effect of increasing dead time on both spectrum shape and counting efficiency.

As previously mentioned, further experiments with other organic extractants in extractive scintillators[61,62] – in addition to those using DIPEX-based extractants – would allow for a better understanding of both the advantages and limitations of using these different extractants to pull one or more of the alpha-emitting isotopes away from the beta/gamma emitters (or vice-versa). The kinetics of liquid-liquid extractions are extremely fast, and the steps for mixing,

centrifuging, and pipetting the organic phase off of the top of each sample could be automated in order to increase sample throughput.

5.3 Conclusion

In an emergency situation involving a potential public exposure to radioactive material, those responding to the incident must take advantage of all available tools. Time- and labor-intensive chemical separations can be avoided while still quantitatively determining both isotopic identification and the activity of each isotope present in a urine sample for a mixture of at least five isotopes. The work presented herein suggests that quantification of activity from additional isotopes may also be possible using similar methods, albeit with increased associated uncertainties for the calculation of each isotope's activity.

REFERENCES

1. Beyer, D.; Dalheimer, A. R.; Gunther, E. W.; Henrichs, K. "Monitoring by Excretion Analysis: Results of Interlaboratory Comparisons." Radiation Protection Dosimetry 79 (1998) 513-516

2. Mingote, R. M.; Barbeira, P. J. S.; Rocha, Z. "Methodology for rapid tritium determination in urine." Journal of Radioanalytical and Nuclear Chemistry 269.2 (2006) 475-479

3. Shiraishi, K.; Ko, S.; Arae, H.; Ayama, K. "Rapid analysis technique for strontium, thorium, and uranium in urine samples." Journal of Radioanalytical and Nuclear Chemistry 273.2 (2007) 307-310

4. Olsen, S. C. "Determination of actinides in a variety of matrices." Czechoslovak Journal of Physics 53.1(Suppl.) (2003) A313-324

5. Maxwell III, S. L. "Rapid column extraction method for actinides and 89/90Sr in water samples." Journal of Radioanalytical and Nuclear Chemistry 267.3 (2006) 537-543

6. Maxwell III, S. L.; Culligan, B. K. "Rapid column extraction method for actinides in soil." Journal of Radioanalytical and Nuclear Chemistry 270.3 (2006) 699-704

7. Duffey, J. M.; Case, F. I.; Metzger, R. L.; Jessop, B. J.; Schweitzer, G. K. "Development of a rapid procedure for the measurement of uranium in drinking water by PERALS® spectrometry." Journal of Radioanalytical and Nuclear Chemistry 221.1-2 (1997) 115-122

8. Chobola, R.; Mell, P.; Daroczi, L.; Vincze, A. "Rapid determination of radiostrontium isotopes in samples of NPP origin." Journal of Radioanalytical and Nuclear Chemistry 267.2 (2006) 297-304

9. Maxwell III, S. L. "Rapid analysis of emergency urine and water samples." Journal of Radioanalytical and Nuclear Chemistry 275.3 (2008) 497-502

10. Maxwell III, S. L.; Culligan, B. K. "New column separation method for emergency urine samples." Journal of Radioanalytical and Nuclear Chemistry 279.1 (2009) 105-111

11. Maxwell III, S. L.; Culligan, B. K.; Jones, V. D.; Nichols, S. T.; Noyes, G. W.; Bernard, M. A. "Rapid Determination of ^{237}Np and Plutonium Isotopes in Urine by Inductively-Coupled Plasma Mass Spectrometry and Alpha Spectrometry." Health Physics 101.2 (2011) 180-186

12. Dai, X.; Kramer-Tremblay, S. "An Emergency Bioassay Method for Actinides in Urine." Health Physics 101.2 (2011) 144-147

13. Thakkar, A. H. “A rapid sequential separation of actinides using Eichrom’s extraction chromatographic material.” Journal of Radioanalytical and Nuclear Chemistry 252.2 (2002) 215-218

14. International Atomic Energy Agency, “Code of Conduct on the Safety and Security of Radioactive Sources,” 14-16. Vienna: IAEA. 2004.

15. Currie, L. A. “Limits for Qualitative Detection and Quantitative Determination.” Analytical Chemistry 40.3 (1968) 586-593

16. McDowell, W. J. *Liquid Scintillation Alpha Spectrometry.* Boca Raton: CRC, 1994.

17. Alzitzoglou, T. “Radioactivity Determination of Individual Radionuclides In A Mixture By Liquid Scintillation Spectra Deconvolution”, presented 3-7 Sep 2007 at 16th ICRM, Cape Town, South Africa.

18. Unpublished CDC file. Provided by K. G. W. Inn, August 2007, Gaithersburg, MD.

19. Ahmedna, M.; Marshall, W. E.; Husseiny, A. A.; Rao, R. M.; Goktepe, I. “The use of nutshell carbons in drinking water filters for removal of trace metals.” Water Research 38.4 (2004) 1062-1068

20. Caccin, M.; Giacobbo, F.; Da Ros, M.; Besozzi, L.; Mariani, M.; “Adsorption of uranium, cesium and strontium onto coconut shell activated carbon.” Journal of Radioanalytical and Nuclear Chemistry 297.1 (2013) 9-18

21. “Specifications: 1220 QUANTULUS Ultra Low Level Liquid Scintillation Spectrometer.” Perkin-Elmer. Web. 10 Mar 2015. http://www.perkinelmer.com/cmsresources/images/46-73870spc_1220quantulus.pdf

22. ICRP, 2012. Compendium of Dose Coefficients based on ICRP Publication 60. ICRP Publication 119. Annals of the ICRP 41(Suppl.)

23. Voelz, G. L. “Plutonium and Health: How great is the risk?” Los Alamos Science 26 (2000) 74-89

24. Moss, W; Eckhardt, R. “The Human Plutonium Injection Experiments.” Los Alamos Science 23 (1995) 177-233

25. Puncher, M.; Harrison, J. D. “Uncertainty analysis of doses from ingestion of plutonium and americium.” Radiation Protection Dosimetry 148.3 (2012) 284-296

26. Fons, J.; Zapata-Garcia, D.; Tent, J.; Llaurado, M. “Simultaneous Determination Of Gross Alpha, Gross Beta And ^{226}Ra In Natural Water By Liquid Scintillation Counting.” Journal of Environmental Radioactivity 125.(2013): 56-60.

27. Todorovic, N.; Nikolov, J.; Tenjovic, B.; Bikit, I.; Veskovic, M. “Establishment Of A Method For Measurement Of Gross Alpha/Beta Activities In Water From Vojvodina Region.” Radiation Measurements 47.11/12 (2012): 1053-1059

28. Bhade, S. P. D.; Reddy, P. J.; Narayanan, K. K.; Babu, D. A. R.; Sharma, D. N. “Standardization Of Calibration Procedures For Quantification Of Gross Alpha And Gross Beta Activities Using Liquid Scintillation Counter.” Journal of Radioanalytical and Nuclear Chemistry 284.2 (2010): 367-375.

29. Kleinschmidt, R. I. “Gross alpha and beta activity analysis in water—a routine laboratory method using liquid scintillation analysis.” Applied Radiation and Isotopes 61.2-3 (2004): 333-338

30. Zapata-Garcia, D.; Llaurado, M.; Rauret, G. “Establishment of a method for the rapid measurement of gross alpha and gross beta activities in sea water.” Applied Radiation and Isotopes 67.5 (2009): 978-981.

31. Happel, S.; Beyermann, M.; Letessier, P.; Bombard, A.; Thakkar, A. H.; Horowitz, E. P. “Gross alpha determination in salt rich water samples using an extraction chromatographic resin and LSC.” Journal of Radioanalytical and Nuclear Chemistry 277.1 (2008) 241-247

32. Jaggi, M.; Rollin, S.; Corcho Alvarado, J. A.; Eikenberg, J. “Determination of 241Pu in nuclear waste slurries: A comparative study using LSC and ICP-MS.” Applied Radiation and Isotopes. 70.2 (2012) 360-364

33. Hou, Xiaolin. “Analysis of Urine for Pure Beta Emitters: Methods and Application.” Health Physics 101.2 (2011) 159-169

34. Oh, J. S.; Warwick, P. E.; Croudace, I. W.; Lee, S. H. “Rapid Measurement Of Pu Activity At Environmental Levels Using Low-Level Liquid Scintillation Analysis.” Journal Of Radioanalytical & Nuclear Chemistry 298.1 (2013): 353-359

35. Karacan, F. “The simple radiochemical determination of Sr-90 in environmental solid samples by solvent extraction.” Journal of Radioanalytical and Nuclear Chemistry 288.3 (2011) 685-691

36. Komosa, A.; Piekarz, M. “Optimization of plutonium extraction with methyltrioctylammonium chloride preceding its determination by liquid scintillation spectrometry.” Nukleonika 55.2 (2010) 137-141

37. Pujol, L. “Simultaneous determination of radium and uranium activities in natural water samples using liquid scintillation counting.” Analyst 123.2 (1998) 399-403

38. Escobar, V. G.; Tome, F. V.; Lozano, J. C.; Sanchez, A. M. “Determination of Rn-222 and Ra-226 in aqueous samples using a low-level liquid scintillation counter.” Applied Radiation and Isotopes 47.9-10 (1996) 861-867

39. Salonen, L. “A Rapid Method for Monitoring of Uranium and Radium in Drinking-Water.” Science of the Total Environment 130 (1993) 23-25

40. Whyte, J. C.; Ungar, R. K. “Low Level ^{90}Sr (Cerenkov) and ^{226}Ra (α/β LSC) analysis in environmental samples using an automated chromatography system and LSC” Proceedings of BAER 47th Annual Conference. Honolulu, Nov 3-8, 2001.

41. Remetti, R.; Franci, D. “ABCD- Tool, A Software Suite For The Analysis Of A/B Spectra From Liquid Scintillation Counting.” Journal of Radioanalytical and Nuclear Chemistry 292.3 (2012): 1115-1122

42. Remetti, R.; Sessa, A. “Beta Spectra Deconvolution For Liquid Scintillation Counting.” Journal of Radioanalytical and Nuclear Chemistry 287.1 (2011): 107-111

43. Neuer, M. J. “Spectral identification of a ^{90}Sr source in the presence of masking nuclides using Maximum-Likelihood deconvolution.” Nuclear Instruments and Methods in Physics Research A 728 (2013): 73-80

44. Pollanen, R.; Karhunen, T.; Siiskonen, T.; Toivonen, H.; Pelikan, A. “Deconvolution of alpha spectra from hot particles.” Radioactive Particles in the Environment (2009) 209-220

45. Yoon, S.; Ha, W. H.; Yoo, J.; Lee, S. S. “Screening of Alpha- and Beta-Emitting Radionuclides Using Liquid Scintillation Counting and Monitoring Procedures in Radiation Emergencies.” Health Physics 107.5 (2014): 382-387

46. Demir, D.; Eroglu, M.; Tursucu, A. “Studying of characteristics of the HPGe detector for radioactivity measurements.” Journal of Instrumentation 8 (2013) P10027

47. Scarpitta, S. C.; Fisenne, I. M. “Calibration of a liquid scintillation counter for alpha, beta, and Cerenkov counting.” Environmental Measurements Laboratory EML-583. New York: July 1996.

48. Villa-Alfageme, M.; Hurtado, S.; Manjon, G.; Garcia-Tenorio, R. “Calibration And Measurement Of 210 Pb Using Two Independent Techniques.” Radiation Measurements 42.9 (2007): 1552-1560

49. Castagnet, X.; Amabile, J. C.; Cazoulat, A.; Lecompte, Y.; de Carbonnieres, H.; Laroche, P. “Diagnosis of Internal Radionuclide Contamination by Mobile Laboratories.” Radiation Protection Dosimetry 125.1-4 (2007) 469-471

50. La Rosa, J.; Outola, I.; Crawford, E.; Nour, S.; Kurosaki, H. “Radiochemical measurement of ^{237}Np in a solution of mixed radionuclides: Experiences in chemical separation and alpha-spectrometry.” Journal of Radioanalytical and Nuclear Chemistry 227.1 (2008) 11-18

51. Pates, Jacqueline M. “Implications of beta energy and quench level for alpha/beta liquid scintillation spectrometry calibration.” Analyst 123.10 (1998) 2201-2207

52. Puhakainen, M.; Heikkinen, T. “Tritium in the urine in Finnish people.” Radiation Protection Dosimetry 128.2 (2008) 254-257

53. Komosa, A.; Slepecka, K. “Effect of liquid scintillating cocktail volume on H-3 and C-14 measurement parameters using a Quantulus spectrometer.” Nukleonika 55.2 (2010) 155-161

54. “Standard Reference Materials.” National Institute of Standards and Technology. 2015. Web. 10 Mar. 2015. http://www.nist.gov/srm/

55. “Full width at half maximum.” Wikipedia, The Free Encyclopedia. Wikimedia Foundation, Inc. 15 November 2014. Web. 10 Mar. 2015.

56. Daniel, H. “Shapes of Beta-Ray Spectra.” Reviews of Modern Physics 40.3 (1968) 659-672

57. Goddu, S. M.; Howell, R. W.; Giuliani, D. C.; Rao, D. V. “Biological dosimetry of bone marrow for incorporated yttrium-90.” Journal of Nuclear Medicine 39.3 (1998) 547-552

58. Li, W. B.; Hollriegl, V.; Roth, P.; Oeh, U. “Human biokinetics of strontium. Part I: Intestinal absorption rate and its impact on the dose coefficient of ^{90}Sr after ingestion.” Radiation and Environmental Biophysics 45 (2006) 115-124

59. Bauer, G. C.; Ray, R.D. “Kinetics of Strontium Metabolism in Man.” Journal of Bone and Joint Surgery 40 (1958) 171-186

60. “Decay Mechanisms.” MIT NSE Virtual Reading Room. Fall 2001. Web. 10 Mar. 2015. http://mightylib.mit.edu/course%20materials/22.01/fall%202001/decay%20mechanisms.pdf

61. Charyulu, M. M. “Extraction of Am(III) from different acid media by di-2-ethyl hexyl phosphoric acid containing phosphorous pentoxide.” Journal of Radioanalytical and Nuclear Chemistry 247.3 (2001) 553-555

62. Grahek, Z.; Eskinja, I.; Kosutic, K.; Lulic, S.; Kvastek, K. “Isolation of radioactive strontium from natural samples: A semi-automatic procedure.” Journal of Radioanalytical and Nuclear Chemistry 241.3 (1999) 617-626

APPENDIX I. CDC CHART OF INTERVENTION LEVELS

Table A1.1 Unpublished CDC chart with intervention levels

50 year Committed Effective Dose Coefficients (Sv/Bq) for Single Inhalation (F, M and S) and Single Ingestion				
List of isotopes	**E(Sv/Bq)_Type F**	**E(Sv/Bq)_Type M**	**E(Sv/Bq)_Type S**	**E(Sv/Bq)_Ingestion**
Co-60	5.26E-09	1.02E-08	3.07E-08	3.41E-09
Sr-90	2.39E-08	3.55E-08	1.57E-07	2.76E-08
Cs-137	4.66E-09	9.68E-09	3.92E-08	1.35E-08
Pu-238	1.07E-04	4.58E-05	1.59E-05	2.26E-07
Am-241	9.59E-05	4.15E-05	1.59E-05	2.03E-07
Intake Excretion Fractions (µCi in 24-h Urine / µCi Intake) at t = 1 day after the intake for Single Inhalation (F, M and S) and Single Ingestion				
List of isotopes	**U-24h (t=1d)_Type F**	**U-24h (t=1d)_Type M**	**U-24h (t=1d)_Type S**	**U-24h (t=1d)_Ingestion**
Co-60	7.94E-02	1.30E-02	6.16E-04	2.75E-02
Sr-90	5.43E-02	8.49E-03	4.17E-04	5.65E-02
Cs-137	5.55E-03	6.40E-04	2.77E-05	1.58E-02
Pu-238	1.97E-03	2.00E-04	2.04E-06	3.37E-06
Am-241	1.50E-02	1.54E-03	2.17E-05	2.96E-05
50 year Committed Effective Dose Coefficient (Sv/µCi) for Single Inhalation (F, M and S) and Single Ingestion				
List of isotopes	**E(Sv/µCi Intake)_Type F**	**E(Sv/µCi Intake)_Type M**	**E(Sv/µCi Intake)_Type S**	**E(Sv/µCi Intake)_Ingestion**
Co-60	1.95E-04	3.77E-04	1.14E-03	1.26E-04
Sr-90	8.84E-04	1.31E-03	5.81E-03	1.02E-03
Cs-137	1.72E-04	3.58E-04	1.45E-03	5.00E-04
Pu-238	3.96E+00	1.69E+00	5.88E-01	8.36E-03
Am-241	3.55E+00	1.54E+00	5.88E-01	7.51E-03
Urinary Excretion Concentration (µCi/L) at 1 day After a Single Intake Corresponding to a Committed Effective Dose of 0.5 Sv				
List of isotopes	**U-24h (t=1d) (µCi/L) @ E=0.5 Sv_Type F**	**U-24h (t=1d) (µCi/L) @ E=0.5 Sv_Type M**	**U-24h (t=1d) (µCi/L) @ E=0.5 Sv_Type S**	**U-24h (t=1d) (µCi/L) @ E=0.5 Sv_Ingestion**
Co-60	1.27E+02	1.08E+01	1.69E-01	6.81E+01
Sr-90	1.92E+01	2.02E+00	2.24E-02	1.73E+01
Cs-137	1.01E+01	5.58E-01	5.97E-03	9.88E+00
Pu-238	1.56E-04	3.69E-05	1.08E-06	1.26E-04
Am-241	1.32E-03	3.13E-04	1.15E-05	1.23E-03

D: Urinary Excretion Concentration (µCi/L) at 1 day After a Single Intake Corresponding to a Committed Effective Dose of 0.5 Sv = 0.5 (Sv) * B / (C * 1.6 L of urine/day)				
	Bq/5ml for .5 Sv type F	Bq/5ml for .5 Sv type M	Bq/5ml for .5 Sv type S	Bq/5ml for .5 Sv ingestion
Co-60	**2.36E+04**	**1.99E+03**	**3.14E+01**	**1.26E+04**
Sr-90	**3.55E+03**	**3.74E+02**	**4.15E+00**	**3.20E+03**
Cs-137	**1.86E+03**	**1.03E+02**	**1.10E+00**	**1.83E+03**
Pu-238	**2.88E-02**	**6.82E-03**	**2.00E-04**	**2.33E-02**
Am-241	**2.44E-01**	**5.80E-02**	**2.13E-03**	**2.28E-01**

Calculation Notes:

A: 50 year Committed Effective Dose Coefficients (Sv/Bq) for Single Inhalation (Types F, M and S) and Single Ingestion; LANL calculations checked against ICRP CD (ICRP Database of Dose Coefficients)

B: Intake Excretion Fractions (µCi in 24-h Urine / µCi Intake) at t = 1 day after the intake for Single Inhalation (Types F, M and S) and Single Ingestion

C: 50 year Committed Effective Dose Coefficient (Sv/µCi) for Single Inhalation (Types F, M and S) and Single Ingestion = A * 37000 (Bq/µCi)

APPENDIX II – SPIKING DATA

Table A2.1 Spiking data, calibration & mixed-isotope samples

U1 – Mixed Isotopes: all isotopes at approx. intervention level

12/25/2014 8:01	Bq	uncert	uncert %
Co-60 Activity (Bq)	**25526**	**97**	0.38%
Sr-90 Activity (Bq)	**3677**	**9**	0.24%
Cs-137 Activity (Bq)	**2083**	**8**	0.37%
Pu-238 Activity (Bq)	**0.02985**	**0.00011**	0.37%
Am-241 Activity (Bq)	**0.2291**	**0.0008**	0.34%

U2 – Mixed isotopes: beta/gamma at approx. intervention level; Pu-238 at 10x int. level, no Am-241

12/24/2014 18:28	Bq	uncert	uncert %
Co-60 Activity (Bq)	**22715**	**86**	0.38%
Sr-90 Activity (Bq)	**3833**	**9**	0.24%
Cs-137 Activity (Bq)	**1768**	**7**	0.38%
Pu-238 Activity (Bq)	**0.3118**	**0.0012**	0.40%
Am-241 Activity (Bq)	**NONE**	**n/a**	n/a

U3 – Mixed isotopes: beta/gamma at approx. int. lvl, Am-241 at 10x int. lvl, no Pu-238

12/25/2014 10:06	Bq	uncert	uncert %
Co-60 Activity (Bq)	**22498**	**85**	0.38%
Sr-90 Activity (Bq)	**3324**	**8**	0.24%
Cs-137 Activity (Bq)	**1688**	**7**	0.39%
Pu-238 Activity (Bq)	**NONE**	**n/a**	n/a
Am-241 Activity (Bq)	**2.614**	**0.009**	0.33%

U4 – Mixed isotopes: beta/gamma at ~10% of int. lvl, Am-241 and Pu-238 at ~10x int. level
***NOTE: Co-60 at 10% of the intervention level was originally intended to be added to this sample; however, it was left out in error.

12/25/2014 11:09	Bq	uncert	uncert %
Co-60 Activity (Bq)	**NONE**	**n/a**	n/a
Sr-90 Activity (Bq)	**339.2**	**1.3**	0.39%
Cs-137 Activity (Bq)	**162.9**	**0.6**	0.39%
Pu-238 Activity (Bq)	**0.3180**	**0.0013**	0.39%
Am-241 Activity (Bq)	**2.638**	**0.009**	0.33%

U5 – Mixed isotopes: no beta/gamma; Am-241 and Pu-241 at ~10x intervention level

12/25/2014 12:11	Bq	uncert	uncert %
Co-60 Activity (Bq)	**NONE**	**n/a**	n/a
Sr-90 Activity (Bq)	**NONE**	**n/a**	n/a
Cs-137 Activity (Bq)	**NONE**	**n/a**	n/a
Pu-238 Activity (Bq)	**0.3064**	**0.0012**	0.40%
Am-241 Activity (Bq)	**2.703**	**0.009**	0.33%

U6 – Mixed isotopes: no alpha; Co-60 at intervention level, Sr-90 & Cs-137 @ ~10% of int. level

12/25/2014 13:14	Bq	uncert	uncert %
Co-60 Activity (Bq)	**23461**	**89**	0.38%
Sr-90 Activity (Bq)	**344.8**	**1.3**	0.39%
Cs-137 Activity (Bq)	**151.3**	**0.6**	0.39%
Pu-238 Activity (Bq)	**NONE**	**n/a**	n/a
Am-241 Activity (Bq)	**NONE**	**n/a**	n/a

U7 – Mixed isotopes: no alpha; Co-60 at 10% of int. level, Sr-90 & Cs-137 at intervention level

12/25/2014 14:16	Bq	uncert	uncert %
Co-60 Activity (Bq)	**2278**	**6**	0.26%
Sr-90 Activity (Bq)	**3364**	**8**	0.24%
Cs-137 Activity (Bq)	**1754**	**7**	0.38%
Pu-238 Activity (Bq)	**NONE**	**n/a**	n/a
Am-241 Activity (Bq)	**NONE**	**n/a**	n/a

U8c – Co-60 calibration source

12/29/2014 21:33	Bq	uncert	uncert %
Co-60 Activity (Bq)	**26631**	**101**	0.38%
Sr-90 Activity (Bq)	**NONE**	**n/a**	n/a
Cs-137 Activity (Bq)	**NONE**	**n/a**	n/a
Pu-238 Activity (Bq)	**NONE**	**n/a**	n/a
Am-241 Activity (Bq)	**NONE**	**n/a**	n/a

U9c – Sr-90 calibration source

12/29/2014 22:35	Bq	uncert	uncert %
Co-60 Activity (Bq)	**NONE**	**n/a**	n/a
Sr-90 Activity (Bq)	**3827**	**9**	0.24%
Cs-137 Activity (Bq)	**NONE**	**n/a**	n/a
Pu-238 Activity (Bq)	**NONE**	**n/a**	n/a
Am-241 Activity (Bq)	**NONE**	**n/a**	n/a

U10c – Cs-137 calibration source

12/29/2014 23:38	Bq	uncert	uncert %
Co-60 Activity (Bq)	**NONE**	**n/a**	n/a
Sr-90 Activity (Bq)	**NONE**	**n/a**	n/a
Cs-137 Activity (Bq)	**5914**	**21**	0.35%
Pu-238 Activity (Bq)	**NONE**	**n/a**	n/a
Am-241 Activity (Bq)	**NONE**	**n/a**	n/a

U11c – Pu-238 calibration source

12/25/2014 3:50	Bq	uncert	uncert %
Co-60 Activity (Bq)	**NONE**	**n/a**	n/a
Sr-90 Activity (Bq)	**NONE**	**n/a**	n/a
Cs-137 Activity (Bq)	**NONE**	**n/a**	n/a
Pu-238 Activity (Bq)	**1.483**	**0.005**	0.34%
Am-241 Activity (Bq)	**NONE**	**n/a**	n/a

U12c – Am-241 calibration source

12/25/2014 4:53	Bq	uncert	uncert %
Co-60 Activity (Bq)	**NONE**	**n/a**	n/a
Sr-90 Activity (Bq)	**NONE**	**n/a**	n/a
Cs-137 Activity (Bq)	**NONE**	**n/a**	n/a
Pu-238 Activity (Bq)	**NONE**	**n/a**	n/a
Am-241 Activity (Bq)	**6.112**	**0.020**	0.32%

U14 – Mixed alpha, no beta: Am-241 and Pu-238 at intervention level

12/31/2014 12:00	Bq	uncert	uncert %
Co-60 Activity (Bq)	**NONE**	**n/a**	n/a
Sr-90 Activity (Bq)	**NONE**	**n/a**	n/a
Cs-137 Activity (Bq)	**NONE**	**n/a**	n/a
Pu-238 Activity (Bq)	**0.03717**	**0.00013**	0.36%
Am-241 Activity (Bq)	**0.2891**	**0.0010**	0.33%

APPENDIX III – ACTIVITY RECOVERIES AFTER AC FILTRATION

Table A3.1 Gravimetric recoveries after carbon filtration

	recovery	**uncert**	**uncert %**
U1	**87.7%**	**1.9%**	**2.2%**
U2	**88.7%**	**2.0%**	**2.2%**
U3	**86.0%**	**1.9%**	**2.2%**
U4	**86.9%**	**2.0%**	**2.3%**
U5	**88.9%**	**2.0%**	**2.3%**
U6	**89.2%**	**2.0%**	**2.2%**
U7	**86.3%**	**1.9%**	**2.2%**
U8	**88.2%**	**2.0%**	**2.2%**
U9	**89.8%**	**2.0%**	**2.2%**
U10	**86.8%**	**2.0%**	**2.2%**
U11	**89.8%**	**2.0%**	**2.2%**
U12	**86.4%**	**1.9%**	**2.2%**
U14	**87.2%**	**2.0%**	**2.2%**
avg	**87.8%**		
stdev	**1.3%**		

Table A3.2 Recoveries calculated from rinses

	Source frac	uncert	uncert %
U1	90.30%	0.02%	0.02%
U2	90.05%	0.02%	0.02%
U3	88.86%	0.02%	0.02%
U4	88.83%	0.08%	0.09%
U5	89.70%	1.50%	1.67%
U6	90.52%	0.02%	0.02%
U7	88.19%	0.02%	0.03%
U8	90.05%	0.02%	0.02%
U9	91.60%	0.03%	0.03%
U10	88.69%	0.03%	0.03%
U11	89.48%	2.30%	2.57%
U12	88.06%	0.95%	1.07%
avg	89.53%		
stdev	1.05%		

APPENDIX IV – HPGE DETECTOR DIAGRAM

CANBERRA

Germanium Detector Chamber Typical Cross-Sectional View

Detector Model GR7023
Cryostat Model 7500 SL
Detector S/N 02076343

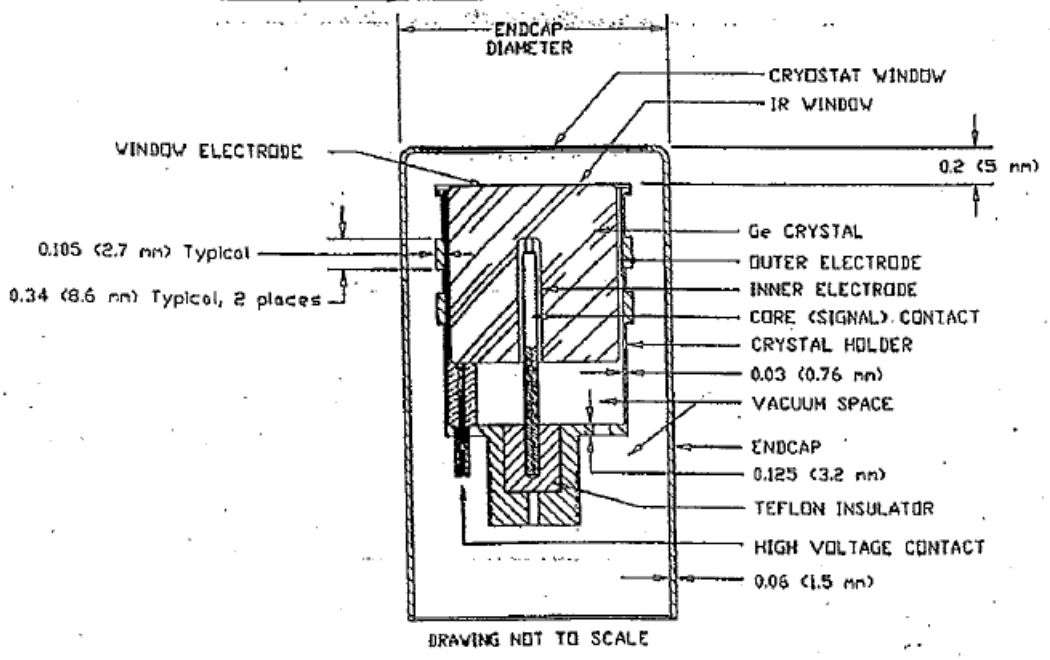

Ge Crystal Details

Outer Electrode Thickness 3x10⁻³ mm (Ge Equivalent)
Inner Electrode Thickness ≈0.5* mm (Ge Equivalent)
Window Electrode Thickness 3x10⁻³ mm (Ge Equivalent)
Crystal Diameter 74.5 mm
Crystal Length 66.5 mm
Core Hole Diameter 20 mm
Core Hole Depth 53 mm

Detector Chamber Material Details

Cryostat Window Material Beryllium Thickness 0.5 mm
IR Window Material 1/3 mil metalized mylar + 4 mil Kapton
Endcap Material Aluminum Thickness 1.6 mm
Crystal Holder Material Aluminum
Additional Comments * typical at time of manufacture

Figure A4.1 HPGe detector diagram